THE UNIVERSITY OF CHICAGO

THE ROLE OF LYSOSOME REMODELING IN PHAGOCYTOSIS

A DISSERTATION SUBMITTED TO

THE FACULTY OF THE DIVISION OF THE PHYSICAL SCIENCES

IN CANDIDACY FOR THE DEGREE OF

DOCTOR OF PHILOSOPHY

DEPARTMENT OF CHEMISTRY

BY

BHAVYASHREE SURESH

CHICAGO, ILLINOIS

JUNE 2021

Dedicated to Mom, Indira and Grandmother, Radha

Table of Contents

List of Figures

List of Tables

Acknowledgements

"If I have seen further, it is by standing on the shoulders of giants". Isaac Newton.

Several people have played important roles during my PhD research. This thesis would be incomplete without acknowledging them for their contributions.

Primarily, I would want to extend my sincere gratitude to my mentor, Prof. Yamuna Krishnan. Prof. Krishnan has not just invested time in my scientific growth, but also taught me how to think independently and to bring out the best in me. I learnt scientific rigor from Yamuna. I deeply appreciate her for giving me the wings to fly in the direction I wanted to. It was a great learning experience working with Yamuna. Her ambitious nature with clear vision is an inspiration for me. Scientific communication and effective collaborations are among many things that I have learnt from her. Yamuna has played a big role in my overall progress as a scientist.

I thank Dr. Lev Becker, our collaborator as well as one of my thesis committee members. Dr. Becker has provided several insightful suggestions and comments while the project was ongoing and during manuscript preparation. My sincere appreciation extends to all my collaborators, Dr. Kasturi Chakraborty, Dr. Anand Saminathan, Dr. Chang Cui and Matthew Zajac who were instrumental in the successful completion of the project.

I want to thank my other thesis committee member, Dr. Bryan Dickinson and his lab members who have been amazing and helpful neighbors. I especially want to thank Dr. Jinyue Pu and Dr. Rahul Kathayat for innumerable insightful scientific discussions and useful suggestions. I also want to thank Prof. He lab members for letting me use his lab resources necessary for carrying out my research.

I joined YK lab in National Center for Biological Sciences (NCBS), Bangalore, India. Dr. Krishnamurthy was my Co-guide at NCBS who provided great scientific guidance at the start of my research career. In NCBS, HariKrishna Adicherla taught and helped me in learning electron microscopy which left me in love with this super technique. Dr. Narayanan Bobby Kasturi and Vandana (Kasturi Lab) and Dr. Vincent De Andrade, Argonne National labs taught sample preparation and x-ray imaging. Dr. Jonathan Austin, University of Chicago, taught me EM techniques like high pressure freezing and freeze substitution etc. Prof. Krishnan lab members, Souvik Modi, Suruchi, Sunaina, Dhiraj, Sonali, Saheli, Saikat, Shareefa, Kasturi, Anand, Maulik, Aneesh, Krishna, Nagarjun, Kaho, Anees, Junyi and Matt have been constant source of learning and helped me in my scientific journey in the lab.

My sincere thanks to my dear friends, Rahul and Jin who were instrumental in keeping me positive every time I hit a roadblock. Thank you, Rahul for so many life lessons which has made me a better person. Also, I want to thank my other friends who also happened to my lab mates, Kasturi, Anand, Shareefa, Maulik, Kaho, Aneesh, Junyi, Matt, Anees who made the journey fun and enjoyable.

Finally, my family especially my Mom, Indira; dad, Suresh and my husband, Jayaram, who were and are my wall of support. They always made me realize my capabilities and short comings and pushed me forward. My brother, Shreyas who inspires me and fills me with energy to propel forward. My brother-in-law, Raghavendra who was so proud of me and made me realize that each time I spoke to him, you will be fondly remembered forever, Raghuanna.

Abstract

Lysosomes are mostly vesicular in morphology performing various functions due to its involvement in several signaling mechanisms. Immune response and autophagy can trigger vesicular lysosomes into morphologically distinct tubular lysosomes. Autophagy mediated tubular lysosomes are mTOR independent while immune mediated tubular lysosomes are mTOR dependent. Tubular lysosomes perform antigen presentation in dendritic cells, provide more fluid retention and aid in enhanced phagocytosis in macrophages while in autophagy, it mediates biogenesis of lysosomes. But studying the role of tubular lysosomes has been difficult as the stimulants of tubular lysosomes also modify the phenotypes of macrophages making it more activated. Here we describe a DNA nanodevice, *Tudor*, which tubulates lysosomes in an alternative pathway in macrophages without affecting its polarization states. *Tudor* binds to cell surface localized Ku70/80 heterodimer proteins and brings about tubulation of lysosomes in various macrophages in TLR independent pathway which was not known before. Further, tubular lysosomes showed lower enzymatic activity as compared to its vesicular counterparts suggesting tubular lysosomal lumenal biochemistry is distinct from vesicular ones. pH correctable calcium sensor, *CalipHluor 2.0* imaging showed the presence of pH and calcium gradients within the lumen of tubular lysosomes. In more than 50% of tubular lysosome population, the part of tubular lysosomes closer to plasma membrane showed high calcium and hypo-acidic lumenal environment. Tubular lysosomes previously discovered to be delivering V-ATPases to phagosome needed for its maturation. We found that tubular lysosomes make physical contact with phagosomes and cells with tubular lysosomes showed better phagosome lysosome fusion. Hence *Tudor* was able to decipher the alternative pathway in which tubular lysosomal formation which poises resting macrophages to phagocytosis.

List of Publications

1. **Suresh, B**., Saminathan, A., Chakraborty, K., Cui, C., Becker, L. and Krishnan, Y., 2020. Tubular lysosomes harbor active ion gradients and poise macrophages for phagocytosis. bioRxiv**.** https://doi.org/10.1101/2020.12.05.413229

2. Saminathan, A., Devany, J., Veetil, A.T., **Suresh, B**., Pillai, K.S. Schwake, M. and Krishnan, Y., 2020. A DNA-based voltmeter for organelles. ***Nature nanotechnology.*** **16,** 96–103 (2021). https://doi.org/10.1038/s41565-020-00784-1

3. Chakraborty, K., **Suresh, B**. and Krishnan, Y., 2020. DNA based sensors for quantitation of lysosomal ions. Current Protocols Journal. (in review)

Chapter 1. Introduction

1.1 Lysosomes are a signaling hub

Lysosomes were a serendipitous discovery by Christian De Duve approximately 50 years ago using the then newly developed experimental procedure, centrifugal sedimentation, and tissue fractionation in rat liver cells while he was studying the enzyme activity of glucose-6-phosphatase[1]. De Duve's experiments showed that lysosomes were basically bags to degrade material and had an acidic pH of 4.5-5.5[1–3]. Lysosomes host more than 60 different degradation enzymes including proteases, hydrolases, nucleases, lipases etc. to degrade a plethora of cargo that enter lysosomes via various pathways like endocytosis, phagocytosis, autophagy. For a long time, lysosomes were considered to only degrade macromolecules into their basic building blocks and recycle them into the cytoplasm of the cells.

Two landmark discoveries changed the outlook of lysosomes; David Sabatini's group showed that mammalian mechanistic target of rapamycin (mTOR), activation and signaling that occurs upon amino acid sensing could occur only if mTORC localized on lysosomes[4]. Another landmark discovery was by Andrea Ballabio's group who showed that upon starvation or stress, lysosome biogenesis was upregulated by the nuclear translocation of the transcription factor denoted transcription factor EB (TFEB). This led to the upregulation of genes associated with lysosomal biogenesis[5,6]. Activation of mTORC1, one of major protein complexes involved in myriad pathways and its involvement in lysosome-to-nucleus signaling with gene expression, led to lysosomes being regarded as one of the signaling hubs in the cell[7,8]. Further studies reveal that lysosomes were also platform for location of 5'-AMP-activated protein kinase (AMPK) along with mTORC1 and other proteins which toggled the delicate catabolic and anabolic balance within cells. This then led to lysosomes emerging as an important metabolic signaling hub in the cells[9,10].

1.1a The role of lysosomes in cellular metabolism: Although lysosomes are the catabolic organelle of the cell, lysosomes can also act as platforms for anabolic pathways involving mTOR needed for cell proliferation, the immune response and survival. Both rowth factors and nutrients bring about activation of receptors on the lysosomal membrane. For example, arginine can be sensed by SLC38A9 and CASTOR1, which are amino acid sensing receptors on the lysosomal membrane. Binding of amino acids to the amino acid sensing domains of SLC38A9 or CASTOR1 leads to the activation of Rag Guanosine tri phosphatases (GTPases) which recruits mTORC1 from the cytosol to the membrane of lysosomes[4,11–16]. Rheb GTPases on the lysosomal membrane then stimulates the kinase activity of mTORC1. V-ATPases interact with RAPTOR and Rag GTPases in an amino acid dependent manner. Knocking down V-ATPases prevents lysosomal anchorage of mTORC1 and thus prevents the activation of mTORC1[17]. mTOR activation on lysosomal membrane leads to its phosphorylation which leads to activation of S-6-Kinase which, in turn triggers biosynthesis of lipids, nucleotides, ribosome biogenesis and switch to glucose metabolism. The main goal of mTOR activation on the lysosomal membrane is to phosphorylate 4EBP leading to increased protein synthesis [10,18–20].

Lysosomes also sense cholesterol through SLC38A9 activating mTOR through the above mentioned Rag GTPase pathway. Cholesterol is transferred via the intracellular cholesterol transporter, (Niemann Pick C type1) NPC1 to other organelles like the ER, Golgi or plasma membrane (PM) thereby inactivating mTOR[20].

Another important lysosomal signaling involves AMPK. AMPK, being an ATP sensor senses the increase in AMP:ATP/ADP:ATP. AMP/ADP binds to γ-subunit of AMPK phosphorylating Thr172 of the catalytic α-subunit hence activating AMPK. Upon glucose deprivation, Liver Kinase B1 (LKB1), a kinase upstream of AMPK forms a complex with AMPK along with the scaffold

protein, AXIN on the lysosomal membrane by binding to lysosomal proteins, LAMTOR1. RAGULATOR and V-ATPase contribute to complex formation and further activation of AMPK [21,22]. LKB1 activates AMPK on the cytosolic side of lysosomal membrane. Activated AMPK prevents ATP harnessing the anabolic pathway and instead triggers the ATP powered catabolic pathway to restore energy homeostasis[7]. AMPK activation on the lysosomal membrane leads to the activation of transcription factors, FOXO/DAF 16 and CRTC/CRTC-1 in *C. elegans* expressing stress resistance genes. Hence AMPK is also involved in enhancing longevity in *C. elegans*. Note that AMPK and mTOR activation promote opposite outcomes, and both kinases use the same downstream effectors. However, AMPK promotes autophagy while mTOR promotes lysosomal biogenesis through TFEB. AMPK inhibits mTOR by two well studied mechanisms; (i) it activates Tuberous Sclerosis complex 2 (TSC2) which has GTPase activating protein (GAP) activity inhibiting Rheb and therefore inhibiting mTOR[23,24], (ii) AMPK phosphorylates S722 and S792 on RAPTOR[25,26]. Hence lysosomes play role in both metabolism and longevity by toggling both AMPK and mTOR-related pathways.

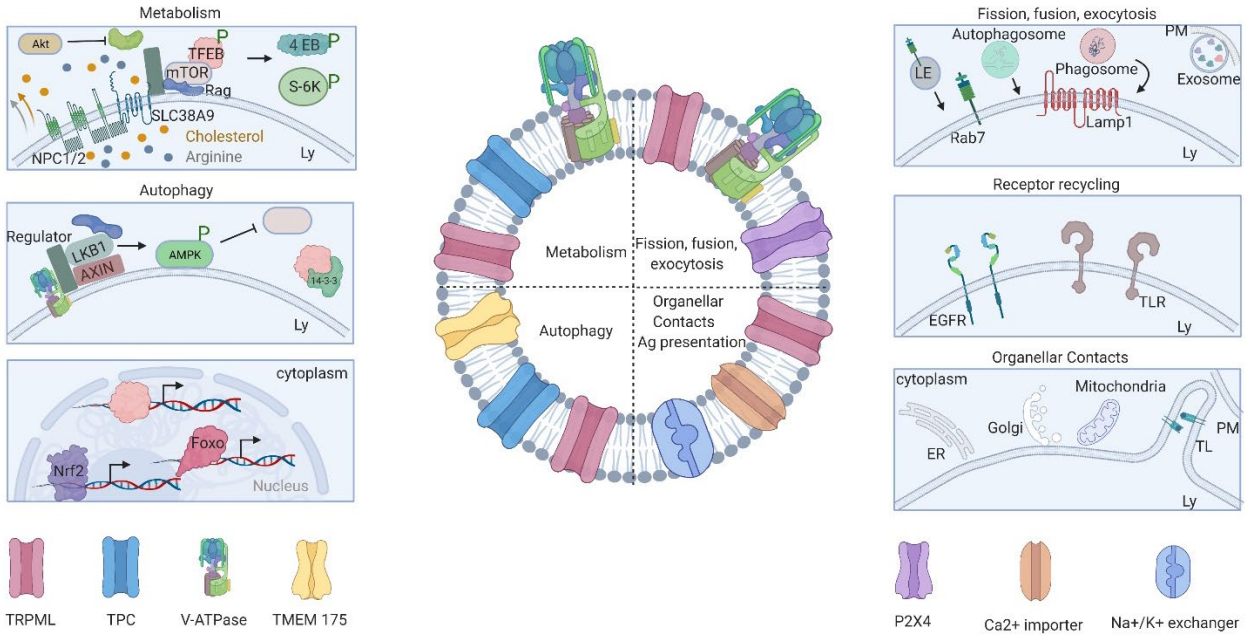

Figure I.1: Lysosome as a signaling hub. Schematic of the various signaling roles performed by lysosomes.

1.1b The role of lysosomes in other signaling pathways: Lysosomes activate other pathways mainly by proteolytic activation of certain signaling ligands or by degrading specific activated receptors. Two examples are detailed below.

<u>Downregulation of receptor mediated signaling at PM:</u> Receptor Tyrosine Kinase (RTK) family receptors are a subclass of tyrosine kinases which play roles in cell-cell communication, cell survival, metabolism etc[27]. Few examples of RTKs includes Epithelial growth factor receptors (EGFR) or platelet derived growth factor (PDGF). EGF binds to EGFR on the cell surface, activating EGFR, leading to its dimerization and cross phosphorylation of its cytosolic phosphorylating domains[27,28]. This enables the binding and activation of Ras-GTPases Phosphotidyl-3- kinases (PI3K) eventually activating the MAPK pathway needed for cell proliferation[29]. To prevent uncontrolled cell proliferation, the ligand-receptor binding is regulated by triggering the endocytosis of phosphorylated EGFR (p-EGFR). This is due to the presence of

self-ubiquitination of p-EGFR by E3 ligases Cbl which is recognized by endocytic adapter proteins, epsin and Eps15[18]. Eventually p-EGFR then reaches the lysosomes where the receptor is degraded, preventing uncontrolled cell division. Downregulation of receptor degradation leads to constitutive activation of EGFR which leads to malignant conditions.

Regulation of receptor mediated activation: Toll like receptors (TLRs) elicit the immune response in immune cells by recognizing and binding with the pathogen associated molecular patterns (PAMPs). Of all the TLRs, TLR 3, 7, 8 and 9 are present in the endosomes and mainly survey the system for any pathogenic nucleic acids. When the recognition of PAMPs occurs via the ectodomain on the lumenal side of endosomal TLRs, it leads to conformational changes in its structure. These structural changes then cause the binding of adapter proteins like TIRF, MyD88 on the lumenal side of endosomes. However, the action of cathepsins and asparagine endopeptidases is needed within lysosomes in order to fully activate TLRs and elicit a strong immune response leading to cytokine production.

1.2 The various functions of lysosomes

1.2a Cargo degradation: Given its role in multiple signaling mechanisms, lysosomes also play multiple roles in maintaining cellular homeostasis. Lysosomes are the end point of endocytosis where cargo breakdown yields monomer building blocks in the lumen. Under certain conditions, lysosomes act as nutrient reservoirs which can either buffer the cytosolic nutrient levels or modify it. Lysosomes are also the endpoint of phagosome maturation where extracellular cargo e.g., apoptotic cells or foreign particle like bacteria or viruses within the phagosome fuses with lysosomes for its degradation. The partially digested cargo is loaded on MHCII peptide followed by display on the plasma membrane. This promotes recognition by T-cells and their activation.

Other organelles that make their way to lysosomes are autophagosomes, which mainly brings the intracellular cargo such as non-functional organelles for degradation and recycling.

1.2b Exocytosis: One of the main sources of membrane for PM recycling is given by lysosomes due to its exocytosis behavior. Upon plasm membrane damage, lysosomes release its highly degradative enzymes mainly Cathepsin B, L, D and acid sphingomyelinases (ASM) by exocytosis at the site of damaged Plasma Membrane. Lysosomal enzymes remodel the extracellular matrix aiding in Plasma Membrane repair. Releasing ASM on the site of damaged Plasma Membrane converts sphingomyelin at damaged site into ceramide. Ceramide rich domains on the Plasma Membrane triggers endocytosis resolving the damage by endocytosed where the damaged membrane cargo is eventually degraded in lysosomes and the monomers are recycled [9]. Secretory lysosomes are a specialized population of lysosomes which perform exocytosis and are found in specialized cells like melanocytes, renal tubular cells, osteoclasts and hematopoietic lineage cells like T cells, neutrophils, macrophages, dendritic cells etc. These cells contains secretory proteins like anti-microbial peptides, perforins, Van Willbrand Factors etc. Secretory lysosomes perform multiple functions such as degradation, storage as well as intercellular communications[30].

1.2c Lysosomes as acidic calcium store: Lysosomes are dynamic, undergoing constant fission and fusion. Not all lysosomes are similar in their composition. They vary based on their lumenal composition as well as membrane protein compositions and these variations dictate their differential cellular functions. Lysosomal ion channels and transporters maintain H^+, Ca^{2+}, Na^+, K^+, Cl^- and potential across the lysosomal membrane. Lysosomal pH is largely maintained by V-ATPases although pH in lysosomes also correlates with lysosome location within the cell, i.e., whether they are present in the cell periphery or perinuclear region and the nutrient state of the

cells[31,32]. While V-ATPases pump protons into lysosomes, the identity of the proton leak channels in lysosomes is still unknown.

One of the hallmarks of lysosomes are that they are acidic and a secondary store for calcium, iron, copper and zinc ions[33]. Lysosomes have ~0.2-0.5 M calcium, which is ~5000 fold higher than that of the cytoplasm[34]. ATP13A2 has being shown as a plausible calcium importer into lysosomes, over and above possible H^+/Ca^{2+} changers which have been posited to exist [35,36]. Ca^{2+} release channels like Mucolipin 1(TRPML1) and P2X4 have been found on lysosomal membranes. TRPML function is closely associated with acidic lysosome lumens. TRPML1 channel activity leads to fission while P2X4 activity leads to fusion events. However, both channels are activated at slightly different pH - TRPML1 needs less acidic lumenal milieu while P2X4 needs more acidic lumenal milieu for activity, thereby promoting lysosomal fission and fusion[37]. Due to these ionic signatures, ion channels and other integral proteins, lysosomes make contact with other organelles in cells especially the peroxisomes, endoplasmic reticulum (ER), and the mitochondria[38]. For example, Lysosomes make contact with ER where Ca^{2+} release channels on the ER such as Inositol triphosphate receptors (IP_3R) which release Ca^{2+} that is taken up by lysosomal Ca^{2+} transporters[39]. Similarly, lysosomes also contact mitochondria to exchange amino acids, lipids and ions like Ca^{2+}[40]. Recently lysosomes were found to regulate the dynamics of ER tubules[41]. Two other lysosomal Ca^{2+} channels are two pore channels, TPC1 and TPC2. The TPC channels are calcium permeable but are Na^{2+} selective and thereby maintain Na^+ dependent membrane potential across lysosomes[38]. In order to meet all of these functional demands, lysosomes have also evolved to adapt morphologically, forming distinct tubular structures as compared to the conventional vesicular shape.

1.3 Lysosome remodeling impacts its function

Lysosomes are mostly vesicular with diameter of 0.5 μm-1.0 μm yet there are several examples where lysosomes are extensively elongated upto 4 μm to 10 μm in length[42–46]. These curvilinear lysosomes are called Tubular lysosomes (TLs) sometimes referred to also as MHC-II compartments in dendritic cells[47]. Cells ranging from epithelial cells, fibroblasts, macrophages such as bone marrow derived macrophages (BMDM) and dendritic cells (BMDC) also show the presence of both vesicular and tubular lysosomes[48]. Tubular lysosomes play roles in lysosomal biogenesis, antigen presentation, and in phagosome resolution[48]. Thus, lysosomes are modulated into either into vesicular or tubular morphologies in order to perform specific cellular functions.

1.4 Different types of tubular lysosomes

Several innate immune cells like Human monocyte derived macrophages (HMDM), BMDM, BMDC and muscles cells in the developing larva of *Drosophila melanogaster* have shown highly reticulate, tubular lysosomes. The trigger for the formation of such constitutively present tubular lysosomes is still unknown. Tubular lysosomes can be triggered in immune cells like macrophages and dendritic cells by activating the immune response with bacteria, lipopolysaccharides (LPS) or Phorbol myristate 13-ester (PMA). LPS, is a ligand for the TLR4 receptor on the Plasma Membrane and tubular lysosome formation in immune cells has been considered to be TLR4-mediated. However, inactivating MyD88, one of the downstream players in TLR4 signaling, could not completely suppress the formation of tubular lysosomes in BMDCs. This suggests the presence of additional pathways to tubulate lysosomes[49]. Starving cells up to 4 hours induced tubular lysosome formation in several epithelial cell types such as normal rat kidney cells, HeLa cells etc[50,51]. Both immune activation and cell starvation trigger two distinct pathways, and both tubulate

lysosomes. However, we still do not know whether the tubular lysosomes associated with either pathway are biochemically or functionally distinct from each other.

1.4a Autophagy mediated tubular lysosomes: Nutrient deprivation upon starvation leads to mTOR inactivation and AMPK activation thereby initiating autophagy. During autophagy, autophagosomes fuse with lysosomes to form autolysosomes and hence the number of lysosomes available for other cellular functions is reduced. However, when lysosomes tubulate, one also observes the formation of spherical proto-lysosomes emanating from the tubular ends. These newly formed proto-lysosomes mature into nascent vesicular lysosomes, are highly acidic and have high proteolytic activity. Hence autophagy triggered tubular lysosomes also leads to the production of smaller, vesicular proto-lysosomes[52]. This process is referred to as Autophagic lysosomal reformation (ALR)[50,52,53]. During autophagy, the lysosomal efflux permease and sugar transporter, Spinster (Spin), regulates ALR by transporting the sugar across lysosomal membrane. During starvation, the general amino acid control (GAAC) pathway is activated by increasing the expression of amino acid transporters on the Plasma Membrane which elevates amino acid uptake. Hence upon nutrient replenishment, mTOR is activated thereby attenuating autophagy. Thus, mTOR signaling acts as a negative feedback mechanism to prevent excessive autophagy. Inhibition of Spin leads to autolysosome accumulation which impedes proto-lysosome formation [50,52,54].

ALR formation initiates with the PI(4,5)P2 microdomains formed by action of PIP5K on PI4P present on the membrane of autolysosomes. Other variants also catalyze this process e.g., PIP5KIIIβ[54,55]. Clathrin binds to PI(4,5)P2 on autolysosomes via its adapter protein (AP2) forming a lattice at makes the membrane bud. The PH domain of KIF5B, binds the PI(4,5)P2 microdomain and drives the tubulation of autolysosomes. The second wave of Clathrin binding to PI(4,5)P2

molecules is catalyzed by PIP5K1α on the tip of the tubule. The subsequent recruitment of dynamin-1/2, helps in scission of proto-lysosomes from tubulated autolysosomes[52,54]. Tubular lysosomes are marked by SNAREs and Syntaxin (SNX17) in larval muscle cells of *D. melanogaster*[56]. ALR also activates Nrf2/FOXO transcription factors thereby activating oxidative stress response genes and lysosomal genes in *C.elegans*[57].

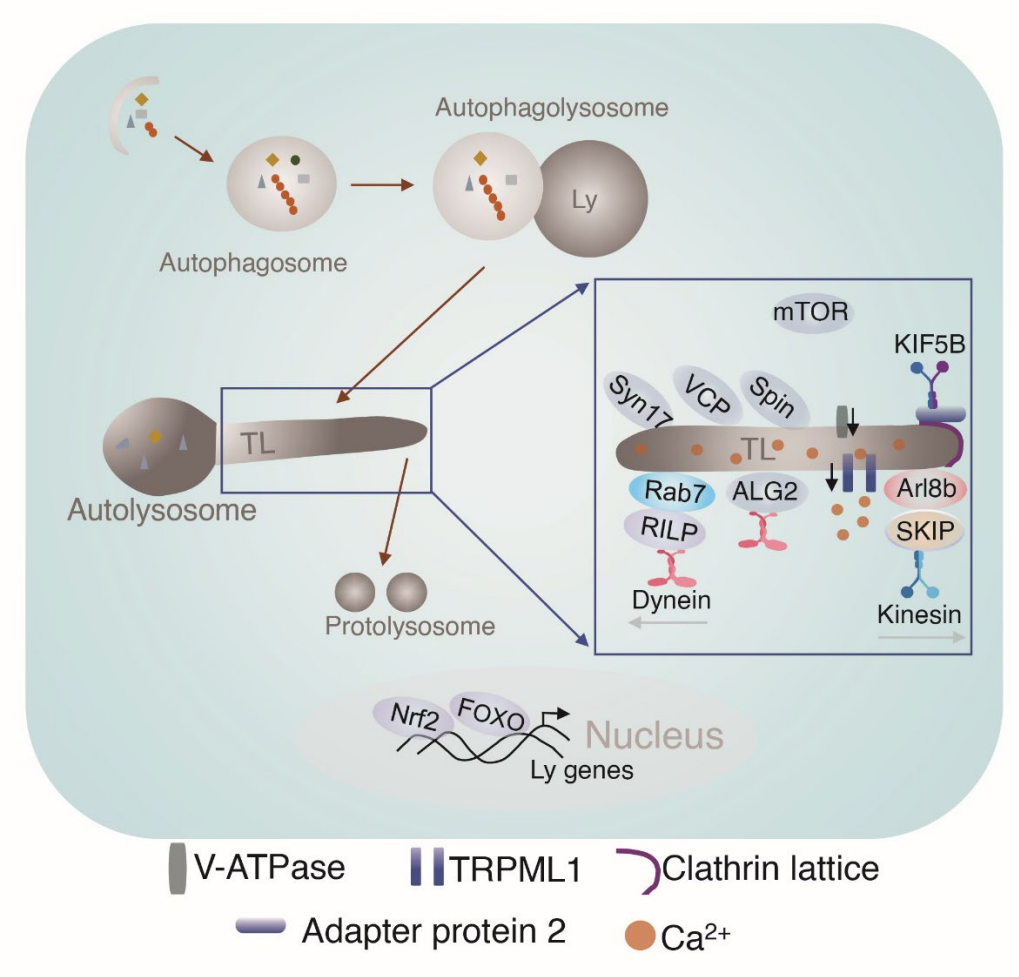

Figure I.2: Autophagy mediated tubular lysosome formation. Schematic of autophagy mediated lysosomes tubulation in response to starvation or during the early development. Autophagy mediated lysosomal tubulation is mTOR independent, eventually leading to lysosomal and oxidative stress response gene expression.

1.4b Physiological relevance of Autophagic Lysosome Reformation (ALR): Spin mutants in Drosophila show carbohydrate accumulation within their autolysosomes and fewer nascent lysosomes[58]. Glucocerebrosidase is important for ALR. Mutations in glucocerebrosidase leads to ALR inhibition and fewer nascent lysosomes needed for autophagic degradation of α-synuclein. Accumulation of α-synuclein is associated with Parkinson's disease [59]. Valosin containing protein (VCP) and AAA-ATPases were found to be important in lysosomal tubulation. VCP mutants prevent lysosomal tubulation in muscles cells of third instar larva of *D. melanogaster*. Similar mutations were associated with autosomal recessive hereditary spastic paraplegia[44]. As revealed by studies on L-4 larvae of *C. elegans* and *D. melanogaster* ALR is crucial for the tissue remodeling necessary during development [56,57,60].

1.4c LPS mediated tubular lysosomes: Tubular lysosomes in immune cells are highly pronounced, almost spanning the entire length of immune cells sometimes reaching up to 10-20 μm. Lipopolysaccharide (LPS) is a well-studied immunostimulant that initiates lysosome tubulation in innate immune cells. Tubular lysosomes in immune cells usually form from the center of the cell and radiate towards the periphery. Tubular lysosomes generally propagate towards phagosomes if the latter is formed within the immune cell[61]. LPS modulates the immune cell polarization into a more pro-inflammatory state and simultaneously vesicular lysosomes tubulate. LPS is a well-known ligand for TLR4 found on Plasma Memebrane. TLR4 activates the PI3K-Akt-mTOR cascade via MyD88. Thus, cytosolic mTOR is recruited to the lysosomal membrane. LPS activation also upregulates ADP ribosylation factors like the GTPase Arl8b.. Arl8b binds to Kinesin-1 through the adapter protein, SifA-kinesin interacting protein (SKIP). Kinesin then moves lysosomes displaying Arl8b towards to periphery of the cell by propagating along the "+" of microtubules. In contrast, Rab7 GTPase, also found on the lysosomal membrane remains bound

to the motor protein dynein. Rab7 binds to dynein through its adapter proteins Rab interacting lysosomal protein (RILP) or FYVE and the Coiled-Coil Domain Autophagy Adaptor 1 (FYCO1). Dynein drives the movement of lysosomes towards the nucleus by propagating towards "-" end of microtubules. This tug of war between dynein and kinesin-1 attached to both lysosomal motility proteins along microtubules drives lysosome tubulation[43,46,62]. LPS treatment also leads to Ca^{2+} efflux from lysosomes through the Ca^{2+} channel TRPML1 which activates ALG2. This further enhances lysosomal movement by its direct association with the dynein-dynactin complex. Both Inhibition or over-expression of TRPML1 prevent tubulation suggesting a delicate balance of expression is needed for the right amount of Ca^{2+} in order to tubulate lysosomes [37,51]. BORC1, a multi-subunit protein complex regulates the localization of Arl8b on the lysosomal membrane and is also needed for tubulation. However, mTOR negatively modulates BORC1 and Arl8b during autophagy[43,63]. Therefore, lysosome tubulation is stringently regulated and does not happen inadvertently.

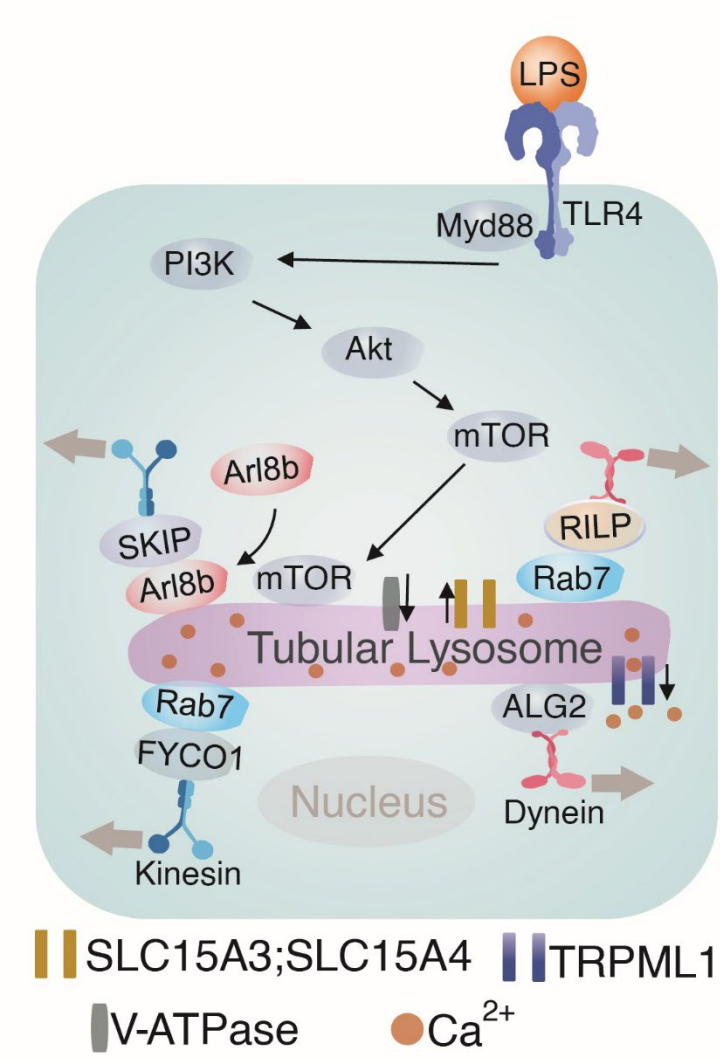

Figure I.3: LPS induced tubulation of lysosomes. LPS mediated tubulation is TLR4 dependent and involves the PI3K-Akt-mTOR pathway. Activation of mTOR enhances the levels of Arl8B on lysosomes which activates kinesin.

Figure 1.3, continued. Rab7 mediated dynein activation acts in concert to tubulates the vesicular lysosomes.

1.4d Physiological relevance of LPS mediated tubular lysosomes: Tubular lysosomes in immune cells play multiple roles. In dendritic cells they contain MHCII and are hence called MHCII compartments[47,49,64–66]. MHCII:peptide complexes are formed within the tubular lysosomes in dendritic cells. MHCII:peptide complex are presented on PLASMA MEMBRANE upon fusion these tubular lysosomes leading to antigen presentation[49,65,67,68]. In macrophages, tubular lysosomes enhance phagosome resolution[45]. Tubular lysosomes also contact phagosomes to deliver V-ATPases needed to acidify phagosomes and for eventually fusing with vesicular lysosomes [69].

1.5 The dynamic nature of tubular lysosomes

Tubular lysosomes are highly dynamic organelles similar to their vesicular counterparts moving along microtubules back and forth. The pH within the lumen of tubular lysosomes is crucial to maintain the tubular morphology. Inhibition of V-ATPase prevented the tubulation of lysosomes. This is because acidic pH within the lysosomal lumen activates PI(3,5)P2 which is needed to activate TRPML1 channels in lysosomes [37,51]. Inhibition of TRPML1 prevents lysosomal tubulation and causes mucolipidosis IV, a lysosomal storage disorder [51]. Thus, the lumenal ionic levels drive lysosome tubulation.

1.6 DNA based sensors to study lysosomes

Macrophage or dendritic cell have both vesicular and tubular lysosomes upon immune stimulation. However, it is not clear as to why would a cell need two morphologically distinct forms of the same organelle. The inner lumenal milieu of tubular lysosomes is still undetermined. Thus, we do

not know how tubular lysosomes are different from vesicular lysosomes. Also, LPS triggers not just the tubulation of lysosomes but also stimulates the immune response. In order to tease out the precise function of tubular lysosomes in the background of inflammation, we need to decouple tubular lysosome formation from immunostimulation or cell starvation.

I have developed a DNA based nanodevice, *Tudor* which triggers the tubulation of lysosomes in various macrophage cells lines in their resting states. It enhances the tubulation of lysosome in primary macrophages without affecting expression profiles of genes related to the immune response or polarizing macrophage. Thus, it is an excellent tool to study the functions of tubular lysosomes without the background of immune stimulation or autophagy.

I decided to test whether the proteolytic activity with tubular lysosomes was different from that in vesicular lysosomes; and how the lumenal pH and calcium were altered during lysosome tubulation. These aspects were not possible to study previously due to the lack of specific, targetable fluorescent probes that localized in the lumen of tubular lysosomes in live cells.

DNA based fluorescent reporters are ideally placed to compare tubular and vesicular lysosomes for several reasons. Firstly, there already exist reporters for lumenal pH, Ca^{2+}, Cl^{-}, enzymatic cleavage, RNS, ROS and physical cue like membrane potential in live cells and *in vivo*[34,70–79]. This due to several reasons. Secondly, DNA-based reporters are targetable to lysosomes with high precision. Thirdly, they are ratiometric; DNA reporters are made from equimolar concentrations of DNA strands containing the reporter fluorophore and a reference fluorophore; hence it is possible to have DNA reporter with a precise 1:1 ratio of reporter: reference fluorophores. The ratio of sensing to reference fluorophore corrects for heterogeneity due to cell uptake or inhomogeneous probe distribution. Lastly, the modular nature of DNA enables one to integrate multiple sensing modalities at appropriate distances to yield combination reporters.

Using the above concepts, I have designed and characterized three DNA based reporters outlined herein: a pH correctable Ca^{2+} sensor, Cathepsin C and B activity reporters and a DNA nanodevice denoted *Tudor*, that localizes in tubular lysosomes.

1.7 Outline of the thesis: Lysosomes are not just lytic bags but are signaling hubs performing multiple functions. Of both vesicular and tubular lysosomes, the latter are not very well studied despite its importance in organismal development as well as in immune defense. This thesis focuses on the characterization of *Tudor*, a unique tool to trigger the formation of tubular lysosomes, to differentiate tubular lysosomes from vesicular lysosomes with respect to its lumenal biochemistry and how the formation of tubular lysosomes enhances phagocytosis in macrophages.

Chapter 2: *Tudor* design, characterization and its specificity for tubular lysosome formation in various cell types will be discussed.

Chapter 3: Molecular mechanism of lysosome tubulation induced by *Tudor* in macrophages will be discussed.

Chapter 4: Proteolytic activity differences in tubular and vesicular lysosomes will be discussed.

Chapter 5: Lumenal pH and Ca^{2+} measurements within tubular and vesicular lysosomes will be discussed.

Chapter 6: The role of tubular lysosomes in promoting phagocytosis and phagolysosome formation will be discussed.

1.8 References

1. de Duve, C. The lysosome turns fifty. *Nat. Cell Biol.* **7,** 847–849 (2005).
2. Blobel, G. Christian de Duve (1917-2013). *Nature* **498,** 300 (2013).

3. De Duve, C., Pressman, B. C., Gianetto, R., Wattiaux, R. & Appelmans, F. Tissue fractionation studies. 6. Intracellular distribution patterns of enzymes in rat-liver tissue. *Biochem. J.* **60,** 604–617 (1955).

4. Sancak, Y. *et al.* The Rag GTPases bind raptor and mediate amino acid signaling to mTORC1. *Science* **320,** 1496–1501 (2008).

5. Sardiello, M. *et al.* A gene network regulating lysosomal biogenesis and function. *Science* **325,** 473–477 (2009).

6. Settembre, C. *et al.* TFEB links autophagy to lysosomal biogenesis. *Science* **332,** 1429–1433 (2011).

7. Savini, M., Zhao, Q. & Wang, M. C. Lysosomes: signaling hubs for metabolic sensing and longevity. *Trends Cell Biol.* **29,** 876–887 (2019).

8. Hesketh, G. G., Wartosch, L., Davis, L. J., Bright, N. A. & Luzio, J. P. The lysosome and intracellular signalling. *Prog Mol Subcell Biol* **57,** 151–180 (2018).

9. Inpanathan, S. & Botelho, R. J. The lysosome signaling platform: adapting with the times. *Front. Cell Dev. Biol.* **7,** 113 (2019).

10. Lawrence, R. E. & Zoncu, R. The lysosome as a cellular centre for signalling, metabolism and quality control. *Nat. Cell Biol.* **21,** 133–142 (2019).

11. Wang, S. *et al.* Metabolism. Lysosomal amino acid transporter SLC38A9 signals arginine sufficiency to mTORC1. *Science* **347,** 188–194 (2015).

12. Saxton, R. A., Chantranupong, L., Knockenhauer, K. E., Schwartz, T. U. & Sabatini, D. M. Mechanism of arginine sensing by CASTOR1 upstream of mTORC1. *Nature* **536,** 229–233 (2016).

13. Rebsamen, M. *et al.* SLC38A9 is a component of the lysosomal amino acid sensing machinery that controls mTORC1. *Nature* **519,** 477–481 (2015).

14. Chantranupong, L. *et al.* The CASTOR Proteins Are Arginine Sensors for the mTORC1 Pathway. *Cell* **165,** 153–164 (2016).

15. Lawrence, R. E. *et al.* A nutrient-induced affinity switch controls mTORC1 activation by its Rag GTPase-Ragulator lysosomal scaffold. *Nat. Cell Biol.* **20,** 1052–1063 (2018).

16. Castellano, B. M. *et al.* Lysosomal cholesterol activates mTORC1 via an SLC38A9-Niemann-Pick C1 signaling complex. *Science* **355,** 1306–1311 (2017).

17. Zoncu, R. *et al.* mTORC1 senses lysosomal amino acids through an inside-out mechanism that requires the vacuolar H(+)-ATPase. *Science* **334,** 678–683 (2011).

18. Lim, C.-Y. & Zoncu, R. The lysosome as a command-and-control center for cellular metabolism. *J. Cell Biol.* **214,** 653–664 (2016).

19. Perera, R. M. & Zoncu, R. The lysosome as a regulatory hub. *Annu. Rev. Cell Dev. Biol.* **32,** 223–253 (2016).

20. Shin, H. R. & Zoncu, R. The lysosome at the intersection of cellular growth and destruction. *Dev. Cell* **54,** 226–238 (2020).

21. Zhang, Y.-L. *et al.* AMP as a low-energy charge signal autonomously initiates assembly of AXIN-AMPK-LKB1 complex for AMPK activation. *Cell Metab.* **18,** 546–555 (2013).

22. Zhang, C.-S. *et al.* The lysosomal v-ATPase-Ragulator complex is a common activator for AMPK and mTORC1, acting as a switch between catabolism and anabolism. *Cell Metab.* **20,** 526–540 (2014).

23. Shaw, R. J. LKB1 and AMP-activated protein kinase control of mTOR signalling and growth. *Acta Physiol (Oxf)* **196,** 65–80 (2009).

24. Inoki, K., Zhu, T. & Guan, K.-L. TSC2 mediates cellular energy response to control cell growth and survival. *Cell* **115,** 577–590 (2003).

25. Inoki, K., Kim, J. & Guan, K.-L. AMPK and mTOR in cellular energy homeostasis and drug targets. *Annu. Rev. Pharmacol. Toxicol.* **52,** 381–400 (2012).

26. Gwinn, D. M. *et al.* AMPK phosphorylation of raptor mediates a metabolic checkpoint. *Mol. Cell* **30,** 214–226 (2008).

27. Paul, M. D. & Hristova, K. The RTK interactome: overview and perspective on RTK heterointeractions. *Chem. Rev.* **119,** 5881–5921 (2019).

28. Lemmon, M. A. & Schlessinger, J. Cell signaling by receptor tyrosine kinases. *Cell* **141,** 1117–1134 (2010).

29. Castellano, E. & Downward, J. RAS Interaction with PI3K: More Than Just Another Effector Pathway. *Genes Cancer* **2,** 261–274 (2011).

30. Blott, E. J. & Griffiths, G. M. Secretory lysosomes. *Nat. Rev. Mol. Cell Biol.* **3,** 122–131 (2002).

31. Johnson, D. E., Ostrowski, P., Jaumouillé, V. & Grinstein, S. The position of lysosomes within the cell determines their luminal pH. *J. Cell Biol.* **212,** 677–692 (2016).

32. Mindell, J. A. Lysosomal acidification mechanisms. *Annu. Rev. Physiol.* **74,** 69–86 (2012).

33. Xu, H. & Ren, D. Lysosomal physiology. *Annu. Rev. Physiol.* **77,** 57–80 (2015).

34. Narayanaswamy, N. *et al.* A pH-correctable, DNA-based fluorescent reporter for organellar calcium. *Nat. Methods* **16,** 95–102 (2019).

35. Morgan, A. J., Platt, F. M., Lloyd-Evans, E. & Galione, A. Molecular mechanisms of endolysosomal Ca2+ signalling in health and disease. *Biochem. J.* **439,** 349–374 (2011).

36. Feng, X. & Yang, J. Lysosomal calcium in neurodegeneration. *Messenger (Los Angel)* **5,** 56–66 (2016).

37. Saffi, G. T. & Botelho, R. J. Lysosome fission: planning for an exit. *Trends Cell Biol.* **29,** 635–646 (2019).

38. Li, P., Gu, M. & Xu, H. Lysosomal ion channels as decoders of cellular signals. *Trends Biochem. Sci.* **44,** 110–124 (2019).

39. Ballabio, A. & Bonifacino, J. S. Lysosomes as dynamic regulators of cell and organismal homeostasis. *Nat. Rev. Mol. Cell Biol.* **21,** 101–118 (2020).

40. Todkar, K., Ilamathi, H. S. & Germain, M. Mitochondria and lysosomes: discovering bonds. *Front. Cell Dev. Biol.* **5,** 106 (2017).

41. Lu, M. e*t al.* The structure and global distribution of the endoplasmic reticulum network are actively regulated by lysosomes. S*ci. Adv.* 6**,** (2020).

42. Swanson, J., Bushnell, A. & Silverstein, S. C. Tubular lysosome morphology and distribution within macrophages depend on the integrity of cytoplasmic microtubules. *Proc. Natl. Acad. Sci. USA* **84,** 1921–1925 (1987).

43. Saric, A. *et al.* mTOR controls lysosome tubulation and antigen presentation in macrophages and dendritic cells. *Mol. Biol. Cell* **27,** 321–333 (2016).

44. Johnson, A. E., Shu, H., Hauswirth, A. G., Tong, A. & Davis, G. W. VCP-dependent muscle degeneration is linked to defects in a dynamic tubular lysosomal network in vivo. *Elife* **4,** (2015).

45. Hipolito, V. E. B. *et al.* Enhanced translation expands the endo-lysosome size and promotes antigen presentation during phagocyte activation. *PLoS Biol.* **17,** e3000535 (2019).

46. Mrakovic, A., Kay, J. G., Furuya, W., Brumell, J. H. & Botelho, R. J. Rab7 and Arl8 GTPases are necessary for lysosome tubulation in macrophages. *Traffic* 1**3,** 1667–1679 (2012).

47. Chow, A., Toomre, D., Garrett, W. & Mellman, I. Dendritic cell maturation triggers retrograde MHC class II transport from lysosomes to the plasma membrane. *Nature* **418,** 988–994 (2002).

48. Hipolito, V. E. B., Ospina-Escobar, E. & Botelho, R. J. Lysosome remodelling and adaptation during phagocyte activation. *Cell Microbiol.* **20,** (2018).

49. Vyas, J. M. *et al.* Tubulation of class II MHC compartments is microtubule dependent and involves multiple endolysosomal membrane proteins in primary dendritic cells. *J. Immunol.* **178,** 7199–7210 (2007).

50. Yu, L. *et al.* Termination of autophagy and reformation of lysosomes regulated by mTOR. N*ature* 4**65,** 942–946 (2010).

51. Li, X. *et al.* A molecular mechanism to regulate lysosome motility for lysosome positioning and tubulation. *Nat. Cell Biol.* **18,** 404–417 (2016).

52. Chen, Y. & Yu, L. Recent progress in autophagic lysosome reformation. *Traffic* **18,** 358–361 (2017).

53. Chen, Y. & Yu, L. Development of Research into Autophagic Lysosome Reformation. *Mol. Cells* **41,** 45–49 (2018).

54. Chen, Y. & Yu, L. Autophagic lysosome reformation. *Exp. Cell Res.* **319,** 142–146 (2013).

55. Ni, S. *et al.* Recent progress in aptamer discoveries and modifications for therapeutic applications. *ACS Appl. Mater. Interfaces* (2020). doi:10.1021/acsami.0c05750

56. Murakawa, T., Kiger, A. A., Sakamaki, Y., Fukuda, M. & Fujita, N. An Autophagy-Dependent Tubular Lysosomal Network Synchronizes Degradative Activity Required for Muscle Remodeling. *BioRxiv* (2020). doi:10.1101/2020.04.15.043075

57. Sun, Y. *et al.* Lysosome activity is modulated by multiple longevity pathways and is important for lifespan extension in C. elegans. *Elife* **9,** (2020).

58. Rong, Y. *et al.* Spinster is required for autophagic lysosome reformation and mTOR reactivation following starvation. *Proc. Natl. Acad. Sci. USA* **108,** 7826–7831 (2011).

59. Magalhaes, J. *et al.* Autophagic lysosome reformation dysfunction in glucocerebrosidase deficient cells: relevance to Parkinson disease. *Hum. Mol. Genet.* **25,** 3432–3445 (2016).

60. Miao, R., Li, M., Zhang, Q., Yang, C. & Wang, X. An ECM-to-Nucleus Signaling Pathway Activates Lysosomes for C. elegans Larval Development. *Dev. Cell* **52,** 21–37.e5 (2020).

61. Mantegazza, A. R. *et al.* TLR-dependent phagosome tubulation in dendritic cells promotes phagosome cross-talk to optimize MHC-II antigen presentation. *Proc. Natl. Acad. Sci. USA* **111,** 15508–15513 (2014).

62. Du, W. *et al.* Kinesin 1 drives autolysosome tubulation. *Dev. Cell* **37,** 326–336 (2016).

63. Pu, J. *et al.* BORC, a multisubunit complex that regulates lysosome positioning. *Dev. Cell* **33,** 176–188 (2015).

64. Nijman, H. W. *et al.* Antigen capture and major histocompatibility class II compartments of freshly isolated and cultured human blood dendritic cells. *J. Exp. Med.* **182,** 163–174 (1995).

65. Barois, N., de Saint-Vis, B., Lebecque, S., Geuze, H. J. & Kleijmeer, M. J. MHC class II compartments in human dendritic cells undergo profound structural changes upon activation. *Traffic* **3,** 894–905 (2002).

66. Kleijmeer, M. J., Morkowski, S., Griffith, J. M., Rudensky, A. Y. & Geuze, H. J. Major histocompatibility complex class II compartments in human and mouse B lymphoblasts represent conventional endocytic compartments. *J. Cell Biol.* **139,** 639–649 (1997).

67. Mantegazza, A. R., Magalhaes, J. G., Amigorena, S. & Marks, M. S. Presentation of phagocytosed antigens by MHC class I and II. *Traffic* **14,** 135–152 (2013).

68. Kleijmeer, M. *et al.* Reorganization of multivesicular bodies regulates MHC class II antigen presentation by dendritic cells. *J. Cell Biol.* **155,** 53–63 (2001).

69. Sun-Wada, G.-H., Tabata, H., Kawamura, N., Aoyama, M. & Wada, Y. Direct recruitment of H+-ATPase from lysosomes for phagosomal acidification. *J. Cell Sci.* **122,** 2504–2513 (2009).

70. Modi, S. *et al.* A DNA nanomachine that maps spatial and temporal pH changes inside living cells. *Nat. Nanotechnol.* **4,** 325–330 (2009).

71. Thekkan, S. *et al.* A DNA-based fluorescent reporter maps HOCl production in the maturing phagosome. *Nat. Chem. Biol.* **15,** 1165–1172 (2019).

72. Surana, S., Bhat, J. M., Koushika, S. P. & Krishnan, Y. An autonomous DNA nanomachine maps spatiotemporal pH changes in a multicellular living organism. *Nat. Commun.* **2,** 340 (2011).

73. Surana, S. & Krishnan, Y. A method to map spatiotemporal pH changes in a multicellular living organism using a DNA nanosensor. *Methods Mol. Biol.* **991,** 9–23 (2013).

74. Saha, S., Prakash, V., Halder, S., Chakraborty, K. & Krishnan, Y. A pH-independent DNA nanodevice for quantifying chloride transport in organelles of living cells. *Nat. Nanotechnol.* **10,** 645–651 (2015).

75. Leung, K., Chakraborty, K., Saminathan, A. & Krishnan, Y. A DNA nanomachine chemically resolves lysosomes in live cells. *Nat. Nanotechnol.* **14,** 176–183 (2019).

76. Veetil, A. T. *et al.* DNA-based fluorescent probes of NOS2 activity in live brains. *Proc. Natl. Acad. Sci. USA* **117,** 14694–14702 (2020).

77. Saminathan, A. *et al.* A DNA-based voltmeter for organelles. *Nat. Nanotechnol.* (2020). doi:10.1038/s41565-020-00784-1

78. Jani, M. S., Zou, J., Veetil, A. T. & Krishnan, Y. A DNA-based fluorescent probe maps NOS3 activity with subcellular spatial resolution. *Nat. Chem. Biol.* **16,** 660–666 (2020).

79. Chakraborty, K., Leung, K. & Krishnan, Y. High lumenal chloride in the lysosome is critical for lysosome function. *Elife* **6,** e28862 (2017).

Chapter 2. *Tudor* triggers tubular lysosome formation in mammalian cells

2.1 Introduction

Lysosomes are conventionally thought to be vesicular in morphology with diameters of 0.5 μm-1.0 μm. Under certain conditions, lysosomes can form extensive tubular networks with lengths ≥ 4 μm[1,2]. Tubular lysosomes are found in a myriad of cells. For example, immune stimulation with the gram-negative bacterial cell wall component, LPS, or NFκ-B activation with PMA triggers the formation of tubular lysosomes in immune cell lines, BMDM and BMDC[1–6]. In addition, during autophagy triggered by starvation, epithelial cells show tubules emanating from autolysosomes that give rise to proto-lysosomes, eventually maturing into nascent vesicular lysosomes (VL), a process called autophagic lysosomal reformation (ALR) [7–9]. Tubular lysosomes have also been found *in vivo* in model organisms, including the muscle cells of third instar larva of *D. melanogaster* and epidermal cells of the molting stage of *C. elegans*, where they play a crucial role in tissue remodeling during development[10–12]. Valosin Containing Protein (VCP) is crucial to maintain the dynamic nature and integrity of ALR-induced tubular lysosomes. Homozygous mutation of VCP in humans disrupts tubular lysosome formation, suggesting that loss of tubular lysosomes contributes to the pathogenesis of VCP-related degenerative diseases[13]. Tubular lysosomes in immune cells play a role in phagocytosis and antigen presentation. Tubular lysosomes are also constitutively present in cell types like CV1 cells and human monocyte derived macrophages (HMDM), but their function is yet to be discovered.

Studying tubular lysosomes has been difficult mainly because the cue which triggers tubulation of lysosomes also causes other physiological changes within the cells. For example, LPS along with inducing lysosome tubulation, also activates macrophages by changing its polarization into pro-inflammatory with cytokine production[14,15]. LPS can even trigger autophagy while stimulating the

immune response[16,17]. Therefore, with LPS or PMA stimulation, it is impossible to tease out the biology of tubular lysosomes without the effect of other parallel pathways directly or indirectly affecting tubular lysosomes. In order to study the biology of tubular lysosomes and its role in immune cells without perturbing the expression profile of macrophages, we have developed a DNA nanodevice called *Tudor. Tudor* triggers tubulation of lysosomes in cell lines and primary cells by interacting with surface localized Ku70/80 heterodimer proteins.

Ku proteins have diverse roles in genome integrity maintenance, telomerase maintenance, anti-apoptosis, gene regulation, cell signaling, immune response and cancer[18–21]. Ku70/80 heterodimers are predominantly found in the nucleus, where they perform non-homologous end-joining (NHEJ)-mediated DNA repair and chromosome maintenance. Ku70/80 brings about gene arrangement by variable (V), diversity (D) and joining (J) of gene segments by V(D)J recombination [22]. Although Ku70/80 heterodimers are present in the nucleus, they also localize to other cellular locations. Immunofluorescence has shown Ku70/80 on the plasma membrane in untransformed cells like erythrocyte progenitors, macrophages, endothelial cells, immune cells and several cancerous cells[22–25]. Structural/sequential analysis of this heterodimer has revealed the hydrophobic nature of the Ku70/80 dimer, suggesting that it may be an integral membrane protein[26]. Ku proteins also localize to membrane lipid rafts in addition to being present in the cytoplasm[27,28]. Ku proteins also act as receptors for various pathogens on the plasma membrane. For example, Ku80 acts as receptor for Human parvovirus B19 while Ku70 acts as receptor for gram negative bacteria and *Rickettsia conorii* which causes Mediterranean spotted fever [29–31]. Ku70 aids in extracellular matrix rearrangement needed for migration of cells by its proteolytic cleavage of pro-matrix metalloproteases 9 (MMP9) into mature MMP9[22]. In monocytes treated with monocyte colony stimulating factor (M-CSF), Ku proteins translocate through endocytic vesicles to the surface of

activated macrophages, which express elevated levels of IL-1β [25]. Autoantibodies for Ku heterodimers were found in sera of patients diagnosed with certain autoimmune diseases, such as systemic lupus erythematosus, Graves' disease and scleroderma[23,32].

Certain tumor cells have upregulated levels of Ku70/80 on their surface, helping in cancer adhesion, migration and invasion [24,33]. To target Ku70/80 for cancer therapy, two DNA aptamers, named SA43 and SA44, were developed to bind cell surface Ku70/80 heterodimer proteins with a dissociation constant (K_d) of 21 nM[34]. Since Ku70/80 proteins found on lipid rafts are also endocytosed, the SA43 aptamer acts as a ligand for Ku70/80 present on the cell surface and hence can be used to trace the endocytic path of Ku70/80 leading to lysosomes.

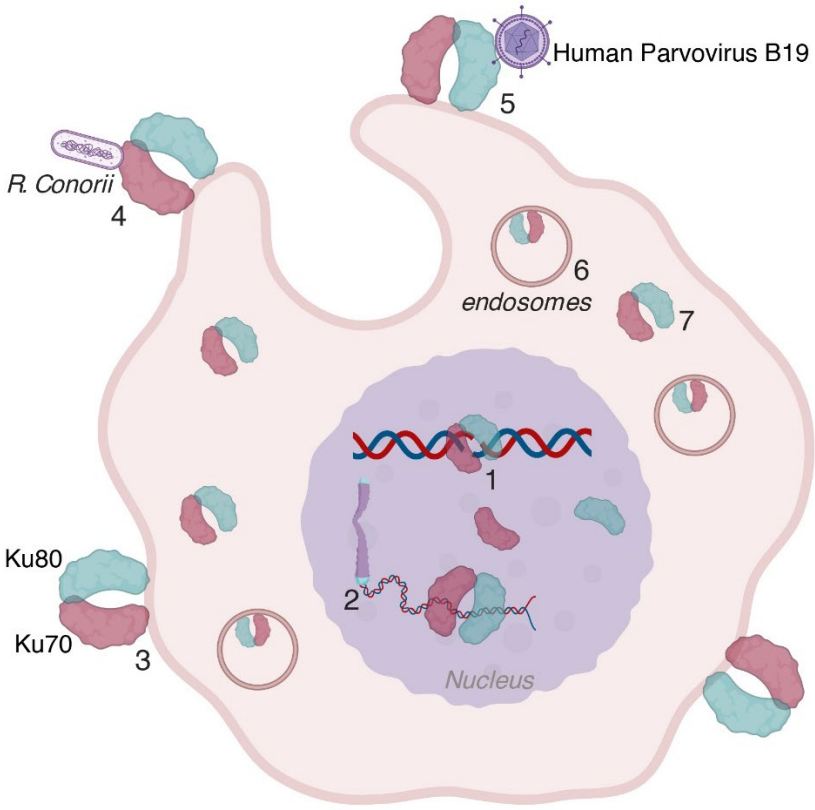

Figure II.1: Non-canonical roles of Ku70/80 heterodimer proteins in eukaryotic cells. Schematic of different localizations and functions of Ku70/80 in eukaryotic cells. (1) Ku70/80 heterodimer proteins along with DNA-Protein Kinase C (PKC), performs DNA double stranded break (DSB) repair by NHEJ and antigen receptor gene rearrangement by V(D)J recombination

Figure II.1, continued. needed for B and T cell development. (2) Chromosome maintenance by Ku70/80 interacting with telomeres to maintain telomere length. (3) Ku70/80 is found on the plasma membrane where it supports migration of cancerous and immune cells. (4 and 5) Ku 70/80 acts as receptors for pathogens and aid in its internalization. (6 and 7) Ku70/80 are found in endosomes including lysosomes and cytoplasm with unknown functions.

DNA aptamers are excellent tools for targeting, as their binding affinity to their cognate target proteins have affinities and specificities comparable to monoclonal antibodies. DNA aptamers have hence been used also to target drugs and DNA nanodevices to specific locations within cells[35–37]. The modular nature of the DNA scaffold makes it easy to incorporate multiple entities with completely different functions independent of each other. For example, aptamers can be fused to duplex (double stranded, ds) DNA to form a DNA nanodevice. The aptamer in this device can be a targeting moiety by acting as a ligand to a protein of choice, while the dsDNA acts as handle to attach fluorophores needed for its visualization within intracellular compartments. The versatile properties of DNA have also been leveraged for quantitative functional imaging in mammalian cells as well as in live organisms in real-time[36,38–50].

The modularity of DNA also enables one to incorporate an analyte-sensing module with an analyte-insensitive (normalizing) module with a precise stoichiometry in a single DNA nanodevice. The sensing module provides a readout of the analyte concentration, while the normalizing module provides ratiometric quantification. These DNA nanodevices can display ligands or functional DNA motifs that target them to specific organellar compartments or trigger signaling mechanisms. We therefore displayed the Ku aptamer SA43, on a DNA nanodevice denoted Tubular lysosome DNA reporter (*Tudor)*. *Tudor* tubulates lysosomes in several cell types, especially primary macrophages and macrophage cell lines, without activating them. Using *Tudor*, we were able to simultaneously stimulate the formation, visualize tubular lysosomes, and using

DNA based sensors to sense the lumenal biochemistry within both vesicular and tubular lysosomes.

2.2 Materials and methods

2.2a Reagents

All oligonucleotides were obtained from Integrated DNA Technologies (IDT, USA).

Sequence name	DNA sequence information (5'-3')
SA43	ACGTTACTCTTGCAACACAAACTTTAATAGCCTCTTATAGTTC
A1	ACGTTACTCTTGCAACACAAACTTTAATAGCCTCTTATAGTTCTT CATCAACACTGCACACCAGACAGCA
A1-Atto647N	ACGTTACTCTTGCAACACAAACTTTAATAGCCTCTTATAGTTCTT CA/A647/TCAACACTGCACACCAGACAGCA
A2	TGCTGTCTGGTGTGCAGTGTTGAT
A3	ATCAACACTGCACACCAGACAGCA
A2-A647N	Alexa 647-TGCTGTCTGGTGTGCAGTGTTGAT
TRG2	GGCTATAGCACATGGGTAAAACGACTTTGCT/Alexa 647/TGTCTGGTGTGCAGTGTTGAT
CpG	Atto 647-TGCTGTCTGGTGTGCAGTGTTGATTTccatgacgttcctgacgtt
ssDNA (B1)	ATCAACACTGCACACCAGACAGCAAGATCCTATATATAACTAC

Table 1: DNA sequences used in for *Tudor,* MUC1-dsDNA, CpG-dsDNA

MUC1-dsDNA	5-TRG2 aptamer linked to A2+A3
CpG-dsDNA	CpG strand linked to A2+ A3
dsDNA	A2 and A3
ssDNA	B1

Table 2: Combinations of DNA used in the study. (Refer Table 1 for sequences).

2.2b Formation of *Tudor*: All HPLC purified oligonucleotides (Table II.1) used to make *Tudor* were purchased from Integrated DNA Technologies (IDT, USA). All fluorophore labeled oligonucleotides were ethanol precipitated before using as per standard procedures. A2 oligonucleotide contained SA43 aptamer with a 3-mer linker followed by 24mer long ssDNA which is complementary to 24mer S1 oligonucleotide to form a dsDNA.

2.2c Annealing of DNA nanodevices: A1 and A2 oligos were mixed in 1:1 ratio to a final concentration of 20 μM in 20 mM Sodium Phosphate buffer (pH 7.2) containing 10 mM KCl and 10 mM $MgSO_4$. This DNA solution was annealed by heating it to 90 °C for 5 mins followed by cooling to RT over 3 hours at the rate of 5 °C/15 mins. The annealed DNA solution was equilibrated at 4 °C overnight before use. The formation of *Tudor* was confirmed by mobility shift assay in 12% native poly acrylamide gel electrophoresis (PAGE)[36,49]. Other DNA nanodevices (dsDNA, *CalipHluor 2.0*, *ImLy 2.0*) were annealed in 20 mM Sodium phosphate buffer, pH 7.2 with annealing protocol as mentioned above.

2.2d Gel electrophoresis (confirmation of formation of *Tudor)*: Gel mobility shift assay was used to confirm the formation of *Tudor*. *Tudor*[647] was used for this purpose, where 5-prime of A2 (24-mer) oligonucleotide was labeled with Alexa Fluor 647 for visualization. A1 and A2

oligonucleotide monomers were run alongside the fully formed *Tudor* in 10 % PAGE in 1X Tris Borate EDTA (TBE buffer) in 100 V.

2.2e Cell culture: Mammalian cell cultures. COS-7 and SIM-A9 cells were sourced from American Type Culture Conditions (ATCC). HepG2 cells, kind gift from Dr. Bryan Dickinson, Department of Chemistry, University of Chicago. RAW 264.7 macrophages, kind gift from Dr. Christine A. Petersen, Department of Epidemiology, College of Public Health, University of Iowa. J774A.1, a kind gift from Prof. Deborah Nelson, Department of Pharmacological and Physiological Sciences, University of Chicago.

COS-7, HepG2, RAW 264.7 and J774A.1 cells were cultured in Dulbecco's modified Eagles medium/F12 (1:1) (DMEM-F12) with 10% FBS as per protocol mentioned in ATCC. SIM-A9 was cultured in DMEM-F12 with 10% Fetal Bovine Serum (FBS) with 5 % Horse serum (Invitrogen co-operation, USA). DMEM Media were supplemented with 100 U/mL of penicillin, 100 µg/mL of streptomycin (Life Technologies).

Bone marrow-derived macrophage (BMDM) isolation and activation. Bone marrow stem cells were used to obtain BMDMs using L-cell conditioned media for six days as previously described protocol[51]. BMDMs were activated into M1 like macrophages by stimulation with LPS (5ng/mL, Sigma) and INFγ (12ng/mL, R&D Systems) for 24 hrs or M2 like macrophages by stimulation with 20ng/mL IL-4 for 48 hrs.

Adipose tissue-macrophages (ATM) isolation. Adipose tissue was minced and digested with 1mg/mL Type I collagenase in 1% BSA/PBS at 37°C shaker at 160 rpm for 40 minutes. The cell pellet was centrifuged, lysed with red blood cell lysis buffer, and passed through 40µm filter.

ATMs were isolated using CD11b microbeads (Miltenyi Biotec) as previously described[51], and purity was assessed by flow cytometry.

Thioglycolate-elicited peritoneal macrophage isolation. Protocol used to isolate peritoneal macrophages (P macs) is as previously described[52]. Briefly, peritoneal macrophages were isolated by lavaging the peritoneal cavity with PBS containing 2% endotoxin-free BSA 5 days after 4% thioglycolate injection (3 mL/mouse). Flow cytometry was used to assess the purity of obtained cells.

2.2f Uptake of *Tudor*

Competition assay with mBSA: RAW264.7 cells were incubated with 0 equivalents of mBSA for 30 mins in Opti-MEM before the treatment with *Tudor* or dsDNA, cells were then treated with 100 nM *Tudor* or dsDNA for 30 mins in Opti-MEM in presence of 30 equivalents of mBSA. Cells were washed with sterile 1X PBS. Cells were chased in culture medium containing mBSA for 1 hour. Those cells not treated with mBSA were pretreated Opti-MEM only followed by pulse and chase with *Tudor*/dsDNA.

Image analysis: Fiji was used for image analysis. Before comparing and quantification, all images were set to the same intensity values of minimum 0 and maximum 20640.

Competition assay with unlabeled Ku aptamer: RAW264.7 were treated with 60 equivalents of unlabeled Ku aptamer in Opti-MEM for 30 mins. Cells were then treated with 50 nM *Tudor* for 30 mins in Opti-MEM. Cells were washed with 1X PBS followed by chase for 1 hour in complete media containing unlabeled Ku aptamer. Only Opti-MEM were used for cells without Ku aptamer before treating them with *Tudor* and chased as mentioned above.

Image Analysis: Fiji was used for all image analysis. Before comparing and quantifications, all images were set to the same intensity values of minimum of 511 and maximum of 23308. Using the bright field image, an outline for each cell was drawn on plasma membrane based. This outline for each cells were used to quantify the total cell intensity for each cell which was plotted as whole cell intensity (WCI).

2.2g Lysosomal tubulation assay: Cells (cell lines: RAW 264.7, J774A.1, SIM A9, HepG2, and COS-7 cells); (Primary cells: ATMs; BMDM (M0, M1 and M2) and P macs (M0, M1 and M2) were treated with 0.5 mg/ mL TMR dextran for 1 hour followed by a chase of 16 hours in complete media unless otherwise mentioned. This was followed by treatment of 100 nM *Tudor* in culture media for 4 hours. Cells were then imaged by confocal microscope.

As positive control, cells were treated with LPS (100 ng/mL for at least 4 hours at 37 °C in culture media.

2.2h Fluorescence microscopy imaging: Microscopes used in these studies are as follows.

Widefield microscope: IX83 inverted widefield microscope (Olympus corporation of the Americas) was used. Objective used are 60x and 100x, 1.42 NA, phase contrast oil immersion objective (PLAPON, Olympus Corporation of the Americas). Detector is the Evolve Delta 512 EMCCD camera (Photometrics). Metamorph Premier Ver 7.8.12.0 (Molecular Devices) was used to control filter wheel, shutter, and charge-coupled device camera. The filters perfectly suitable for the fluorophores used during the course of this study.

Filters used to image Atto 647 channel were 640/30 band-pass excitation filter: 705/72 band-pass emission filter and 89016 dichroic. Filters used for TMR dextran and pHrodo^{TM} Red zymosan were 530/30 band pass excitation filter: 575/40 band pass emission filter and 49014 long pass dichroic filter. 300 ms exposure time and 300 EM Gain was used to acquire images in Alexa 488

channel while 100 ms exposure and 100 ms EM Gain were used to acquire images in channels, TMR dextran, pHrodo^{TM} red and Atto 647,

Confocal microscopy: The confocal microscope used in the study is Leica TCS SP5 II STED laser scanning confocal microscope (Leica Microsystems, Inc.). Laser lines used were Argon ion laser for 488-nm excitation, DPS laser for 564-nm excitation, He-Ne laser for 594-nm, 633-nm excitation. Objectives used was using HCX PIApo 63x/1.4 UV oil 0.14mm WD objective. Argon laser at 488 nm laser was used to excite ER Tracker^{TM} Green, Mito Tracker^{TM} Green, FITC dextran; DPSS laser at 561 nm was used to excite TMR dextran; Red HeNe laser 633 nm was used to excite Lyso Tracker^{TM} deep red, Atto 647N. Acousto-optical beam splitter (AOBS) was used to filter all emission signals with suitable settings for each fluorophore. hybrid detectors (HyD) were used for recording all images.

2.2i Colocalization studies

Mitotracker and ER tracker with tubular lysosomes: 10 kDa TMR dextran (0.5 mg/ml) was used to mark all lysosomes in RAW 264.7 macrophages. Lysosomal tubulation was stimulated in these cell line using 100 nM *Tudor* for 4 hours at 37° C. This was followed by treatment of either 200 nM Mitotracker green or 50 nM ER tracker in HBSS for 15-20 mins. Cells were washed using HBSS and imaged in Leica TCS SP5 II STED laser scanning confocal microscope.

2.2j Analysis of tubular lysosomes using Tubeness

Quantification of Tubular lysosomes: The Tubeness plugin of Fiji was used to identify and quantify any tubular structures in the cell images (ref). The image was then thresholded in Fiji. A Feret value of 0-10 is used to identify tubular structures between 0-10 μM in length. A circularity of 0-0.5 was used to identify tubular structures and a circularity of 0-1 was used to identify all lysosomes. Analyze Particles in Fiji was used with the above-mentioned parameters to display the

results of all lysosomes analyzed in a cell. Lysosomes of Feret length ≥ 4.0 μm were considered to be tubular lysosomes.

Analysis: % tubular lysosomes (TL) per cell was done as indicated: Number of TLs (≥ 4.0 μm) were counted as a percentage of all lysosomes. The number of TLs were divided by the total number of lysosomes, and percentage TLs per cell was calculated.

% Area of TLs per cell: Area of TLs and VLs was measured using Analyze Particles in Fiji as described above. Mean area of TLs was divided by mean area of total lysosomes for each cell and percentage of mean area of TLs for each cell was calculated. The mean percentage area of TL was plotted using origin software.

2.2k Immunofluorescence studies

Labeling of Ku70 on plasma membrane: Cells used for this assay as RAW, SIM A9, J774 A.1, Hep G2, COS 7 cell lines, BMDM (M0, M1 and M2) and P macs (M0, M1 and M2). The similar protocol was followed for each cell types mentioned above where primary cells were fixed with 2% PFA for 10 mins on ice and washed 3 times with ice cold 1X PBS. 1% BSA with 0.3 M Glycine in 1X PBS was used as blocking agent for 30 mins, RT. Cells were then incubated with Ku70 antibody (100X) (Novus Biologicals) in above mentioned blocking buffer for 1 hour, RT. Cells were washed in 1X PBS, 3 times followed by secondary antibody (1000X) incubation in above mentioned blocking buffer for 30 mins, RT. Cells were again washing in 1X PBS, 3 times. Cells were imaged on the Leica SP5 confocal microscope.

2.3 Results and discussion

2.3a *Tudor* formation and its characterization

Tudor (**Tu**bular lysosome **D**NA **r**ep**or**ter) is a DNA nanodevice which tubulates lysosomes in a wide variety of macrophages through a new signaling pathway. This DNA nanodevice is made of A1 and A2 strands comprising a 43-base long DNA aptamer (SA43) raised against Ku70/80 which is attached to a 24-basepair long ds DNA (Figure. II.2 and Table. II.1 and Table. II.2). The formation of *Tudor* was confirmed by gel shift assay[36,42,49,53].

A1 is a 24mer oligonucleotide containing the Alexa 647N for visualization of the nanodevice within the intracellular compartments. A2 comprises SA43 followed by a short 3-mer linker into a 24mer oligonucleotide complementary to A1. A1 (lane 1) is smaller in length, so it showed a lower mobility shift compared to A2 (lane 2) as shown in EtBr-stained gel. The formation of *Tudor* was further confirmed by imaging the gel in Alexa 647 channel.

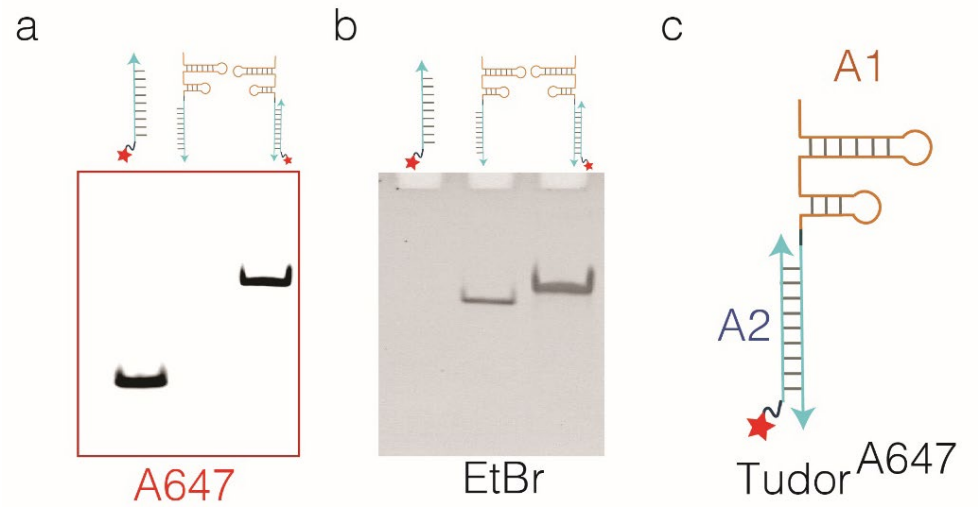

Figure II.2: Formation of *Tudor* confirmed by gel mobility shift assay. (a) and (b) 10% native PAGE showing formation of *Tudor*: lane 1: A1 strand with Alexa 647N; Lane 2: A2 strand and Lane 3: $Tudor^{A647}$ in EtBr and Alexa 647 channels respectively. (c) Schematic of $Tudor^{A647}$.

2.3b Uptake pathway for *Tudor*

The negative backbone DNA is a well-known ligand for scavenger receptors (SR), leading to uptake of DNA into lysosomes by receptor mediated endocytosis[36,46,54]. Since *Tudor* is a DNA nanodevice, we studied the mode of uptake of *Tudor* in macrophages by a competition assay. In this assay, macrophages were pretreated with 60 eq of specific Ku 70/80 DNA aptamer (SA43) containing no fluorophore (unlabeled) for 30 mins followed by treatment of Alexa 647N labeled *Tudor* in presence of unlabeled SA43 for 30 mins. *Tudor* showed uptake only in the absence of excess SA43, suggesting that *Tudor* uptake occurs by binding to Ku70/80 on cell surface. It is not taken up via anionic ligand binding receptor (ALBR) mediated endocytosis, as revealed by competition experiments with maleylated BSA (mBSA). dsDNA on the other hand shows efficient uptake in cells and the uptake of DNA is abolished in the presence of 60 eq excess mBSA (Figure II.3).

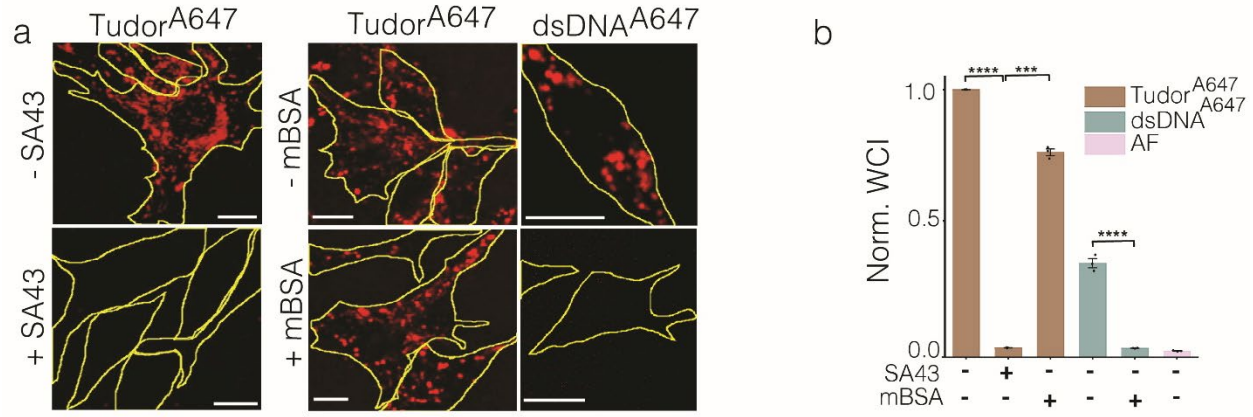

Figure II.3: Uptake of *Tudor*^{A647} in macrophages. (**a**) Representative images of RAW 264.7 cells showing uptake of *Tudor*^{A647} in the presence of unlabeled SA43 aptamer and maleylated BSA. (**b**) Quantification showing the normalized whole cell intensity (WCI) of (a) upon mentioned conditions (n=100 cells). ***P< 0.0005; *P< 0. 05; (one-way ANOVA with Tukey *post hoc* test). Experiments were performed in triplicate with similar results. Error bars indicate the mean of three independent experiments ± s.e.m. Scale bar, 10 μm.

2.3c: Plasma membrane labeling of Ku proteins

Ku70/80 proteins are present on the plasma membrane, in addition to being present predominantly in the nucleus in several cancerous cells and circulating macrophages. Surface labeling of Ku70 by immunofluorescence without permeabilization showed the presence of Ku70 on the surface of cell lines like RAW 264.7, J774A.1 and SIM A9.1, and stimulated murine BMDMs into M0, M1 and M2 macrophages, suggesting that Ku70/80 proteins might play a significant role in internalization and promoting tubular lysosome formation (Figure II.4).

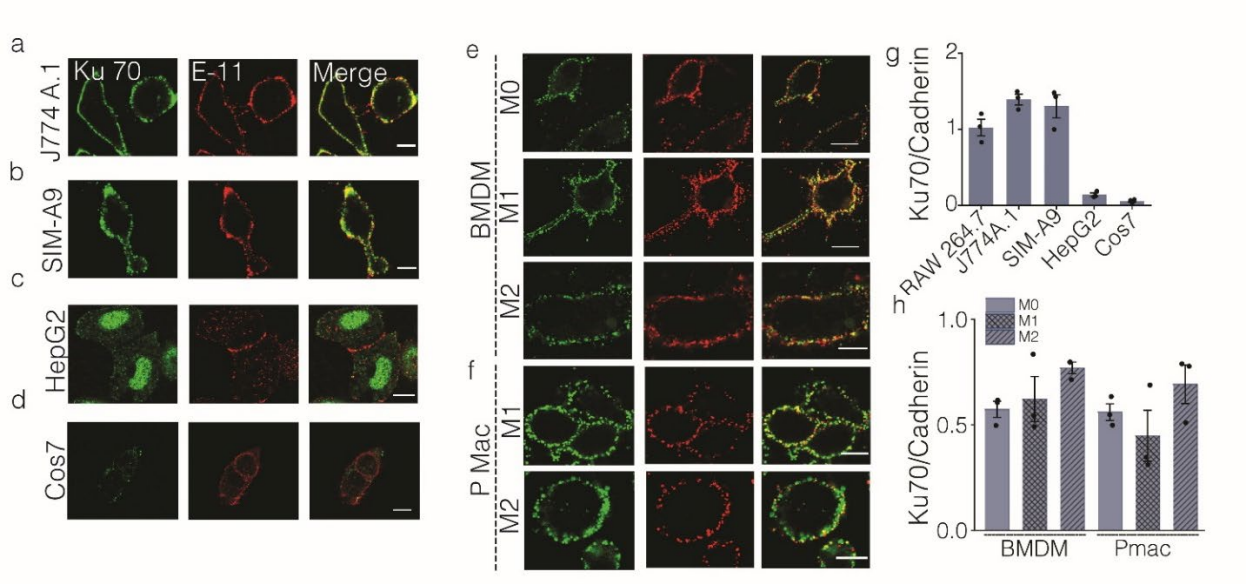

Figure II.4: Ku70 localizes on the plasma membrane of various cell lines and primary macrophages. (a-f) Representative images showing colocalization of Ku70 (green) with Pan Cadherin (E-11, red) in (a) J774A.1; (b) SIM A9; (c) HepG2; (d) COS-7; (e) naïve (M0), LPS/INF-γ activated- (M1), or IL4-activated (M2) BMDM and (f) naïve (M0), LPS/INF-γ activated- (M1), or IL4-activated (M2) Pmac, Scale bar = 10 μm. (**g** and **h**) Normalized intensity ratio of Ku70/Pan Cadherin for each indicated cell types. Data represents three independent experiments shown here (n=50 cells). Error bars represent standard error of mean (s.e.m) from three independent experiments.

2.3d Lysosomal tubulation and its quantification

Tudor triggered tubulation of lysosomes in diverse cell lines such as RAW 264.7, J774A.1, SIM A9 cell lines. While cell lines like HepG2 and COS-7 also showed tubular lysosome formation in presence of *Tudor* but the extent of lysosomal tubulation in these cells were lower than macrophages (Figure II.5). This was consistent with the fact that Ku70 expression on the plasma membrane of macrophage cells lines was higher than on HepG2 and COS-7 cells (Figure. II.4).

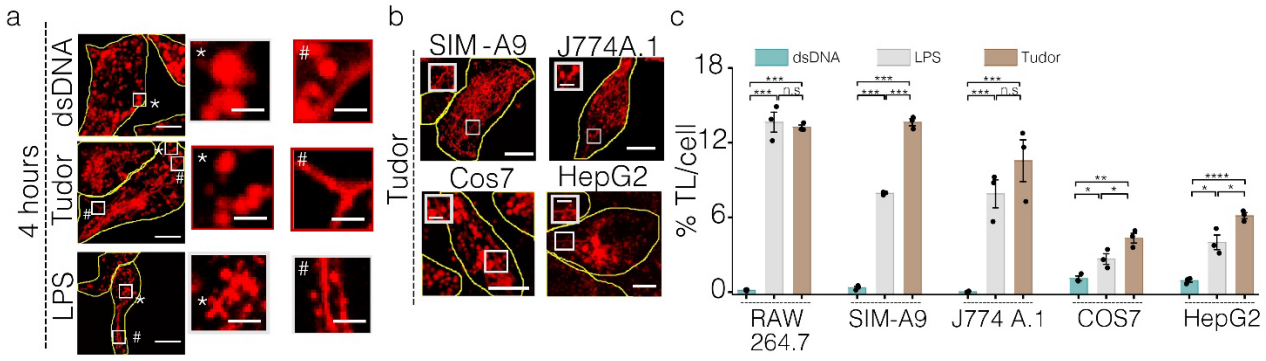

Figure II.5: *Tudor* triggers tubulation of lysosomes in various cell lines. (a) Representative images of RAW 264.7 with lysosomes marked with TMR dextran followed by treatment of dsDNA, *Tudor* and LPS with zoomed region of white box on the right. (b) Representative images of cells lines mentioned showing TMR dextran in presence of *Tudor*. (c) % TLs per cells quantified for (a) and (b) (n=20 cells per experiment). ***P< 0.0005; **P< 0.005 (one-way ANOVA with Tukey *post hoc* test). n.s: non-significant. Experiments repeated atleast three times with similar results. Error bars represents s.e.m. Scale bar: 10 µm and inset scare bars: 4 µm.

2.3d.1 *Tudor* enhances tubular lysosome formation in primary murine macrophages.

Ku70/80 heterodimer proteins are found on the plasma membrane of primary cells like monocyte derived macrophages and other macrophages like THP-1 and HL-60[22]. Although the presence of Ku70/80 on Peritoneal macrophages (P macs) was not known earlier, our experiments show the presence of Ku70/80 proteins on the plasma membrane of P macs (Fig. II.4f). Tubular lysosomes were also identified in primary macrophages like BMDM and BMDCs[2,3]. M1 and M2

macrophages from BMDM and P mac both showed comparable levels of tubulation in presence of either dsDNA, LPS and *Tudor*. M0 macrophages showed significant levels of tubular lysosomes in presence of LPS and *Tudor* as compared to dsDNA (Figure II.6 a, b, d). Similar trends were seen in Adipose Tissue Macrophages (ATMs) (Figure II.6 c, d). These experiments demonstrated that *Tudor* tubulated lysosomes in cell lines as well as enhanced lysosomal tubulation in naïve, unpolarized macrophages from diverse sources.

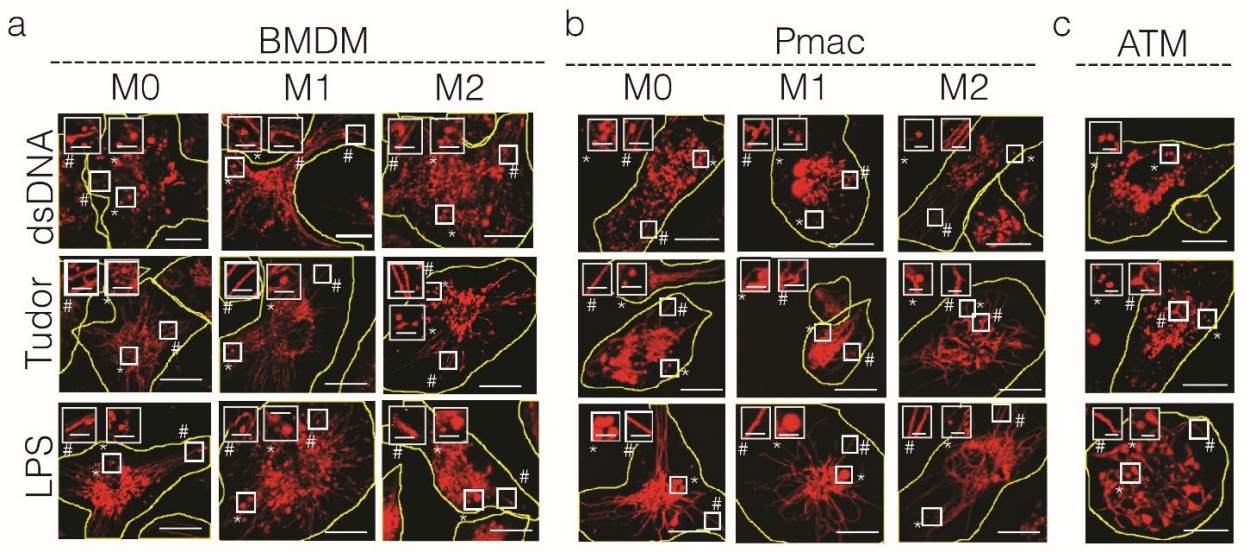

Figure. II.6: Tudor enhances tubulation of lysosomes in primary macrophages.

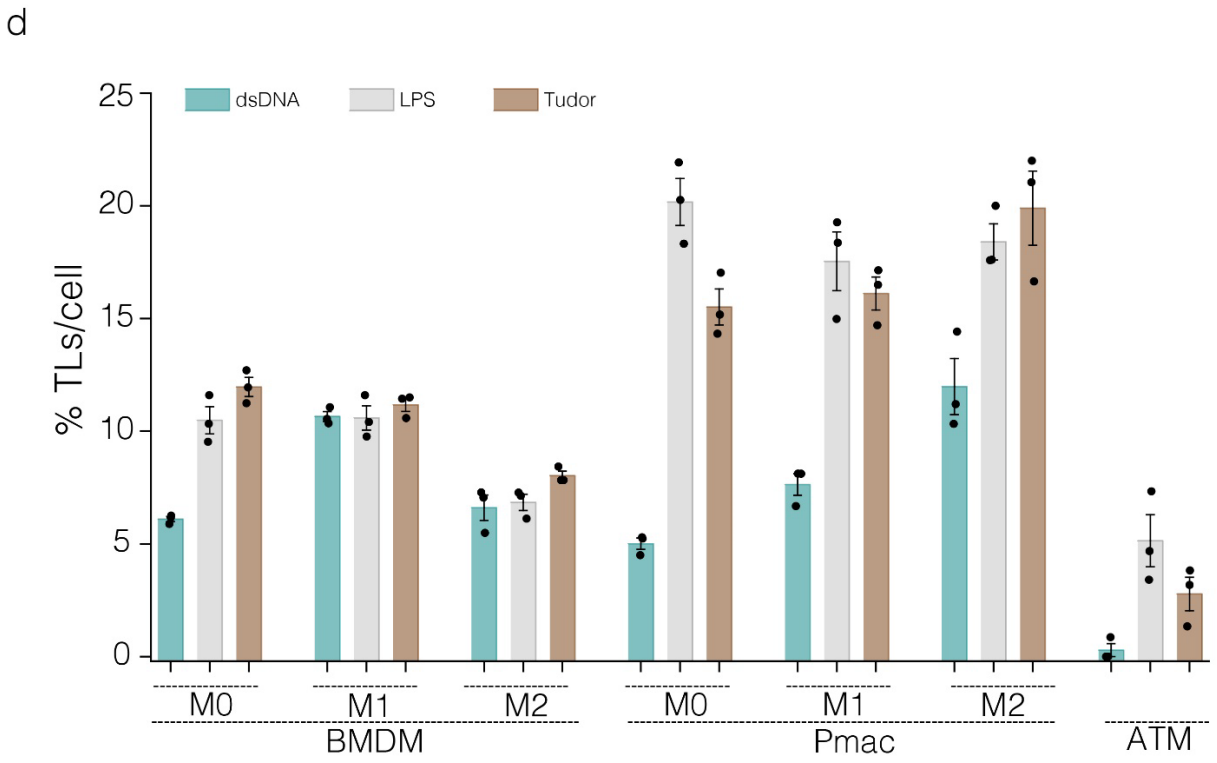

Figure. II.6, continued. *Tudor* enhances tubulation of lysosomes in primary macrophages. (**a-c**) Representative images of TMR dextran labeled lysosomes of M0, M1 and M2 of BMDM (a), Pmacs (b) and ATM (c) either untreated or in presence of dsDNA, LPS and *Tudor*. (**d**) %TLs per cell quantification shown for (a, b and c). (n= 50 cells), Scale bar: 10 µm and inset scare bars: 4 µm. Experiments repeated atleast three times with similar results. Error bars represent s.e.m. ***P< 0.0005; **P< 0.005 (one-way ANOVA with Tukey *post hoc* test). n.s: non-significant.

2.3d.2 Analysis and quantification of tubular lysosomes

Tubeness plugin in Fiji was used to analyze curvilinear structures previously[55–57]. Hence Tubeness was also used to identify and quantify Tubular lysosomes. A raw image of SIM A9 cell is shown here where lysosomes in these cells were marked with TMR dextran followed by treatment with *Tudor* for tubulation of lysosomes. The fluorescence confocal image was separated from its brightfield image and background subtracted. The Tubeness filter was applied using the default sigma value on the background subtracted image. Tubeness filter highlights all structures.

This image was then converted into a binary image by thresholding where the pixel intensity of white is 0 [minimum] and black is 255 [maximum]. After Tubeness was applied, Analyze Particles was selected based on 2 parameters: circularity and feret length. Circularity ranges between 0 representing elongated organelles (tubular lysosomes) and 1 being a circle (vesicular lysosomes). Hence circularity range of 0.0 to 0.5 was used. Feret length range between 1-20 µm was used to cover all curvi-linear structures ranging between 1-20 µm. Analyze Particle feature was used to generate a report in the output box containing details of vesicular and tubular lysosomes which includes the area within vesicular and tubular lysosomes, feret distance etc. Any lysosome ≥ 4 µm long was considered as a tubular lysosomes and used for statistical analysis[1,2]. Using the above information, the magnitude of *Tudor*-mediated tubular lysosomes formation across different cell types was analyzed in three different methods, i. % TLs per cell, ii. % area of TLs and iii. number of TLs per cell (Figure II.7).

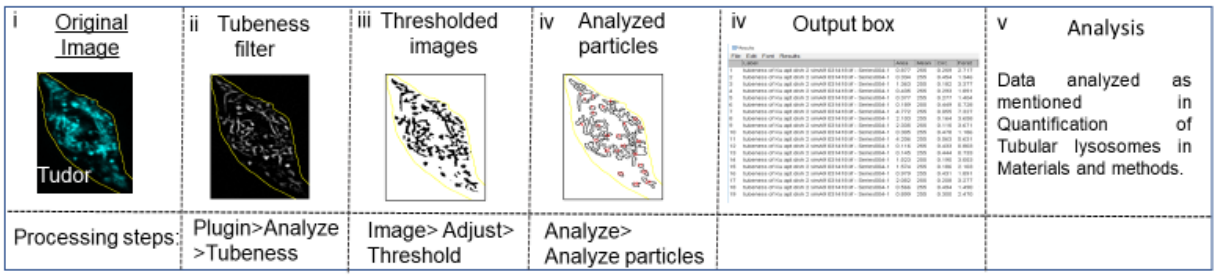

Figure II.7: Image analysis framework for quantification of tubular lysosomes. (i) Fluorescent images of *Tudor* treated cells were background subtracted. (ii) The image was subjected to Tubeness filter which highlights all curvilinear structures. (iii) Raw image in (ii) was then converted into a binary image by thresholding (0, 255). (iv) The image in (iii) was used to find all structures (VLs and TLs) using analyze particles in Fiji based on two parameters: Feret values (0-10) and circularity (range:0.0-0.5). (v) Tubular structures ≥4 µm only are considered for statistical analysis and quantification. (vi) The data obtained were analyzed in multiple methods, %TLs per cells, Number of TLs per cell, % Area of TLs per cell.

2.3e Tubular lysosomes do not colocalize with ER and Mitochondria

Here, we confirm that tubular structures triggered by *Tudor* are not the endoplasmic reticulum (ER) or mitochondria in Raw 264.7 and BMDMs. Lysosomes in these cells were prelabeled with 10 kDa TMR-dextran where cells were incubated with TMR-dextran for 1 hour (which is referred to as pulse) and chased for 16 hours such that the TMR-dextran marked all the lysosomes in the cells. Cells were then treated with *Tudor* to tubulate lysosomes. Cells were then labeled with either endoplasmic reticulum (ER) tracker, Mitotracker or Lysotracker (Figure. II.8). Tubular structures triggered by *Tudor* showed no colocalization with either ER tracker or Mitotracker, but did so with Lysotracker, suggesting that the tubular organelles could be lysosomes.

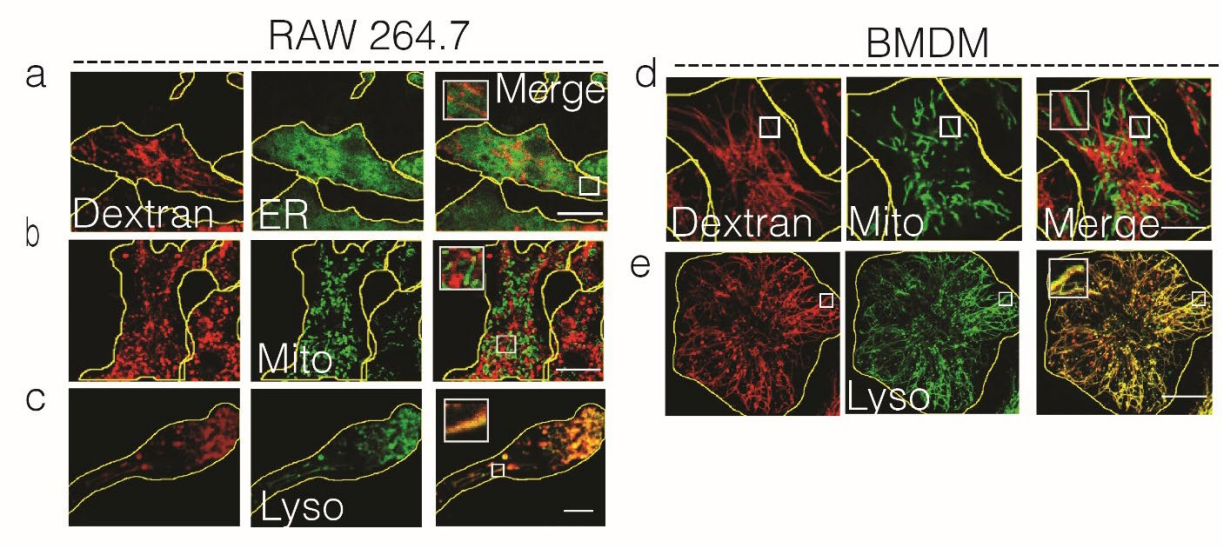

Figure. II.8: *Tudor* triggered tubular lysosomes do not colocalize with Endoplasmic reticulum or Mitochondria. (a-e) Representative confocal images showing lysosomes marked with TMR dextran [red] and organellar marker (for ER: ER tracker; mitochondria (Mito): Mitotracker; lysosomes (Lyso): Lysotracker) [green] and merge [yellow] shown for RAW 264.7 (a-c) and BMDN (d and e) with zoomed region for white box shown as inset. All independent experiments were repeated at least three times with similar results. Scale bar = 10 μm.

2.3f: SA43 aptamer in *Tudor* triggers tubulation of lysosomes

To show that the SA43 aptamer triggers tubulation of lysosomes, we compare tubulation in cells treated with other similar DNA nanodevices. MUC1-dsDNA is a DNA nanodevice that incorporates 5-TRG2[38], a DNA aptamer which binds to hypo-glycosylated MUC-1 protein (*Kd*: 18 nM). The latter upregulated on the plasma membrane of certain cancer cells[58]. CpG-ODN, a TLR-9 ligand, can trigger innate immune response in mammalian cellst[59]. Briefly, 5-TRG2 aptamer is fused to 24mer DNA (A2) through a short 3-nt linker. 5-TRG2 fused to the A2 strand along with its complementary A3 strand forms MUC1-dsDNA. CpG-dsDNA was also adopted from prior work where the CpG strand is linked via short 3-nt linker to 24mer (A2) oligonucleotide which is complementary to A3 strand forming CpG-dsDNA[50]. CpG-dsDNA is visualized by Alexa 647N present on A2 strand while MUC1-dsDNA was visualized by Alexa 647N present on A2 strand. *Tudor*, MUC1-dsDNA and CpG-dsDNA have a similar design where a single functional overhang (aptamer) is displayed on a dsDNA module of identical length and sequence. RAW264.7 were treated with either MUC1-dsDNA, CpG-dsDNA, SA43 aptamer or *Tudor* for 4 hours. SA43 and *Tudor* treated cells showed significantly higher lysosomal tubulation than MUC1-dsDNA and CpG-dsDNA treated cells, suggesting lysosome tubulation is specifically induced by the SA43 aptamer in *Tudor* (Figure II.9).

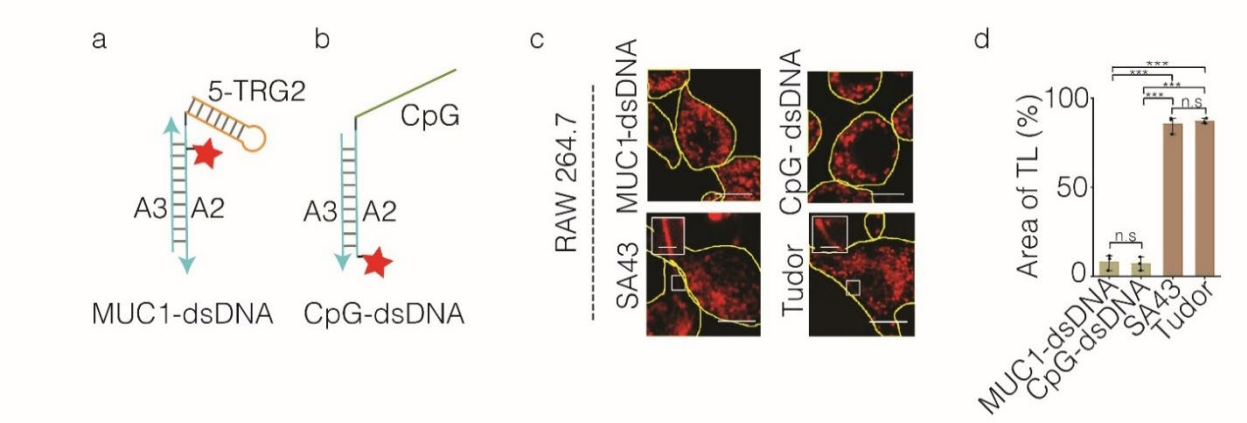

Figure II.9: *Tudor* triggers tubulation of lysosomes in macrophage cell lines. (**a** and **b**) Schematic of MUC1-dsDNA consisting of 5-TRG2 fused to A2 DNA which is complementary to A3 and CpG-dsDNA where CpG strand is fused to A2 DNA complementary to A3. (c) Representative confocal images of RAW 264.7 in presence of MUC1-dsDNA, CpG-dsDNA, SA43 aptamer and *Tudor*. Scale bar: 10 µm, inset scale bar: 4 µm. (d) Quantification showing % Area of TLs plotted for RAW 264.7 in indicated ligands. Error bars represent s.e.m from 3 independent experiments, (n= 20 cells per experiment); ***P< 0.0005; **P< 0.005 (one-way ANOVA with Tukey *post hoc* test). n.s: non-significant.

2.3f.1 Specificity of *Tudor* in triggering tubulation of lysosomes

Tudor consists of a 43-nt long ssDNA SA43 aptamer and a 24-mer long dsDNA. In order to interrogate the role of each motif in *Tudor* in lysosome tubulation, we used a 43-nucleotide long ssDNA of different sequences with the same GC content as SA43 aptamer and 24mer dsDNA sequence and size similar to that used in *Tudor*. This experiment revealed that neither ssDNA nor dsDNA triggered tubulation even at 8 hours suggesting that the tubulation of lysosomes is triggered by *Tudor* and is not non-specific (Figure II.10).

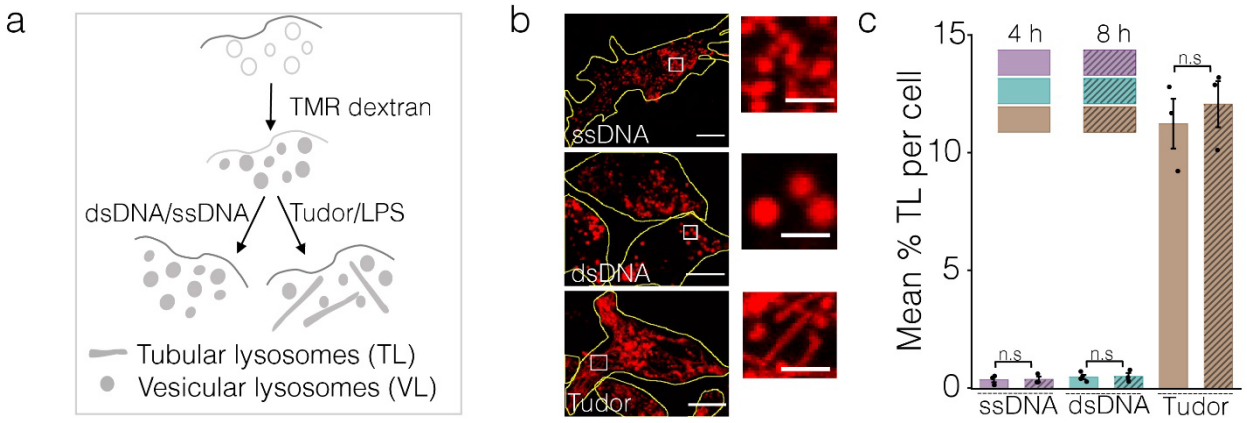

Figure II.10: Specificity of *Tudor* in triggering tubulation of lysosomes. (**a**) Schematic of lysosomal tubulation assay (**b**) Representative images of TMR-dextran labeled lysosomes of RAW 264.7 upon treatment with ssDNA; dsDNA and *Tudor*. Inset: Magnified images of VLs and TLs on the right. (**c**) Quantification of (b) as % TLs per cell 4 and 8 hours of treatment (n = 25 cells). n.s: non-significant; ****P*< 0.0005; **P< 0.005; *P< 0.05 (one-way ANOVA with Tukey *post hoc* test). Error bars represent standard error of mean (s.e.m) for all experiments shown here. Data represented from at least 3 independent experiments. Scale bar: 10 µm and inset scale bar: 4 µm.

2.3g *Tudor* does not change the polarization of macrophages

LPS, a well-known ligand of TLR4, also tubulates lysosomes and polarizes M0 macrophages into M1-like macrophages. LPS-treated macrophages express higher levels of IL-1β, and TNF-α, which are classic M1 macrophage markers [60,61]. In order to check if *Tudor* also polarized naïve M0 macrophages into M1 or M2 like macrophages, murine M0 macrophages of BMDM and Pmacs were treated with 100 nM *Tudor* over 24 hours. This was followed by M1 and M2 marker gene analysis performed by qRT PCR. Briefly, *Tudor* treatment did not alter the polarization of M0 macrophages into either M1 and M2 in both BMDM and Pmacs (Figure II. 11-12).

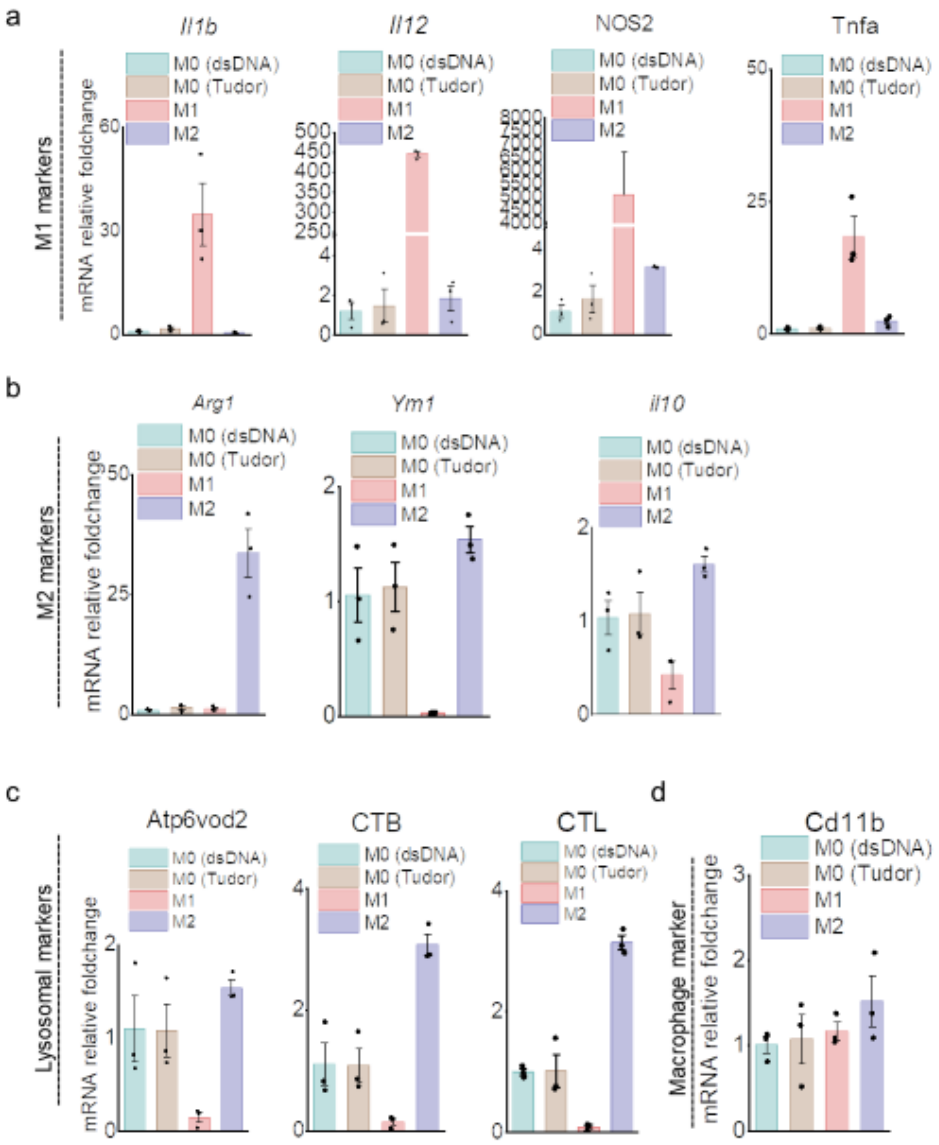

Figure II.11: *Tudor* does not alter polarization states of BMDM macrophages. (a-d) Expression levels of M1(a) and M2 (b) lysosomal genes (c) and macrophage marker (d) genes shown in BMDM (M0) upon dsDNA and *Tudor* treatment. All error bars represent standard error of mean (s.e.m) from three independent experiments with similar results.

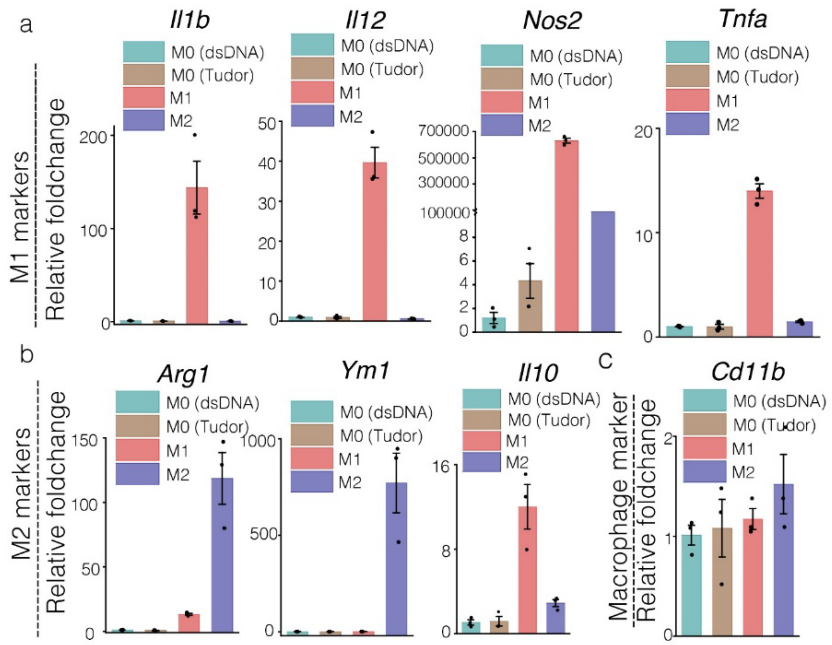

Figure II.12: *Tudor* does not alter polarization states of macrophages from Pmacs. (**a-c**) Expression levels of M1(a) and M2 (b) and macrophage marker (c) genes shown in Pmac (M0) upon dsDNA and *Tudor* treatment. All error bars represent standard error of mean (s.e.m) from three independent experiments.

2.4 Conclusion

LPS activates the immune response in innate immune cells likes macrophages and dendritic cells, which leads to lysosome tubulation. Similarly autophagy, stimulated either by starvation or during development *in vivo* leads to lysosome tubulation[7,10–12]. *Tudor*, a DNA based nanodevice consisting of an aptamer, SA43, triggers tubulation of lysosomes in several macrophage cell lines such as RAW 264.7, SIM-A9, J774A.1; fibroblasts such as COS-7 and epithelial cells such as HepG2. *Tudor* also increased the number of tubular lysosomes in primary cells like BMDMs, Pmacs and ATMs. *Tudor* stimulates tubulation by binding to Ku70/80 proteins present on the plasma membrane of the cells. Although Ku70/80 has been reported to act as receptors for *Rickettsia conorii* bacteria and thereby internalize bacteria, the physiological ligand for Ku70/80

present on plasma membrane is still not known [29,30]. *Tudor* internalizes into the cell by binding to Ku70/80 and brings about lysosomal remodeling in macrophages without affecting its polarization into either M1 or M2 like macrophages.

2.5 References

1. Saric, A. *et al.* mTOR controls lysosome tubulation and antigen presentation in macrophages and dendritic cells. *Mol. Biol. Cell* **27,** 321–333 (2016).
2. Hipolito, V. E. B. *et al.* Enhanced translation expands the endo-lysosome size and promotes antigen presentation during phagocyte activation. *PLoS Biol.* **17,** e3000535 (2019).
3. Hipolito, V. E. B., Ospina-Escobar, E. & Botelho, R. J. Lysosome remodelling and adaptation during phagocyte activation. *Cell Microbiol.* **20,** (2018).
4. Robinson, J. M., Chiplonkar, J. & Luo, Z. A method for co-localization of tubular lysosomes and microtubules in macrophages: fluorescence microscopy of individual cells. *J. Histochem. Cytochem.* **44,** 1109–1114 (1996).
5. ROB, J., CHIPLONKAR, J. & LU, Z. I A Method for Co-localization of Tubular Lysosomes and.
6. Swanson, J., Bushnell, A. & Silverstein, S. C. Tubular lysosome morphology and distribution within macrophages depend on the integrity of cytoplasmic microtubules. *Proc. Natl. Acad. Sci. USA* **84,** 1921–1925 (1987).
7. Yu, L. *et al.* Termination of autophagy and reformation of lysosomes regulated by mTOR. *Nature* **465,** 942–946 (2010).
8. Chen, Y. & Yu, L. Autophagic lysosome reformation. *Exp. Cell Res.* **319,** 142–146 (2013).
9. Chen, Y. & Yu, L. Recent progress in autophagic lysosome reformation. *Traffic* **18,** 358–361 (2017).
10. Miao, R., Li, M., Zhang, Q., Yang, C. & Wang, X. An ECM-to-Nucleus Signaling Pathway Activates Lysosomes for C. elegans Larval Development. *Dev. Cell* **52,** 21–37.e5 (2020).
11. Sun, Y. *et al.* Lysosome activity is modulated by multiple longevity pathways and is important for lifespan extension in C. elegans. *Elife* **9,** (2020).
12. Murakawa, T., Kiger, A. A., Sakamaki, Y., Fukuda, M. & Fujita, N. An Autophagy-Dependent Tubular Lysosomal Network Synchronizes Degradative Activity Required for Muscle Remodeling. *BioRxiv* (2020). doi:10.1101/2020.04.15.043075

13. Johnson, A. E., Shu, H., Hauswirth, A. G., Tong, A. & Davis, G. W. VCP-dependent muscle degeneration is linked to defects in a dynamic tubular lysosomal network in vivo. *Elife* **4,** (2015).

14. Fujihara, M. *et al.* Molecular mechanisms of macrophage activation and deactivation by lipopolysaccharide: roles of the receptor complex. *Pharmacol. Ther.* **100,** 171–194 (2003).

15. Mosser, D. M. & Zhang, X. Activation of murine macrophages. *Curr. Protoc. Immunol.* **Chapter 14,** Unit 14.2 (2008).

16. Yuan, H. *et al.* LPS-induced autophagy is mediated by oxidative signaling in cardiomyocytes and is associated with cytoprotection. *Am. J. Physiol. Heart Circ. Physiol.* **296,** H470–9 (2009).

17. Bermúdez, V., Tenconi, P. E., Giusto, N. M. & Mateos, M. V. Lipopolysaccharide-Induced Autophagy Mediates Retinal Pigment Epithelium Cells Survival. Modulation by the Phospholipase D Pathway. *Front. Cell Neurosci.* **13,** 154 (2019).

18. Abdelbaqi, K., Di Paola, D., Rampakakis, E. & Zannis-Hadjopoulos, M. Ku protein levels, localization and association to replication origins in different stages of breast tumor progression. *J. Cancer* **4,** 358–370 (2013).

19. Chai, W., Ford, L. P., Lenertz, L., Wright, W. E. & Shay, J. W. Human Ku70/80 associates physically with telomerase through interaction with hTERT. *J. Biol. Chem.* **277,** 47242–47247 (2002).

20. Skorokhod, O. M., Kravchuk, I. V., Teleheiev, H. D. & Maliuta, S. S. [Role of Ku protein in normal and cancer cells]. *Ukr Biokhim Zh (1999)* **78,** 5–15 (2006).

21. Kim, H. DNA repair Ku proteins in gastric cancer cells and pancreatic acinar cells. *Amino Acids* **34,** 195–202 (2008).

22. Monferran, S., Paupert, J., Dauvillier, S., Salles, B. & Muller, C. The membrane form of the DNA repair protein Ku interacts at the cell surface with metalloproteinase 9. *EMBO J.* **23,** 3758–3768 (2004).

23. Prabhakar, B. S., Allaway, G. P., Srinivasappa, J. & Notkins, A. L. Cell surface expression of the 70-kD component of Ku, a DNA-binding nuclear autoantigen. *J. Clin. Invest.* **86,** 1301–1305 (1990).

24. Muller, C., Paupert, J., Monferran, S. & Salles, B. The double life of the Ku protein: facing the DNA breaks and the extracellular environment. *Cell Cycle* **4,** 438–441 (2005).

25. Paupert, J., Dauvillier, S., Salles, B. & Muller, C. Transport of the leaderless protein Ku on the cell surface of activated monocytes regulates their migratory abilities. *EMBO Rep.* **8,** 583–588 (2007).

26. Chan, J. Y. *et al.* Cloning and characterization of a cDNA that encodes a 70-kDa novel human thyroid autoantigen. *J. Biol. Chem.* **264,** 3651–3654 (1989).

27. Lucero, H., Gae, D. & Taccioli, G. E. Novel localization of the DNA-PK complex in lipid rafts: a putative role in the signal transduction pathway of the ionizing radiation response. *J. Biol. Chem.* **278,** 22136–22143 (2003).

28. Morio, T. *et al.* Ku in the cytoplasm associates with CD40 in human B cells and translocates into the nucleus following incubation with IL-4 and anti-CD40 mAb. *Immunity* **11,** 339–348 (1999).

29. Martinez, J. J., Seveau, S., Veiga, E., Matsuyama, S. & Cossart, P. Ku70, a component of DNA-dependent protein kinase, is a mammalian receptor for Rickettsia conorii. *Cell* **123,** 1013–1023 (2005).

30. Chan, Y. G. Y., Cardwell, M. M., Hermanas, T. M., Uchiyama, T. & Martinez, J. J. Rickettsial outer-membrane protein B (rOmpB) mediates bacterial invasion through Ku70 in an actin, c-Cbl, clathrin and caveolin 2-dependent manner. *Cell Microbiol.* **11,** 629–644 (2009).

31. Munakata, Y. *et al.* Ku80 autoantigen as a cellular coreceptor for human parvovirus B19 infection. *Blood* **106**, 3449–3456 (2005).

32. Koike, M. Dimerization, translocation and localization of Ku70 and Ku80 proteins. *J Radiat Res* **43**, 223–236 (2002).

33. Fransson, J. & Borrebaeck, C. A. K. The nuclear DNA repair protein Ku70/80 is a tumor-associated antigen displaying rapid receptor mediated endocytosis. *Int. J. Cancer* **119,** 2492–2496 (2006).

34. Aptekar, S. *et al*. Selective Targeting to Glioma with Nucleic Acid Aptamers. *PLoS One* **10**, e0134957 (2015).

35. Ni, S. *et al.* Recent progress in aptamer discoveries and modifications for therapeutic applications. *ACS Appl. Mater. Interfaces* (2020). doi:10.1021/acsami.0c05750

36. Saminathan, A. *et al.* A DNA-based voltmeter for organelles. *Nat. Nanotechnol.* (2020). doi:10.1038/s41565-020-00784-1

37. He, F. *et al.* Aptamer-Based Targeted Drug Delivery Systems: Current Potential and Challenges. *Curr. Med. Chem*. **27**, 2189–2219 (2020).

38. Jani, M. S., Zou, J., Veetil, A. T. & Krishnan, Y. A DNA-based fluorescent probe maps NOS3 activity with subcellular spatial resolution. *Nat. Chem. Biol.* **16,** 660–666 (2020).

39. Modi, S., Nizak, C., Surana, S., Halder, S. & Krishnan, Y. Two DNA nanomachines map pH changes along intersecting endocytic pathways inside the same cell. *Nat. Nanotechnol.* **8,** 459–467 (2013).

40. Surana, S., Bhat, J. M., Koushika, S. P. & Krishnan, Y. An autonomous DNA nanomachine maps spatiotemporal pH changes in a multicellular living organism. *Nat. Commun.* **2,** 340 (2011).

41. Surana, S., Bhatia, D. & Krishnan, Y. A method to study in vivo stability of DNA nanostructures. *Methods* **64,** 94–100 (2013).

42. Leung, K., Chakraborty, K., Saminathan, A. & Krishnan, Y. A DNA nanomachine chemically resolves lysosomes in live cells. *Nat. Nanotechnol.* **14,** 176–183 (2019).

43. Thekkan, S. *et al.* A DNA-based fluorescent reporter maps HOCl production in the maturing phagosome. *Nat. Chem. Biol.* **15,** 1165–1172 (2019).

44. Modi, S. *et al.* A DNA nanomachine that maps spatial and temporal pH changes inside living cells. *Nat. Nanotechnol.* **4,** 325–330 (2009).

45. Saha, S., Prakash, V., Halder, S., Chakraborty, K. & Krishnan, Y. A pH-independent DNA nanodevice for quantifying chloride transport in organelles of living cells. *Nat. Nanotechnol.* **10,** 645–651 (2015).

46. Chakraborty, K., Leung, K. & Krishnan, Y. High lumenal chloride in the lysosome is critical for lysosome function. *Elife* **6,** e28862 (2017).

47. Veetil, A. T. e*t al.* DNA-based fluorescent probes of NOS2 activity in live brains. P*roc. Natl. Acad. Sci. USA* 1**17,** 14694–14702 (2020).

48. Veetil, A. T. *et al.* Cell-targetable DNA nanocapsules for spatiotemporal release of caged bioactive small molecules. *Nat. Nanotechnol.* **12,** 1183–1189 (2017).

49. Narayanaswamy, N. *et al.* A pH-correctable, DNA-based fluorescent reporter for organellar calcium. *Nat. Methods* **16,** 95–102 (2019).

50. Veetil, A. T., Jani, M. S. & Krishnan, Y. Chemical control over membrane-initiated steroid signaling with a DNA nanocapsule. *Proc. Natl. Acad. Sci. USA* **115,** 9432–9437 (2018).

51. Kratz, M. *et al.* Metabolic dysfunction drives a mechanistically distinct proinflammatory phenotype in adipose tissue macrophages. *Cell Metab.* **20,** 614–625 (2014).

52. Reardon, C. A. *et al.* Obesity and Insulin Resistance Promote Atherosclerosis through an IFNγ-Regulated Macrophage Protein Network. *Cell Rep.* **23**, 3021–3030 (2018).

53. Dan, K., Veetil, A. T., Chakraborty, K. & Krishnan, Y. DNA nanodevices map enzymatic activity in organelles. *Nat. Nanotechnol.* **14**, 252–259 (2019).

54. Fukasawa, M. *et al.* SRB1, a class B scavenger receptor, recognizes both negatively charged liposomes and apoptotic cells. *Exp. Cell Res.* **222,** 246–250 (1996).

55. Schindelin, J. *et al*. Fiji: an open-source platform for biological-image analysis. *Nat. Method*s **9**, 676–682 (2012).

56. Kalkofen, D. N., de Figueiredo, P. & Brown, W. J. Methods for analyzing the role of phospholipase A_2 enzymes in endosome membrane tubule formation. *Methods Cell Biol.* **130**, 157–180 (2015).

57. Sato, Y. *et al.* Three-dimensional multi-scale line filter for segmentation and visualization of curvilinear structures in medical images. *Med Image Anal* **2,** 143–168 (1998).

58. Ferreira, C. S. M., Cheung, M. C., Missailidis, S., Bisland, S. & Gariépy, J. Phototoxic aptamers selectively enter and kill epithelial cancer cells. *Nucleic Acids Res.* **37,** 866–876 (2009).

59. Chuang, T.-H., Lee, J., Kline, L., Mathison, J. C. & Ulevitch, R. J. Toll-like receptor 9 mediates CpG-DNA signaling. *J. Leukoc. Biol.* **71,** 538–544 (2002).

60. Cho, J.-S. *et al.* Lipopolysaccharide induces pro-inflammatory cytokines and MMP production via TLR4 in nasal polyp-derived fibroblast and organ culture. *PLoS On*e **9**, e90683 (2014).

61. Segura, M., Vadeboncoeur, N. & Gottschalk, M. CD14-dependent and -independent cytokine and chemokine production by human THP-1 monocytes stimulated by Streptococcus suis capsular type 2. *Clin. Exp. Immunol*. **127**, 243–254 (2002).

Chapter 3. Mechanistic basis of lysosome remodeling by *Tudor*

3.1 Introduction

Both lipopolysaccharide (LPS) and *Tudor* showed similar kinetics of tubular lysosome formation. This suggested that both treatments might utilize a similar pathway with the possibility of a positive feedback mechanism that would be needed for sustained tubular lysosome formation over hour long durations. LPS mediated tubulation of lysosomes in macrophages occurs via TLR4. Yet, MyD88 deficient dendritic cells also show tubulated lysosomes suggesting the presence of alternative pathways to tubulate lysosomes in immune cells[1]. Studying alternative pathways of lysosome tubulation has not been possible thus far, due to the lack of tools to tubulate lysosomes without affecting other cellular mechanisms. This is because in addition to tubulating lysosomes LPS also activates immune cells and triggers autophagy. The DNA nanodevice *Tudor* tubulates lysosomes without activating macrophages and therefore could be used to reveal an additional lysosome tubulation pathway in macrophages. This pathway converges on previously known protein players involving in lysosome tubulation and is discussed in detail in this chapter.

Tubulation of lysosomes was assayed by labeling lysosomes in immune cells with tetramethyl rhodamine - dextran (TMR-Dextran), pretreated with a given inhibitor against protein targets and then tubuluation was induced with LPS or *Tudor*. If the protein target played a role in the tubulation pathway, its inhibition would prevent lysosomal tubulation.

LPS, the ligand for TLR4 triggers tubular lysosome formation through Myd88 pathway by activating PI3K, Akt, mTOR pathway[2,3]. LPS mediated tubulation of lysosome also involves the lysosomal motility proteins like Ras related protein Rab7, Arl8b, Asparagine-Linked Glycosylation 2 (ALG2). Rab7 brings about the movement of lysosomes towards perinuclear and

peripheral region through its adapter proteins Rab Interacting Lysosome protein (RILP) and FYVE and coiled-coil domain containing protein (FYCO1) bound to dynein and kinesin respectively. The GTPase Arl8b plays a role in lysosomal positioning, trafficking whereby lysosome tethered Arl8b binds to SifA-kinesin interacting protein (SKIP). SKIP binds to kinesin-1 which moves lysosomes along minus end of microtubule towards the plasma membrane[2–5]. Calcium efflux from the TRPML1 channel is crucial for the continued elongation of tubulation of lysosomes. Release of lysosomal calcium activates cytosolic ALG2 which binds to the cytosolic face of the lysosomal membrane and to kinesin further enhancing lysosome movement towards the plasma membrane. Recruitment of ALG2 on increases the tension between RAB7 and Arl8b through their respective adapter proteins. Hence lysosome is pulled along both end of microtubules elongating into tubular lysosomes[2,3,5,6]. siRNA or constutitively inactivating GTPases such as Rab7, Arl8b or any of their adapter proteins prevents lysosomal tubulation in LPS treated macrophages[2,3]. Similar results were seen in non-immune cells when lysosomes tubulation was triggered with gram negative bacteria, *S. Typhimurium*[7].

Tudor triggers lysosome tubulation upon binding to the Ku70/80 heterodimer resident on the plasma membrane. Our studies revealed an additional pathway that causes tubuluation that independent of TLR4 and could potentially function in resting cells of diverse cell types, not restricted to immune cells.

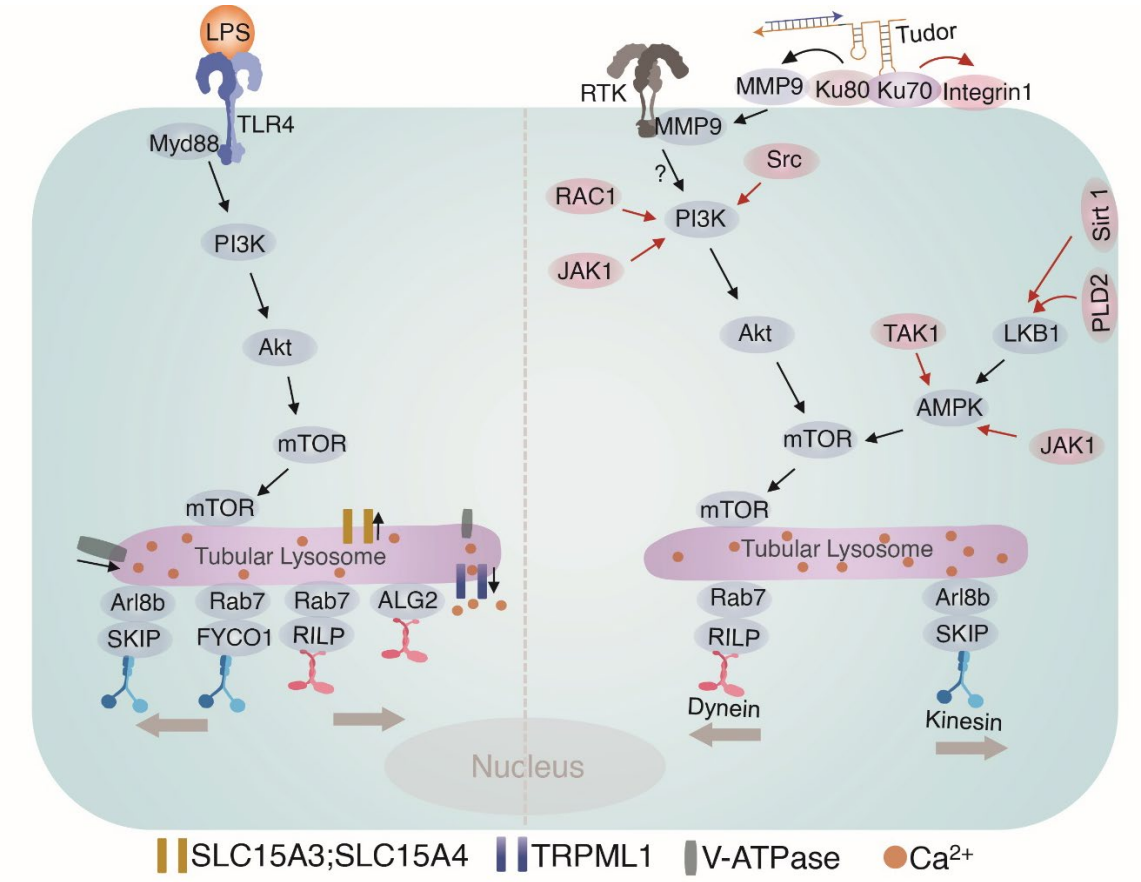

Figure III.1: Mechanistic basis of lysosome tubulation induced by LPS or *Tudor*. LPS mediated pathway of tubular lysosome formation is shown on left with *Tudor* mediated pathway on the right side of the macrophage cell. Black and red arrows represent players that either involved or not respectively, in lysosomal tubulation as outlined in this chapter.

3.2 Materials and methods

3.2a: siRNA gene silencing: Trans IT-TKO (Mirus Biol LLC) was used to perform siRNA gene silencing in RAW 264.7 as per supplier's instructions. Two DsiRNA (IDT DNA, USA) against mouse *Arl8b* (GENE ID: 67166) were used along with negative control. quantitative real time PCR was used to confirmation of *Arl8b* gene silencing after 72 hours of transfection.

After 72 hours of transfection, lysosomal tubulation assay was performed (Refer to Chapter 2, Materials and methods, 2.2g). 18S was used as internal control. Following are the primers used in this study (F=forward, R= reverse):

Arl8b F: AGATCTGGGACATAGGCGGA, R: AGGACCATGTCCTGGGAAGT

18s F: GCCGCTAGAGGTGAAATTCTT; R: CGTCTTCGAACCTCCGACT

3.2b: MMP9 activity assay: MMP9 assay kit was used to study MMP9 activity assay (Anaspec Inc) was performed as per supplier's instructions. Approximated 100,000 cells were seeded in each 96 well plate. Cells were grown with standard culturing conditions. APMA (final concentration of 1 mM) for 2 hours; MMP 9inhibitor-I (100 µM for 1 hour) or 500 nM *Tudor* for 4 hours was replaced in assay buffer (50 mM Tris, 10 mM $CaCl_2$, 150 mM NaCl, 0.05 % BrijW L23, pH 7.5). 200 X final concentration of peptide substrate diluted in assay buffer was added to the above mixture on cells. The cells were incubated with substrate containing buffer for 24 hours. The reaction was stopped using stop solution provided in the kit. Synergy™ Neo 2 Multi -Mode Microplate Reader was used to measure Relative fluorescence unit (RFU) at Ex/Em at 480 /520 nm. RFU from three independent experiments were used to calculate and plot Mean fluorescence unit (MFU) was calculated and plotted. Signal from APMA containing wells were normalized to 1. Normalized percentage activity where the MFU of background hydrolysis (BH) was subtracted from the other samples (APMA, MMP9-i, dsDNA and *Tudor*) was set to 0 % and APMA to 100 %.

3.2c: Western blot analyses. Cells were lysed with Ice cold RIPA buffer containing phosphatase inhibitors (Sigma), and protein was quantified with the BCA Protein Assay Kit (Thermo Fisher). Proteins (10-20 µg) were resolved on 8-12.5 % SDS-PAGE gels, transferred to PVDF membranes

(Millipore). The blots were blocked with 5% BSA (Sigma) in 0.1% TBS/Tween-20 at RT for 1 hour, stained with primary and secondary antibodies, and visualized using the Super Signal™ Femto Maximum sensitivity substrate (Thermo Fisher). BioRad ChemiDoc MP Molecular imager. Antibodies include: pSTAT1 (7649), tubulin (2125), pNF-kB (3033) from Cell Signaling Technologies.

3.2d: RT PCR: Raw 264.7 macrophages were used for this assay where total RNA from cells were isolated using Trizol as per instructions by manufacturer (Invitrogen). First strand synthesis was performed using Super Script III as per manufacturer's instructions (Thermo Scientific). 10 µL of PCR product was run on 2.0 % agarose gel in TAE buffer.

MMP9 and GAPDH specific primers used were as follows:

MMP9 F: CCTGTGTGTTCCCGTTCATCT, R: CGCTGGAATGATCTAAGCCCA

GAPDH F: CCCAGAAGACTGTGGATGG, R: CACATTGGGGGTAGGAACAC

3.2e: Time-dependent lysosomal tubulation assay: Time-dependent tubulation: RAW 264.7 with TMR-dextran labeled lysosomes were treated with unlabeled 100 nM *Tudor*, 100 nM dsDNA, or 100 ng/ mL LPS. Addition of Tudor, dsDNA or LPS is taken as t=0 mins. Cells were then imaged in fluorescence microscope at the indicated time points and scored for the formation of tubular lysosomes.

3.2f: Inhibitor assay: Lysosomes in RAW 264.7 and BMDMs were treated with 10 kDa TMR dextran to label lysosomes. Cells were then incubated with specific inhibitors for proteins which might be playing role in lysosomal tubulation. Inhibitor treatment was followed by (100 nM) *Tudor* for 4 hours at 37° C in the presence of the inhibitors. Cells were then imaged using a confocal microscope.

Details of the concentration and incubation times of each inhibitor used are provided in Table II.1.

Table 3: Details of inhibitors used in the study.

Protein	**Inhibitor**	**Concentration/duration**	**Cat no.**	**Source**
TLR 4	TAK-242	10 µM, 18 hours	13871	Cayman chemicals, USA
mTORC1	Rapamycin	100 nM, 1 hour	13346	Cayman chemicals, USA
mTORC2	Torin 1	100 nM, 1 hour	10997	Cayman chemicals, USA
AMPK	Dorsomorphin	20 µM, 30 mins	21207	Cayman chemicals, USA
PI3K	Zstk474	1 µM, 30 mins	17381	Cayman chemicals, USA
Akt	Akt inhibitor VIII	5 µM, 30 mins	14870	Cayman chemicals, USA
Src1	Dasatinib	1 µM, 1 hour	11498	Cayman chemicals, USA
JAK	JAK inhibitor I	1 µM, 48 hours	15146	Cayman chemicals, USA
Rac1	NSC 23766	50 µM, 12 hours	13196	Cayman chemicals, USA

TAK1	(5Z)-7-Oxo Zeaenol	300 nM, 6 hours	17459	Cayman chemicals, USA
PLD1	CAY10594	1 µM, 30 mins	13207	Cayman chemicals, USA
MMP9	MMP-9 inhibitor I	100 µM, 1 hour	15942	Cayman chemicals, USA
Integrin 1	RGD peptide	0.3 mg/mL, 4 hours	14501	Cayman chemicals, USA
Pan Cathepsin	E64	50 µM, 24 hours	10007963	Cayman chemicals, USA
TLR3	CuCPT-4a	27 µM, 24 hours	4884	Tocris, USA
TLR5	TH 1020	0.37 µM, 24 hours	6191	Tocris, USA
TLR2/6	GIT-27	10ug/mL, 24 hours	3270	Tocris
Myd88	Myd88 Inhibitor peptide	100 µM, 24 hours	NBP-2 29328	Novus Biologicals, USA
LKB1	LKB1-i	380 nM, 24 hours	A3556	APExBio
IRS1	NT-157	1 µM, 72 hours	S8228	Selleckchem
Sirtuin1	EX527	1 µM, 24 hours	100099798	Cayman chemicals, USA
TLR1/2-i	CuCPT-22	8 µM, 24 hours	4884	Tocris, USA
Nrf2	ML385	5 µM, 72 hours	21114	Cayman chemicals, USA
NFkB	JSH-23	300 µM, 1 hour	481408	Sigma Aldrich, USA

Table 3, Continued: Details of inhibitors used in the study.

3.3 Results and Discussion

3.3a: Rate of tubulation induced by *Tudor* is similar to that observed with LPS

LPS (100 ng/mL) treatment for 4 hours tubulates lysosomes in immune cells. The rate of tubulation induced by *Tudor* is similar to that observed with LPS treatment. After 4 hours of treatment with either LPS or *Tudor*, the area of tubular lysosomes corresponded to 80% of total area occupied by lysosomes in macrophages. When treated with duplex DNA (dsDNA) no tubulation was observed. In addition, both LPS and *Tudor* continued to tubulate lysosomes even after 8-12 hours of treatment suggesting that the existence of a mechanism for the sustained tubulation of lysosomes. Given that both LPS and *Tudor* treatment led to similar kinetics of tubulation, we hypothesized that the *Tudor*-mediated pathway and the LPS-mediated pathway could share common players.

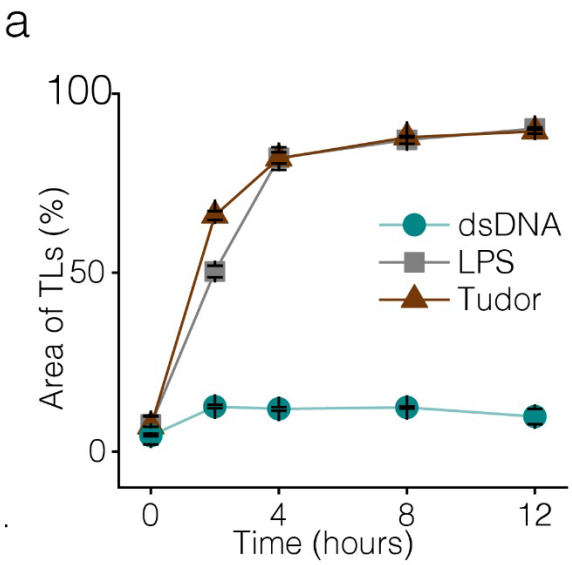

Figure III.2: Rate of *Tudor* mediated tubulation is similar to that of LPS. (**a**) Percentage area

Figure III.2, continued: of TLs w.r.t. time upon addition of *Tudor*, LPS or dsDNA in RAW 264.7 cells (n= 20 cells). Error bars represent standard error of mean (S.E.M) from three independent experiments.

3.3b: Signaling Pathway of *Tudor* mediated tubulation of lysosomes

LPS is known to trigger lysosome tubulation by interacting with TLR4 present on the plasma membrane followed by MyD88[8]. Although *Tudor* internalization occurs via the Ku70/80 heterodimer, in order to study the role of TLR4 or Myd88 if any we inhibited TLR4 and Myd88 using the inhibitors TAK242 and Myd88 inhibiting peptide respectively. We found that *Tudor* induced tubulation was not affected while LPS induced lysosomal tubulation was abolished (Figure III.3 a, b). Thus despite the similar kinetics of tubulation observed by LPS treatment *Tudor* *Tudor* induced tubulation is TLR-4 and Myd88 independent.

In order to check if *Tudor* and LPS pathways shared common downstream players, mTOR1 and mTOR2 protein complexes were inhibited using specific inhibitors, Rapamycin and Torin 1. This prevented tubulation of lysosomes (Figure III.3 a, b) suggesting that mTOR plays crucial role in lysosomal tubulation. Furthermore, inhibiting PI3K and Akt with ZSTK474 or Akt-I respectively revealed that PI3K-Akt-mTOR axis was indispensable *Tudor* mediated tubulation. Thus both LPS and *Tudor* did indeed share common downstream players.

5'-AMP-activated protein kinase (AMPK) is a serine/threonine kinase that is activated under metabolic stress[9]. AMPK is a key player in the activation of innate immune cells when they encounter pathogens such as Ebola, HCV etc[10]. AMPK regulates the anti-inflammatory response and can also activate the Pi3K-Akt pathway[11]. Treating macrophages with an activator of AMPK leads to their polarization to an anti-inflammatory phenotype[11]. AMPK activation by AICAR enhances phagocytosis, bactericidal activity against pathogens like *S. aureus* in microglia,

macrophages and neutrophils[12]. LKB1 is the direct activator of AMPK[13]. Interestingly, LKB1 was played a role in *Tudor* mediated tubulation but had no effect on LPS induced tubulation (Figure III.3a, b). Additionally, AMPK also inhibits mTOR by phosphorylating mTOR at S722 and S792 [14,15]. Previous studies by Botelho *et al* had discounted the role of AMPK in lysosomal tubulation based on pharmacological activation using A769662[2]. However, our studies that used pharmacological inhibition of AMPK with dorsomophin (Compound C), revealed that it does play a role in tubulating lysosomes[16].

Another protein which was found to be crucial for tubulation was MMP9. The core region (222-372 amino acids) of Ku80 of the Ku70/80 heterodimer present on the plasma membrane interacts with the hemopexin domain (514-707 amino acids) found at the C-terminus of MMP9[17]. When MMP9 was inhibited both LPS and *Tudor* induced tubulation were completely abolished (Figure III.3 a, b). Further, *Tudor* treatment also activated MMP9 on the plasma membrane as revealed by an MMP9 activity assay (Figure III.3c).

Taken together, this suggests that AMPK activity is highly regulated. Both hyper-activation and complete inhibition of AMPK will prevents lysosome tubulation. One of the well-known upstream activators of AMPK is LKB1[13,18]. Pharmacological inhibition of LKB1 (LKB1-inhibitor) prevented lysosomes tubulation upon *Tudor* treatment but not upon LPS treatment. This reveals two new protein players in lysosomal tubulation namely AMPK and LKB1. Given that AMPK is also negatively regulates mTOR, we hypothesize that the main role of AMPK is to maintain the delicate balance of activated mTOR since PI3K-Akt positively regulate mTOR activity. This likely prevents complete inhibition or hyperactivation of mTOR to bringing about sustained tubulation (Figure III.3a, b).

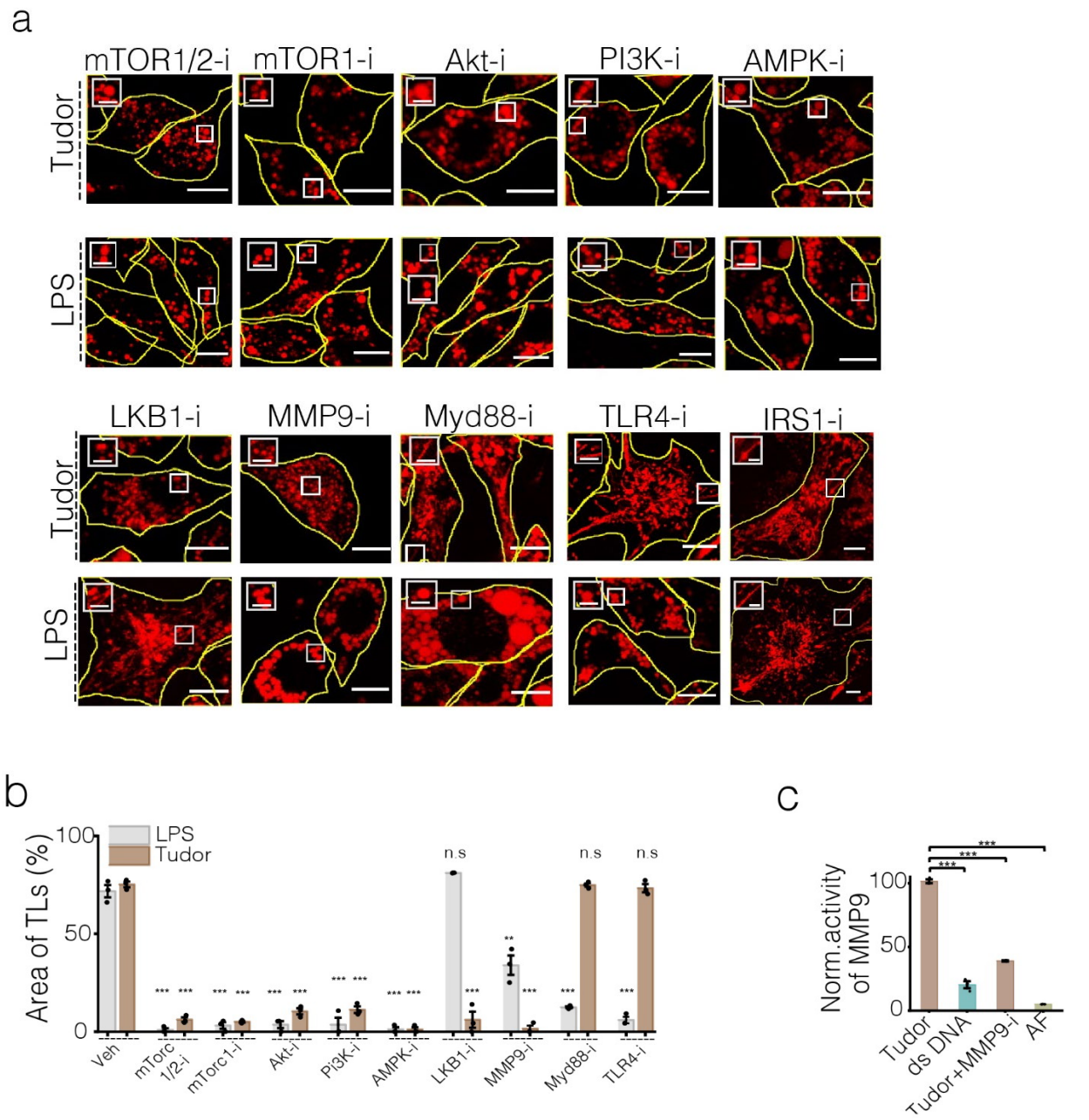

Figure III.3: Inhibitor screen of protein players that prevent *Tudor* or LPS-induced tubular lysosome formation. (**a**) Representative confocal images of TMR dextran labeled lysosomes in *Tudor* or LPS treated cells in the presence of indicated pharmacological inhibitors. Scale bar: 10 µm, inset scale bar: 4 µm. (**b**) Percentage area of TLs in 646 the presence *Tudor* or LPS and pharmacological inhibitors for indicated protein (*protein-i)* in RAW 264.7 cells, (n=20 cells). (**c**) Normalized activity of MMP9 in RAW 264.7 upon treatment with *Tudor* (in absence or presence of MMP9 inhibitor-1) and dsDNA where mean fluorescence unit of *Tudor* was normalized to maxima (100%). AF represents autofluorescence of cells without any treatment. n.s: non-significant; ***P< 0.0005; **P< 0.005; *P< 0.05 (one-way ANOVA with Tukey *post hoc* test).

Figure III.3, continued. Error bars 649 represent standard error of mean (s.e.m) for all experiments shown here. Data represented from at 650 least 3 independent experiments.

3.3b.1 Protein players that are not involved in lysosomal tubulation

LPS is a well known activator of TLR4/2. TLR4 activation by LPS leads to its dimerization and activation of Myd88, which subsequently initiate a signalling cascade resulting in lysosome tubulation. On the contrary, TLR4 and Myd88 were not involved in *Tudor* mediated tubulation. In order to check if other TLRs played any role in *Tudor* mediated tubulation, various plasma membrane resident TLRs were pharmacologically inhibited using TH 1020 (TLR5), GIT 27 (TLR2/6), CuCPT-4a (TLR3) and CuCPT-22 (TLR 1/2). Our experiments revealed that tubulation was unaffected by any of these inhibitors demonstrating no role of TLRs in *Tudor* induced lysosomal tubulation (Figure III.4 a, c).

We tested a range of protein players based on their known roles in activating PI3K, Akt and mTOR to test their involvement in lysosomal tubulation. For example, PI3K can be activated by various means; cSrc activates PI3K by interacting with p85, the regulatory subunit of PIi3K [19] and also through c-Cbl[20]. Further, cSrc, c-Cbl and PI3K activity are involved in Ku70 mediated entry of *R. conorii* in the nonphagocytic cells[21]. Treating cells with a potent inhibitor for cSrc such as dasatinib did not abolish lysosome tubulation by either LPS or *Tudor* treatment (Figure III.4 b, c). An independent study in innate immune cells showed that TLR2 activation leads to the activation of Rho GTPase, RAC1, c-Cbl and PI3K. This signaling cascade eventually leads to transactivation of NFκB through PI3K-Akt activation[22]. However, inhibiting RAC1 with RAC1-i did not prevent tubulation. Yet another potential player that can activate PI3K is JAK1/2 that is activated by IL2 as seen in adult T-cell leukemia [23]. However, the JAK1/2 inhibitor, barcitinib did not abolish

tubulation (Figure III.4 b, c). These experiments demonstrated that PI3K is not activated by either cSrc, Rac1, c-Cbl, JAK1/2 mediated pathway but by alternative protein players upstream. We also tested the role of transforming growth factor β (TGF β) activating Kinase 1 (TAK1)[25,26]. However, the TAK1 inhibitor ((5Z)-7-Oxozeaenol) did not prevent tubular lysosome formation in both LPS and *Tudor* treated cells (Figure III.4 b,c). This precludes the role of TAK1 in *Tudor* induced lysosomal tubulation.

LKB1 can be activated by phosphotidic acid (PA) produced by phospholipase D2 (PLD2) at the plasma membrane of normal cells[27]. Sirt1, a class III NAD^+ dependent histone/protein deacetylases can activate AMPK through LKB1[28]. Treatment with a PLD2 inhibitor, CA105297 or a Sirt1 inhibitor, EX527 had no effect on TL formation in both *Tudor* and LPS treated macrophages (Figure III.4 b,c).

Ku70/80 heterodimer shows structural homology with the Integrin A domain involved in fibronectin binding. The metal ion dependent adhesion site (MIDAS) in Ku70/80 heterodimer is required for ligand binding and activation of Integrins[29–31]. However, inhibition of Integrin1 had no effect on tubulation of lysosomes. These experiments demonstrate that the players upstream of LKB1 and downstream of MMP9 still needs to be identified. One possible hypothesis which needs to be tested is a potential receptor tyrosine kinase (RTK) which might get activated upon MMP9 activation on the cytosolic side of the receptor. The activation of this RTK could in turn activate PI3K[24].

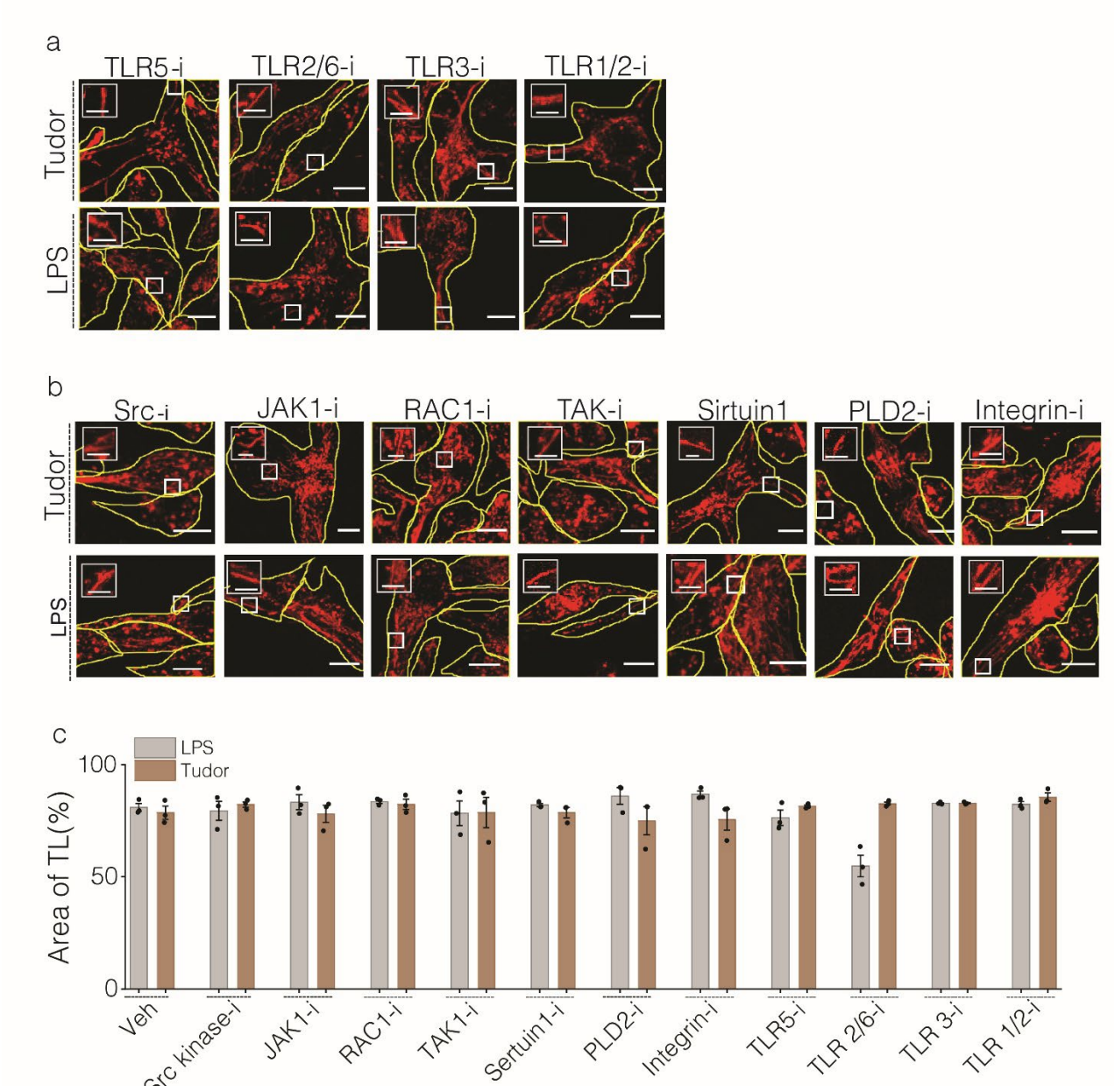

Figure III. 4: Pharmacological inhibition of proteins not involved in *Tudor* and LPS mediated pathways. (**a, b**) Representative confocal images of TMR dextran labeled lysosomes in *Tudor* or LPS treated cells in the presence of indicated pharmacological inhibitors. Scale bar: 10 µm, inset scale bar: 4 µm. (**c**) Quantification of mean % Area of TL over total lysosomes shown in (a, b), (n=20 cells), (Veh=DMSO). ***P< 0.0005; (one-way ANOVA with Tukey *post hoc* test). Error bars represent s.e.m from three independent experiments.

3.3b.2 *Tudor* mediated lysosome tubulation is conserved in primary macrophages

In order to check if the *Tudor* triggered lysosomal tubulation is conserved in primary cells, BMDMs were chosen as model primary cells mainly because these cells express Ku70/80 on their plasma membrane from previous experiments as well as our own ones. Hence we inhibited key players such as mTOR1/2, LKB1, MMP9 and TLR4 with the previously mentioned specific inhibitors in M0, M1 and M2 macrophages derived from BMDMs (Figure III. 5 a-e). M0 macrophages of BMDMs showed reduced tubulation upon treatment with mTOR1/2 inhibitor (Torin1). Abolishing LKB1 activity abrogated tubulation in both LPS and *Tudor* treated M0 macrophages (figure III.5 a, d). As anticipated, TLR-4 inhibition showed no effect on tubulation in *Tudor* treated M0 macrophages while LPS-treated cells showed reduced tubulation. This suggests the existence of an additional pathway for LPS mediated tubulation that is TLR-4 independent in primary cells. Interestingly, MMP9 inhibition showed complete abolition of tubular lysosomes in both LPS and *Tudor* treated M0 macrophages (Figure III. 5 a, d). Similar results were also found in M1 and M2 macrophages of BMDMs upon similar treatment as shown in Figure III. 5 d, c and e. This suggests that the pathway of *Tudor* mediated tubulation is conserved in primary M0 macrophages of BMDM.

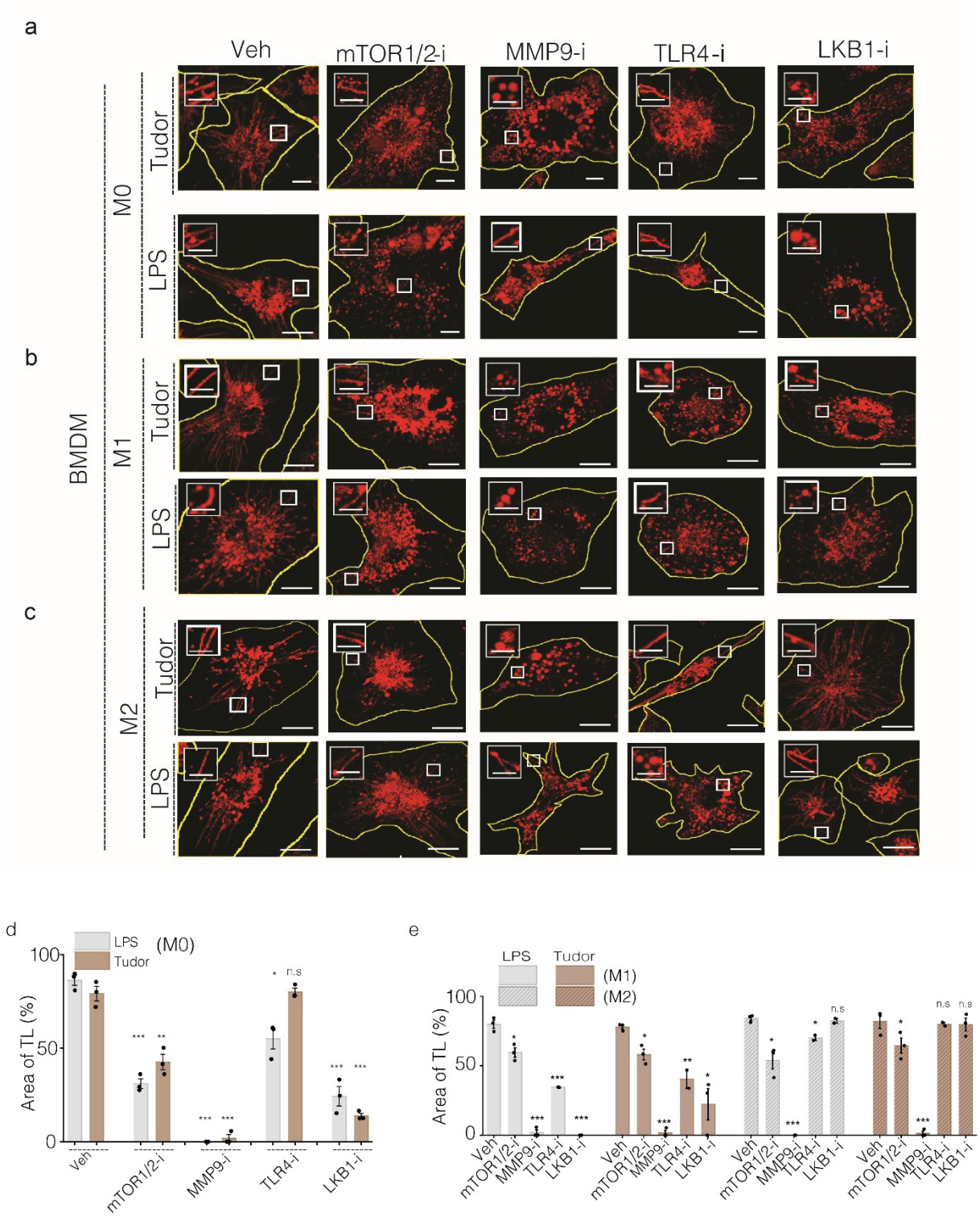

Figure III.5: Lysosome tubulation pathway induced by *Tudor* is conserved in BMDMs. (a-c) Representative confocal images of TMR-dextran-labeled lysosomes of murine BMDMs treated either with *Tudor* or LPS where the indicated proteins are pharmacologically inhibited. (d) % Area

Figure III.5, continued. of TL over total lysosomes shown for M1 (left) and M2 (right) obtained from (b and c). ***P< 0.0005; **P< 0.005; *P< 0.05 (one-way ANOVA with Tukey *post hoc* test). Veh=DMSO; n.s: non-significant. Error represents s.e.m from three independent experiments with n= 20 cells per experiment. Scale bar: 10 µm, Inset scale bars: 4 µm.

3.3c: MMP9 activity is important for tubulating lysosomes

Pharmacological inhibition of MMP9 revealed it to be integral for tubulating lysosomes in mouse macrophages (RAW 264.7 and BMDM (M0, M1 and M2). To establish whether MMP9 indeed played a key role, M0 of BMDMs were isolated from MMP9 knockout (KO) mouse and polarized into M0, M1 and M2 macrophages. Murine M0, M1 and M2 (BMDM) macrophages lacking MMP-9 showed highly reduced tubular lysosomes compared to wildtype macrophages (Figure III.6 a-f). This reveals that MMP9 is indeed a critical player for lysosome tubulation.

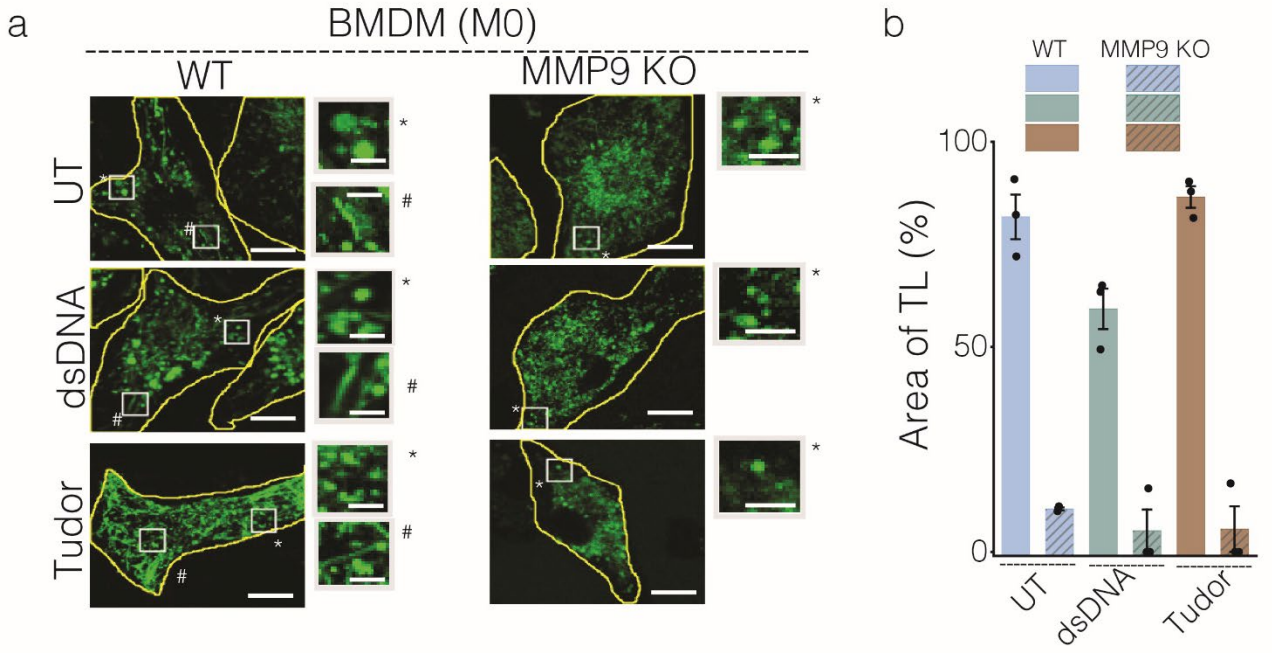

Figure III.6: MMP9 is necessary for tubulation of lysosomes in BMDM

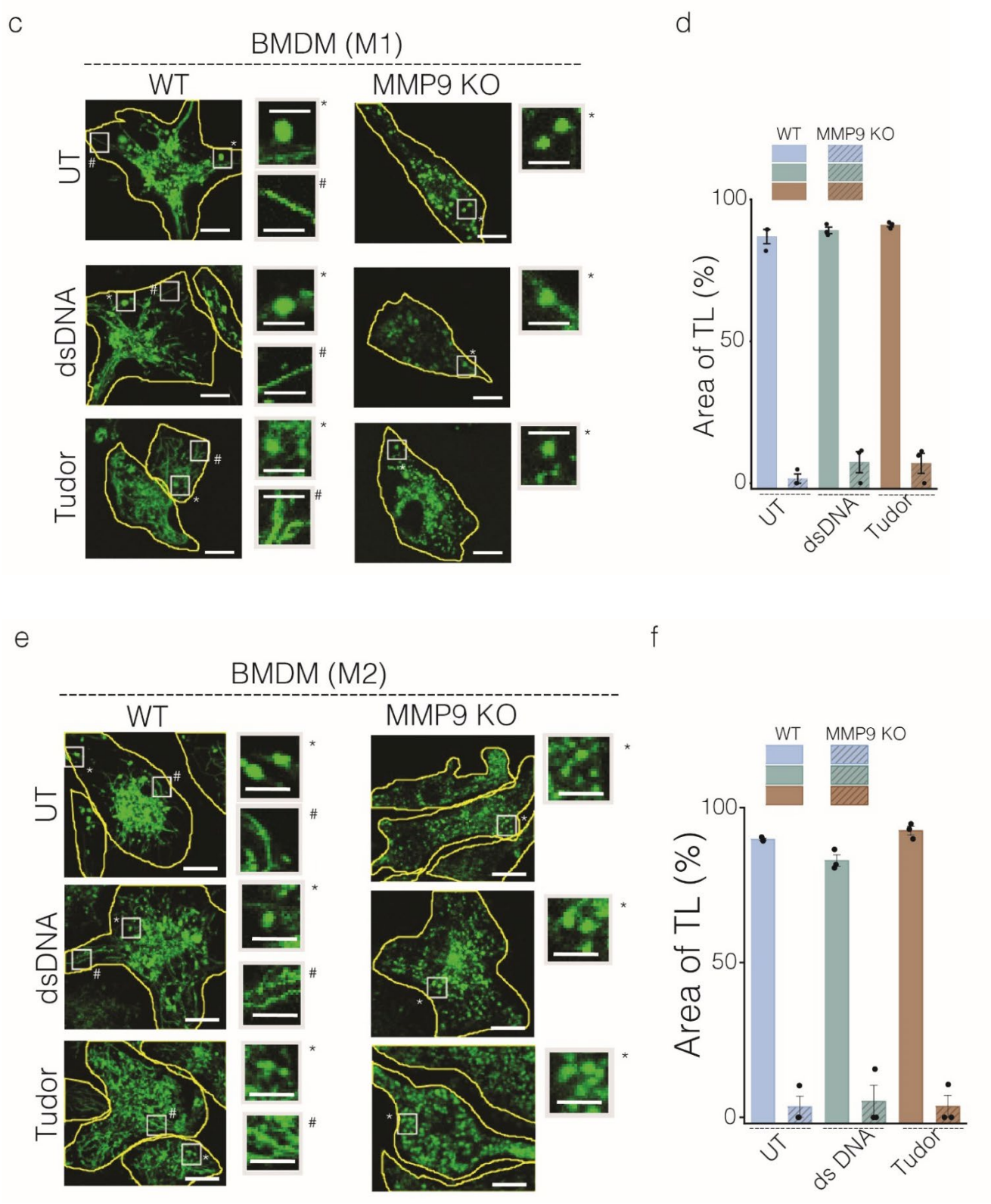

Figure III.6, continued. MMP9 is necessary for tubulation of lysosomes in BMDM. (a, c and e) Representative confocal images in wildtype (WT) and MMP9 knocked out (MMP9 KO) murine

Figure III.6, continued. BMDM M0 (a), M1 (c) and M2 (e) with TMR dextran labeled lysosomes either untreated (UT) or treatment with dsDNA and *Tudor*. Scale bar 10 μm. Inlet showing the zoomed in area shown in the white box with * representing VLs and # representing TLs. (**b,d and f**) Quantification showing Area of TL (%) over total lysosomes for M1 (b), M2 (d) and M3 (f), (n= 45 cells). Error bar represents SEM from three independent experiments.

3.3d: MMP9 expression levels are unaltered by *Tudor* treatment

Tudor triggers tubulation of lysosomes in macrophages via the PI3K-Akt-mTOR axis and involves AMPK, LKB1 and MMP9. Previous studies have shown that activation of PI3K and Akt increases MMP9 expression levels leading to greater MMP9 on the cell surface that in turn further increases MMP9 activity[32]. Alternatively, activation of LKB1- AMPK also increases the expression of MMP9 during autophagy[33]. Our experiments showed that MMP9 activity was essential for lysosome tubulation (Figure III. 3, 5 and 6). and that *Tudor* treatment also increased MMP9 activity (Figure III. 3c). Given that *Tudor* treatment led to a slow increase in tubulation which then reached saturation after 8 hours suggests a potential feedback mechanism for sustained lysosomal tubulation pathway (Figure III.2). We hypothesized that the PI3K-Akt pathway activation could increase the expression levels of MMP9 via an as yet unidentified transcription factor. Such increased expression of MMP9 could lead to to increased release of Pro-MMP9 on to plasma membrane which could then get activated due to interaction with Ku80 of Ku70/80 heterodimer.

MMP9 can be regulated at three steps namely, expression (mRNA); post-translational (cleavage of Pro-MMP9) and activity (mature MMP9 on PM) levels[34]. We therefore probed the involvement of selected transcription factors associated MMP9 transcription. NF-κB is one of the well-studied transcription factors of MMP9[36–38]. Nrf2, a transcription factor for lysosomal genes, can also trnascribe MMP9 by binding to specific sites on the MMP9 promoter during starvation or oxidative stress[33,39]. NF-κB and Nrf2 were chemically inhibited using JSH-23 and ML385 respectively and

scored for formation for tubular lysosomes[40,41]. Both these treatments did not affect the formation of tubular lysosomes (Figure III.7 a, b). Western blots also reinforced that neither NF-κB nor STAT3 were activated upon *Tudor* treatment in primary M0 macrophages of BMDM (Figure III.7c). Taken together these experiments demonstrated that increased activity of MMP9 is not due to increased MMP9 transcription by Nrf2 or NF-κB.

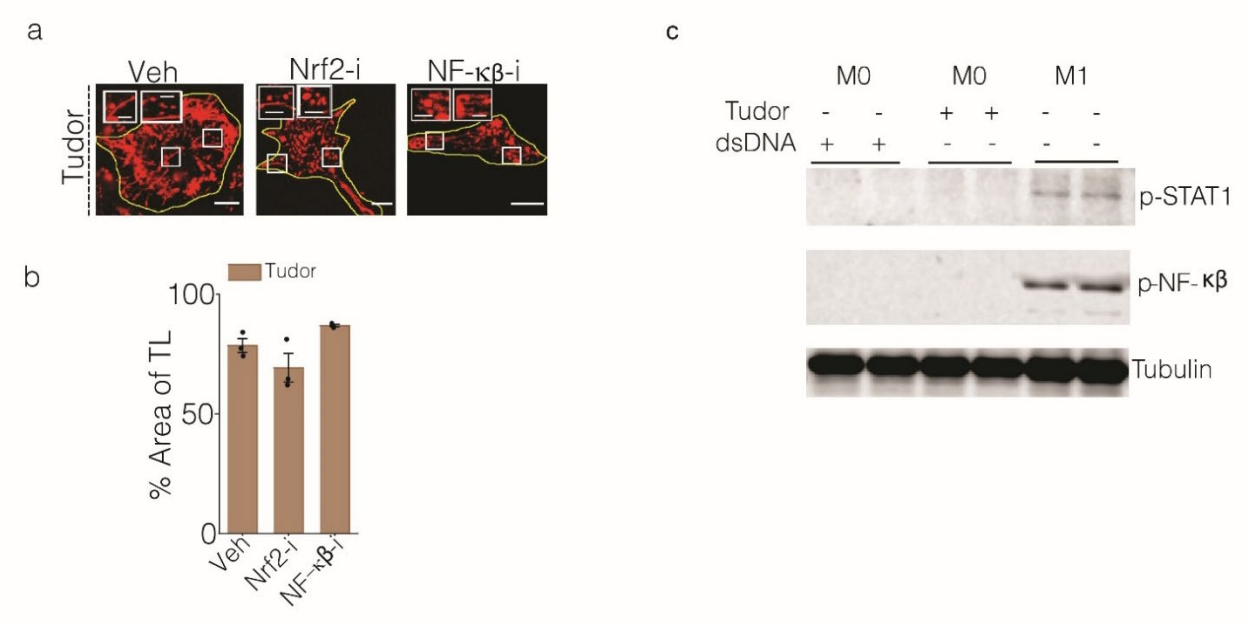

Figure III.7: Nrf2 and NF-κβ activity in *Tudor* treated cells. (a) Representative images of TMR dextran labeled lysosomes in *Tudor* treated RAW 264.7 cells in presence or absence of Nrf2 inhibitor (ML385) or NF-kB inhibitor (JSH-23), (Veh=DMSO). (b) Percentage Area of TLs in the presence or absence of inhibitors. Error bars represent s.e.m from three independent experiments (n =20 cells per experiment). Scale bar: 10 µm; Inset scale bars: 4 µm. (c) Representative western blots of p-STAT1, p-NF-kB and tubulin in M0 BMDM treated with dsDNA or *Tudor* for 24 hours. M1 BMDM are shown as positive control for inflammatory pathway.

To rule out the participation of unknown transcription factors we probed the mRNA levels of MMP9 in untreated, dsDNA and *Tudor* treated cells at 4 hours and 8 hours by RT-PCR. This revealed no change in mRNA levels of MMP-9, suggesting that MMP9 activity is unaffected by transcription when cells are treated with *Tudor*.

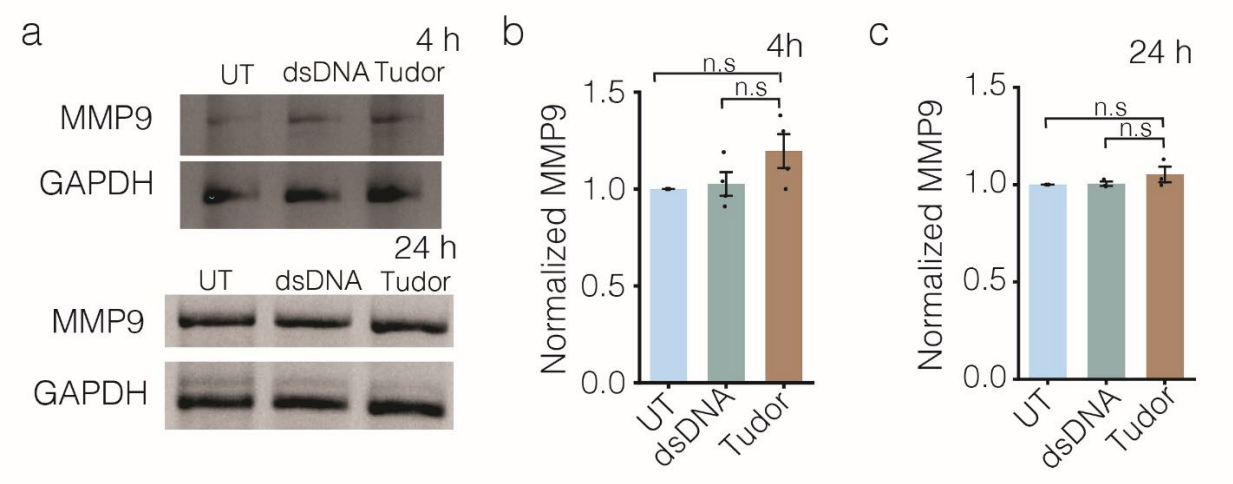

Figure III.8: *Tudor* mediated tubulation of lysosomes do not alter MMP9 expression levels. (**a**) Expression levels of MMP9 in RAW 264.7 cells with or without dsDNA or *Tudor* treatment at indicated times. GAPDH is the loading control. (**b** and **c**) Normalized intensity ratio of MMP9 to GAPDH at (a) 4 h and (b) 24 h (c). n.s: non-significant, (one-way ANOVA with Tukey *post hoc* test). Error bars represents standard error of mean (s.e.m) from three independent experiments.

3.3e: Arl8b is essential for *Tudor* mediated tubulation of lysosomes

The lysosomal motility protein, Arl8b is a small Arf like GTPase which regulates the lysosomal positioning within the cytosol. Arl8b aids in lysosomal movement towards the periphery of the cell by governing the motility of lysosomes towards the "+" end of microtubule by interacting with Kinesin1, through an adapter protein, SKIP[4]. The significance of Arl8b in the formation and movement of LPS triggered TLs has been previously demonstrated [2,7]. We therefore knocked down Arl8b in RAW 264.7 cells by siRNA and assayed for tubular lysosomes formation upon *Tudor* treatment. We found that Arl8b depleted cells showed significantly reduced tubular lysosomes reaffirming that the mechanism of tubulation downstream of PI3K involved the same players as identified for LPS-induced tubulation.

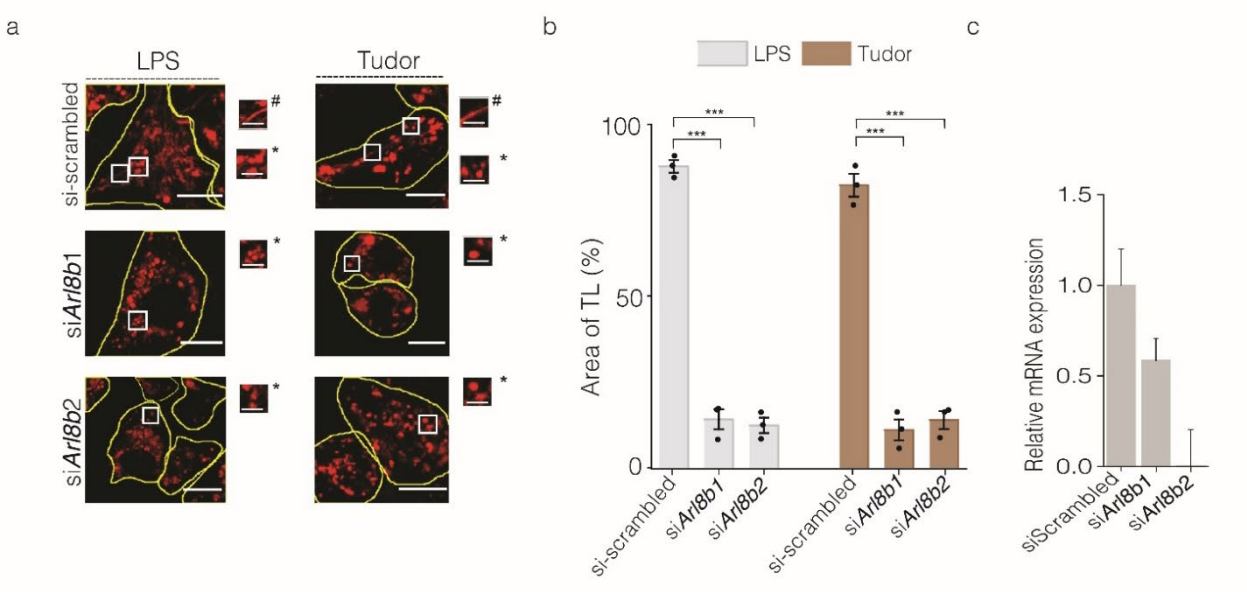

Figure. III.9: Arl8b regulates *Tudor* mediated tubulation of lysosomes. (a) Representative images of TMR dextran labeled lysosomes in *Tudor* or LPS treated RAW 264.7 transfected with siRNA against *Arl8b* (si*Arl8b1* and si*Arl8b2*). Scale bar: 10 µm, with inset scale bar: 4 µm. * in inset represent VLs; # represents TLs. (b) Percentage Area of TLs as a measure of extent of lysosomal tubulation upon *Tudor* and LPS treatment and *Arl8b* knockdown, (n=20 cells). ***$P<$ 0.0005; (one-way ANOVA with Tukey *post hoc* test). (c) Relative mRNA expression levels in RAW 264.7 treated with siRNA against *Arl8b* (si*Arl8b1* and si*Arl8b2*) and scrambled siRNA. Error bars represent s.e.m. from 3 three independent experiments.

3.4 Conclusion

Tudor triggers tubulation of lysosomes via a pathway that shares common protein players with the LPS-mediated tubulation pathway downstream of PI3K. However, unlike LPS, which mediates tubulation through TLR4, *Tudor* mediated tubulation occurs by interacting with plasma-membrane resident Ku70/80. Ku80 interacts with pro-MMP9 at the plasma membrane generating active MMP9. Our studies suggest the potential involvement of an as yet unidentified RTK found at the plasma membrane that could get activated by MMP9 and in turn activated PI3K [24]. The actual mechanism of tubulation still utilizes Arl8b and likely all the partner downstream players.

One of the new players we identified for lysosome tubulation as mediated by *Tudor* or LPS is LKB1. LKB1 activates AMPK which negatively regulates mTOR. In concert with PI3K activation that promotes mTOR activity, this suggests that mTOR activity is stringently controlled to prevent hyperactivation. The participation of inhibitory and activating pathways of mTOR likely prevents runaway activation or complete inhibiton of mTOR.

Importantly lysosomes tubulation absolutely requires MMP9 activity. Interestingly *Tudor* treatment did not show increased transcription of MMP9, suggesting that MMP9 activation is controlled post-transcriptionally. However, the gradual increase of tubulation followed by the sustained tubulation of MMP9 upon *Tudor* treatment suggests the existence of a positive feedback pathway that we address in the subsequent chapter.

3.5 References

1. Vyas JM, Kim Y-M, Artavanis-Tsakonas K, et al. Tubulation of class II MHC compartments is microtubule dependent and involves multiple endolysosomal membrane proteins in primary dendritic cells. *J. Immunol.* 2007;178(11):7199–7210.
2. Saric A, Hipolito VEB, Kay JG, et al. mTOR controls lysosome tubulation and antigen presentation in macrophages and dendritic cells. *Mol. Biol. Cell*. 2016;27(2):321–333.
3. Mrakovic A, Kay JG, Furuya W, Brumell JH, Botelho RJ. Rab7 and Arl8 GTPases are necessary for lysosome tubulation in macrophages. *Traffic*. 2012;13(12):1667–1679.
4. Khatter D, Sindhwani A, Sharma M. Arf-like GTPase Arl8: Moving from the periphery to the center of lysosomal biology. *Cell Logist*. 2015;5(3):e1086501.
5. Li X, Rydzewski N, Hider A, et al. A molecular mechanism to regulate lysosome motility for lysosome positioning and tubulation. *Nat. Cell Biol.* 2016;18(4):404–417.
6. Hipolito VEB, Ospina-Escobar E, Botelho RJ. Lysosome remodelling and adaptation during phagocyte activation. *Cell Microbiol.* 2018;20(4):
7. Kaniuk NA, Canadien V, Bagshaw RD, et al. Salmonella exploits Arl8B-directed kinesin activity to promote endosome tubulation and cell-to-cell transfer. *Cell Microbiol.* 2011;13(11):1812–1823.

8. Pålsson-McDermott EM, O'Neill LAJ. Signal transduction by the lipopolysaccharide receptor, Toll-like receptor-4. *Immunology*. 2004;113(2):153–162.

9. Lin S-C, Hardie DG. AMPK: Sensing Glucose as well as Cellular Energy Status. *Cell Metab.* 2018;27(2):299–313.

10. Silwal P, Kim JK, Yuk J-M, Jo E-K. AMP-Activated Protein Kinase and Host Defense against Infection. *Int. J. Mol. Sci.* 2018;19(11):

11. Zhu YP, Brown JR, Sag D, Zhang L, Suttles J. Adenosine 5'-monophosphate-activated protein kinase regulates IL-10-mediated anti-inflammatory signaling pathways in macrophages. *J. Immunol.* 2015;194(2):584–594.

12. Kumar A, Giri S, Kumar A. 5-Aminoimidazole-4-carboxamide ribonucleoside-mediated adenosine monophosphate-activated protein kinase activation induces protective innate responses in bacterial endophthalmitis. *Cell Microbiol.* 2016;18(12):1815–1830.

13. Shackelford DB, Shaw RJ. The LKB1-AMPK pathway: metabolism and growth control in tumour suppression. *Nat. Rev. Cancer*. 2009;9(8):563–575.

14. Inoki K, Kim J, Guan K-L. AMPK and mTOR in cellular energy homeostasis and drug targets. *Annu. Rev. Pharmacol. Toxicol.* 2012;52:381–400.

15. Gwinn DM, Shackelford DB, Egan DF, et al. AMPK phosphorylation of raptor mediates a metabolic checkpoint. *Mol. Cell*. 2008;30(2):214–226.

16. Yi C-O, Jeon BT, Shin HJ, et al. Resveratrol activates AMPK and suppresses LPS-induced NF-κB-dependent COX-2 activation in RAW 264.7 macrophage cells. *Anat. Cell Biol.* 2011;44(3):194–203.

17. Monferran S, Paupert J, Dauvillier S, Salles B, Muller C. The membrane form of the DNA repair protein Ku interacts at the cell surface with metalloproteinase 9. *EMBO J.* 2004;23(19):3758–3768.

18. Shaw RJ. LKB1 and AMP-activated protein kinase control of mTOR signalling and growth. *Acta Physiol (Oxf)*. 2009;196(1):65–80.

19. Beadnell TC, Nassar KW, Rose MM, et al. Src-mediated regulation of the PI3K pathway in advanced papillary and anaplastic thyroid cancer. *Oncogenesis*. 2018;7(2):23.

20. Song JJ, Kim J-H, Sun BK, et al. c-Cbl acts as a mediator of Src-induced activation of the PI3K-Akt signal transduction pathway during TRAIL treatment. *Cell Signal.* 2010;22(3):377–385.

21. Chan YGY, Cardwell MM, Hermanas TM, Uchiyama T, Martinez JJ. Rickettsial outer-membrane protein B (rOmpB) mediates bacterial invasion through Ku70 in an actin, c-Cbl, clathrin and caveolin 2-dependent manner. *Cell Microbiol.* 2009;11(4):629–644.

22. Arbibe L, Mira JP, Teusch N, et al. Toll-like receptor 2-mediated NF-kappa B activation requires a Rac1-dependent pathway. *Nat. Immunol.* 2000;1(6):533–540.

23. Yamada O, Ozaki K, Akiyama M, Kawauchi K. JAK-STAT and JAK-PI3K-mTORC1 pathways regulate telomerase transcriptionally and posttranslationally in ATL cells. *Mol. Cancer Ther.* 2012;11(5):1112–1121.

24. Castellano E, Downward J. RAS Interaction with PI3K: More Than Just Another Effector Pathway. *Genes Cancer*. 2011;2(3):261–274.

25. Neumann D. Is TAK1 a direct upstream kinase of AMPK? *Int. J. Mol. Sci.* 2018;19(8):

26. Herrero-Martín G, Høyer-Hansen M, García-García C, et al. TAK1 activates AMPK-dependent cytoprotective autophagy in TRAIL-treated epithelial cells. *EMBO J.* 2009;28(6):677–685.

27. Dogliotti G, Kullmann L, Dhumale P, et al. Membrane-binding and activation of LKB1 by phosphatidic acid is essential for development and tumour suppression. *Nat. Commun.* 2017;8:15747.

28. Lan F, Cacicedo JM, Ruderman N, Ido Y. SIRT1 modulation of the acetylation status, cytosolic localization, and activity of LKB1. Possible role in AMP-activated protein kinase activation. *J. Biol. Chem.* 2008;283(41):27628–27635.

29. Martinez JJ, Seveau S, Veiga E, Matsuyama S, Cossart P. Ku70, a component of DNA-dependent protein kinase, is a mammalian receptor for Rickettsia conorii. *Cell*. 2005;123(6):1013–1023.

30. Muller C, Paupert J, Monferran S, Salles B. The double life of the Ku protein: facing the DNA breaks and the extracellular environment. *Cell Cycle*. 2005;4(3):438–441.

31. Monferran S, Muller C, Mourey L, Frit P, Salles B. The Membrane-associated form of the DNA repair protein Ku is involved in cell adhesion to fibronectin. *J. Mol. Biol.* 2004;337(3):503–511.

32. Cheng C-Y, Hsieh H-L, Hsiao L-D, Yang C-M. PI3-K/Akt/JNK/NF-κB is essential for MMP-9 expression and outgrowth in human limbal epithelial cells on intact amniotic membrane. *Stem Cell Res.* 2012;9(1):9–23.

33. Endo H, Owada S, Inagaki Y, Shida Y, Tatemichi M. Glucose starvation induces LKB1-AMPK-mediated MMP-9 expression in cancer cells. *Sci. Rep.* 2018;8(1):10122.

34. Ogata Y, Itoh Y, Nagase H. Steps involved in activation of the pro-matrix metalloproteinase 9 (progelatinase B)-tissue inhibitor of metalloproteinases-1 complex by 4-aminophenylmercuric acetate and proteinases. *J. Biol. Chem.* 1995;270(31):18506–18511.

35. Reinhard SM, Razak K, Ethell IM. A delicate balance: role of MMP-9 in brain development and pathophysiology of neurodevelopmental disorders. *Front. Cell Neurosci.* 2015;9:280.

36. Dorrington MG, Fraser IDC. NF-κB Signaling in Macrophages: Dynamics, Crosstalk, and Signal Integration. *Front. Immunol.* 2019;10:705.

37. Shihab PK, Al-Roub A, Al-Ghanim M, et al. TLR2 and AP-1/NF-kappaB are involved in the regulation of MMP-9 elicited by heat killed Listeria monocytogenes in human monocytic THP-1 cells. *J. Inflamm. (Lond.)*. 2015;12:32.

38. Bond M, Chase AJ, Baker AH, Newby AC. Inhibition of transcription factor NF-kappaB reduces matrix metalloproteinase-1, -3 and -9 production by vascular smooth muscle cells. *Cardiovasc. Res.* 2001;50(3):556–565.

39. Sun Y, Li M, Zhao D, et al. Lysosome activity is modulated by multiple longevity pathways and is important for lifespan extension in C. elegans. *Elife*. 2020;9:

40. Singh A, Venkannagari S, Oh KH, et al. Small Molecule Inhibitor of NRF2 Selectively Intervenes Therapeutic Resistance in KEAP1-Deficient NSCLC Tumors. *ACS Chem. Biol.* 2016;11(11):3214–3225.

41. Shin H-M, Kim M-H, Kim BH, et al. Inhibitory action of novel aromatic diamine compound on lipopolysaccharide-induced nuclear translocation of NF-kappaB without affecting IkappaB degradation. *FEBS Lett.* 2004;571(1-3):50–54.

28. Lan F, Cacicedo JM, Ruderman N, Ido Y. SIRT1 modulation of the acetylation status, cytosolic localization, and activity of LKB1. Possible role in AMP-activated protein kinase activation. J. *Biol. Chem. 2*008;283(41):27628–27635.

29. Martinez JJ, Seveau S, Veiga E, Matsuyama S, Cossart P. Ku70, a component of DNA-dependent protein kinase, is a mammalian receptor for Rickettsia conorii. Ce*ll.* 2005;123(6):1013–1023.

30. Muller C, Paupert J, Monferran S, Salles B. The double life of the Ku protein: facing the DNA breaks and the extracellular environment. Cel*l Cycle. 2*005;4(3):438–441.

31. Monferran S, Muller C, Mourey L, Frit P, Salles B. The Membrane-associated form of the DNA repair protein Ku is involved in cell adhesion to fibronectin. *J. Mol. Biol.* 2004;337(3):503–511.

32. Cheng C-Y, Hsieh H-L, Hsiao L-D, Yang C-M. PI3-K/Akt/JNK/NF-κB is essential for MMP-9 expression and outgrowth in human limbal epithelial cells on intact amniotic membrane. *Stem Cell Res.* 2012;9(1):9–23.

33. Endo H, Owada S, Inagaki Y, Shida Y, Tatemichi M. Glucose starvation induces LKB1-AMPK-mediated MMP-9 expression in cancer cells. *Sci. Rep.* 2018;8(1):10122.

34. Ogata Y, Itoh Y, Nagase H. Steps involved in activation of the pro-matrix metalloproteinase 9 (progelatinase B)-tissue inhibitor of metalloproteinases-1 complex by 4-aminophenylmercuric acetate and proteinases. *J. Biol. Chem.* 1995;270(31):18506–18511.

35. Reinhard SM, Razak K, Ethell IM. A delicate balance: role of MMP-9 in brain development and pathophysiology of neurodevelopmental disorders. *Front. Cell Neurosci.* 2015;9:280.

36. Dorrington MG, Fraser IDC. NF-κB Signaling in Macrophages: Dynamics, Crosstalk, and Signal Integration. *Front. Immunol.* 2019;10:705.

37. Shihab PK, Al-Roub A, Al-Ghanim M, et al. TLR2 and AP-1/NF-kappaB are involved in the regulation of MMP-9 elicited by heat killed Listeria monocytogenes in human monocytic THP-1 cells. J. *Inflamm. (Lond.).* 2015;12:32.

38. Bond M, Chase AJ, Baker AH, Newby AC. Inhibition of transcription factor NF-kappaB reduces matrix metalloproteinase-1, -3 and -9 production by vascular smooth muscle cells. *Cardiovasc. Res.* 2001;50(3):556–565.

39. Sun Y, Li M, Zhao D, et al. Lysosome activity is modulated by multiple longevity pathways and is important for lifespan extension in C. elegans. *Elife*. 2020;9:

Chapter 4. Proteolytic activity in vesicular and tubular lysosomes

4.1 Introduction

4.1a Proteolytic activity in tubular and vesicular lysosomes

Tubulation of lysosomes is crucial for antigen processing and presentation, selective trafficking of lysosomal proteins to plasma membrane, retention of pinocytic cargo and exchange of phagosomal cargo, yet, the precise properties that lysosomes acquire upon adopting the tubular morphology has remained elusive. Essentially, the biochemical distinction between vesicular lysosomes and tubular lysosomes has remained enigmatic. One of the most critical functions of lysosomes is its degradative behavior. Lysosomes, are conventionally thought to be lytic bags housing more than 60 different hydrolases that act to proteolytically digest cargo[1]. Gene expression levels of lipopolysaccharide (LPS) stimulated BMDMs show upregulation of lysosomal hydrolases such as Cathepsins B, S, H, L, V-ATPase etc[2,3]. Various experimental systems have shown differential results, where autophagy-triggered tubular and vesicular lysosomes showed varying proteolytic activity. For example, similar hydrolytic activity was found in both vesicular and tubular lysosomes of larval Drosophila muscle cells while reduced hydrolytic activity was found in tubular lysosomes compared to vesicular ones in normal rat kidney cells[4,5]. Further, the epidermis of *C. elegans* in the molting stage showed similar proteolytic activity in both tubular and vesicular lysosomes yet the overall proteolysis within tubular and vesicular lysosomes was higher compared to lysosomes in cells lacking tubular lysosomes[6]. This suggests that lysosomes might alter their proteolytic activity upon tubulation.

Apart from autophagy, immunostimulation can also trigger tubular lysosome formation in immune cells[7–9]. Tubulation in such a context shows elevates overall lysosomal proteolysis in

macrophages[10]. LPS also stimulates the autophagic response, however its effect on proteolytic activity within tubular lysosomes specifically, is still unclear[11]. Since LPS tubulates lysosomes but is also an immune trigger while *Tudor* tubulates lysosomes without activating immune cells, we sought to carry out a head to head comparison of proteolytic acitivty in vesicular and tubular lysosomes both in an unperturbed scenario as well as during immune activation. We reasoned that this might reveal whether the nature of tubular lysosomes in resting cells and activated cells were different.

Proteolytic activity is also influenced by the lumenal ionic content of lysosomes such as optimal pH. The acidic environment of lysosomes provides the optimal pH for the activity of most lyosomal enzymes[12]. Cathepsin C, one of the most abundant lysosomal enzymes requires a pH of 5.0 for optimal function[13]. When lysosomal enzyme function is disrupted, lysosomes are unable to degrade the cargo into its monomers. This leads to accumulation of cargo within the lysosomal lumen, leading to lysosome storage diseases. One of the reasons for hypoacidification of lysosomal the lumen is seem when chloride ion levels are reduced, which in turn can affect lysosomal calcium levels. Ionic imbalance differentially affect lysosomal enzymes. For example, while Cathepsin C activity can be affected, its upstream activator Cathepsin L can still be functional[14]. Hence it is crucial to understand proteolytic activity in vesicular and tubular lysosomes to study the biochemical differences between tubular lysosomes and vesicular lysosomes.

4.1b Reporters for proteolytic activity

Fluorescence based assays are widely used to study proteolytic activity using caged fluorophores that are pseudo-substrates of lysosomal enzymes. Enzymatic reactions with the caged fluorophores either increase or decrease in fluorescence signal intensity, which is monitored using a fluorimeter or a fluorescence microscope[15–17]. Studying proteolytic activity within native lysosomes is

challenging. One of ways of detecting lysosomal enzyme activity is the use of artificial 4-methylumbelliferyl (4-MU) or fluorescein-based substrates that are specific for given lysosomal enzymes. The cells are lysed and the lysates are subsequently used to cleave the probe-substrates to measure enzymatic activity[18,19]. Alternatively, specific substrates with a caged fluorophore are added to cells that then permeates throughout the cells. Specific lysosomal enzymes cleave the fluorogenic substrates increasing the fluorescence which can be studied using a fluorescence plate reader. Such assays while useful, lacks the spatial information related to the proteolytic activity. Hence, in order to probe the differences in proteolytic activity between tubular and vesicular lysosomes, we must design reporters that can provide spatial information on activity with the resolution of single lysosomes. DNA-based enzyme reporters serves this purpose where a duplex DNA consisting of a normalizing fluorophore that is insensitive to proteolytic activity and second fluorophore that can quantitatively report specific proteolytic activity are covalently attached to the DNA in a precise ratio. Scavenger receptor mediated endocytosis traffics such DNA reporters specifically to lysosomes to enable quantitative measurements.

4.1c Targeting DNA-based reporters for lysosomes

Scavenger receptors (SR) comprise SR classes A-J and are present on the Plasma Membrane of mammalian cells[20,21]. Class A scavenger receptors are homotrimeric proteins with collagen binding activity[21]. There are six members of Class A scavenger receptors; Class A1-A6. SR class A6 is present on the Plasma Membrane of macrophages of peritoneum, lymph node, liver and marginal zone of spleen[20,22,23]. LPS can activate SR class A6 receptor bringing about a pro-inflammatory response[24]. SR-class A1 is associated with phagocytosis by lipid raft dependent mechanisms[20]. DNA uptake in macrophages occurs through interaction of negatively charged DNA backbone with anion ligand binding receptors (ALBRs), also known as scavenger

receptors[25]. DNA nanodeivces such as *I-switch*, *ChloropHluor*, *CalipHluor*, I_m^{LY}, *Voltair* etc. were previously targeted to lysosomes of live mammalian cells as well as *in vivo* in model organisms via scavenger receptor mediated endocytosis[14,26–33].

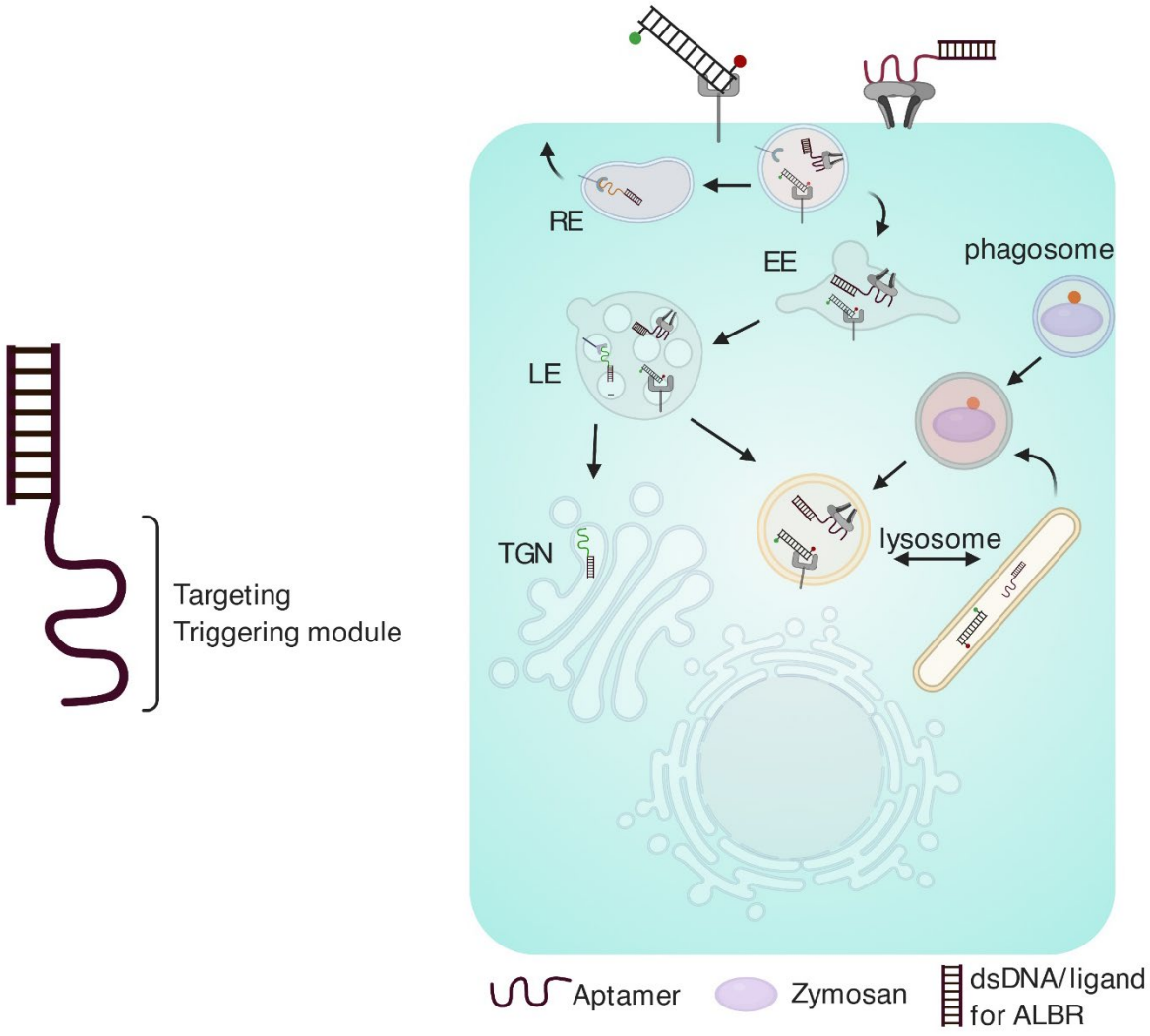

Figure IV.1: Targeting DNA nanodevices to endocytic organelles. Aptamers bind to specific receptors on cell surface and are therefore used to traffic DNA nanodevices into different intracellular compartments; Transferrin aptamer targetw DNA nanodeivces to recycling endosomes (RE); MUC1- aptamer binds to hypo-glycocylated MUC-1 and targets nanodevices to trans-Golgi network (TGN). SA43, aptamer against Ku70/80 stimulates tubular lysosome formation. Thus dsDNA is a ligand for ALBR and hence can be targeted to lysosomes (both vesicular and tubular lysosome). Early endosomes (EE); Late endosomes (LE).

4.2 Materials and methods:

4.2a Oligoneucleotides: Following are the oligoneucleotides used in this study.

Oligo name	Sequence (5'-3')
D1	DBCO-ATCAACACTGCACACCAGACAGCAAGATCCTATATATA
D2	Alexa 647-TATATATAGGATCTTGCTGTCTGGTGTGCAGTGTTGAT

Table 4: DNA sequences used to make Cathepsin C and B reporters

4.2b *Tudor* formation and Lysosomal tubulation (Refer to Chapter 2, Materials and methods, 2.2 b-c, and g).

4.2c DQ^{TM} BSA assay: Alexa 488 conjugated dextran (10 kDa) were used to mark the lysosomes in RAW 264.7. *Tudor* was used to tubulate lysosomes (dsDNA was used as negative control) where cells were treated with 100 nM *Tudor* or dsDNA in complete media followed by pulsed of DQ^{TM}-BSA red (10 µg/ mL) for 10 mins in HBSS. The cells were washed thoroughly in 1X PBS. The washed cells were chased for 30mins in HBSS. Cells were again washed and imaged using a confocal microscope.

4.2e Immunofluorescence of Cathepsins B: Lysosomes in RAW 264.7 macrophages were tubulated as per protocol described above. The cells with fixed for 15 mins in mixture containing 2% PFA, 0.2% GA in 1X PBS at room temperature. 0.1% glycine in 3% BSA in 1X PBS for 5 mins, RT was used quench any unreacted formaldehyde. Cells were washed thoroughly with 1X PBS and permeabilized with 0.2% Triton^{TM} X100 for 5 mins in 1X PBS. Cells were against washed well and blocked in 4% FBS and 3% BSA in 1X PBS for 2 hours. The cells were then incubated with primary Cathepsin B antibody (1:100) (CST 31718, Cell Signaling technology) in above mentioned blocking buffer overnight at 4 °C in a moist chamber. After 5 washed in 1X PBS, cells were incubated with secondary antibody for 1 hour in RT. Again, blocked-in blocking buffer for

2 hours followed by LAMP1 antibody (1:400) (ab24170, Abcam) for 1-hour, RT. After thourgh washing, cells were treated with secondary antibody for 30 mins, RT. Confocal microscopy was used to image these cells.

4.2f Conjugations of azido-Rhodamine110 to DBCO D1 DNA: 5 equivalence of carboxy rhodamine110 azide was mixed with 30 μM of DBCO containing D1 DNA in 10 mM sodium phosphate buffer, pH 7.2. The reaction mixture mixed well with a rice-grain magnetic bead overnight at RT in dark. Ethanol precipitation was used to remove un-incorporated dye. UV spectrophotometer was used to quantify the concentration of DNA and dye in the mixture. 15% denaturing native PAGE was used to confirm the extent of conjugation. Similarly, cathepsin C and B probes were also conjugated to DBCO containing D1 DNA. Purification, quantification and confirmation of conjugation of probes to DNA was performed as mentioned above. Both D1 DNA conjugated with Rhodamine 110 or Cathepsin C/B and Alexa 647N containing D2 oligoneucleotides were annealed as per protocol mentioned above in 1:1 ratio. 12% native PAGE was used to confirm the formation of annealed sensors (Cat_{ON}, Cat_C, Cat_B).

4.2g Cathepsin C/B activity assay: Unlabeled 100 nM *Tudor* was used to tubulate lysosomes in macrophages (cell lines and primary cells). Cells are pulsed with 500 nM Cat_C or Cat_B or Cat_{ON} in Opti-MEM™ for 30 min followed by a chase of 30 mins at 37 °C in complete media. Cells were thoroughly washed and imaged in HBSS using a confocal microscope.

Cat_{OFF} measurement: Cells were treated with Pan Cathepsin inhibitor, 50 μM of E64 inhibitor for 24 hours at 37 °C. This was followed by treatment of either 500 nM of Cat_C or Cat_B in presence of 50 μM of E64 for 30 mins. Cells were washed with 1X PBS followed by a chased for 30 mins in complete media containing 50 μM E64. Cells were imaged in confocal microscopy.

Image analysis for proteolytic activity: Alexa 647 channel is considered to be red (R) (excitation maxima λ_{max} = 650 nm) and Rhodamine 110 as green (G) (excitation maxima λ_{max} = 500 nm). Fiji was used for image analysis. Tubeness plugin in Fiji was used to find any tubular and vesicular structures in the R channel image. The images was then thresholded followed by ROIs for vesicular and tubular lysosomes were obtained from Analyze particles. The ROIs were applied to both G and R images separately. Mean G/R was plotted for each experiment in Cat_{off} (G/R_{min}), Cat_{ON} (G/R_{max}) and real time measurements of activity of either Cat_C or Cat_B (G/R_{probe}) for vesicular and tubular lysosomes. % Response was calculated using the following equation.

$$\% \text{ Response} = \frac{(G/R_{probe} - G/R_{min}}{(G/R_{max} - G/R_{min})} \times 100$$

4. 3 Results and Discussion

4.3a Overall proteolytic activity in vesicular and tubular lysosomes

Tubular lysosomes when triggered by autophagy show lower proteolytic activity as compared to vesicular lysosomes in cultured cell lines while in epidermis of L-4 stage *C. elegans* they show higher proteolytic activity[4,6]. Although muscle cells in *D. melanogaster* showed no change in the overall proteolytic activity in vesicular and tubular lysosomes[5]. Overall proteolytic activity using DQ^{TM} BSA assay in Alexa 488 dextran labeled vesicular and tubular lysosomes in RAW 264.7 macrophages showed that vesicular lysosomes have higher proteolytic activity as compared to tubular lysosomes (Figure. IV.2a, b).

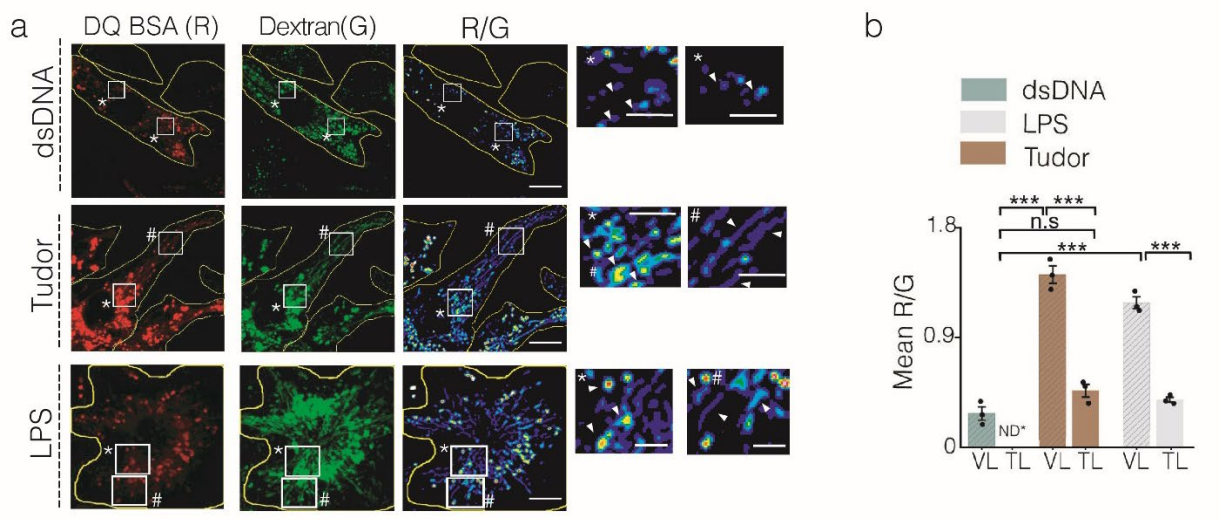

Figure IV.2: Differential hydrolysis in vesicular and tubular lysosomes of RAW 264.7 cells. (a) Representative images of Alexa 488 dextran-labeled lysosomes (G) in RAW 264.7 cells treated with dsDNA, *Tudor* or LPS followed by 10 µg/mL of DQ™ BSA Red (R) with pseudocolored R/G images. Magnified images shown in white box (right). Insets show magnified regions indicated * represents VLs and # represents TLs. Scale bar: 10 µm and inset scale bar: 4 µm. (**b**) Quantification of (a) as mean R/G ratio at single lysosome resolution (n = 50 cells; m = 200 lysosomes).

4.3b Immunofluorescence assay for Cathepsin B

Fixation of tubular lysosomes has been challenging as tubular lysosomes disproportionate into vesicular lysosomes in presence of a range of fixatives. Fixation of tubular lysosomes would prove advantageous for super-resolution microscopy and importantly, to assay the content of various endogenous enzymes with single lysosome resolution. Hence lysosomes in RAW 264.7 macrophages were exposed to several fixatives and we developed a new method mentioned in the table in Figure IV.3 that for the first time preserves the tubular morphology of lysosomes (Figure IV.3 a, b).

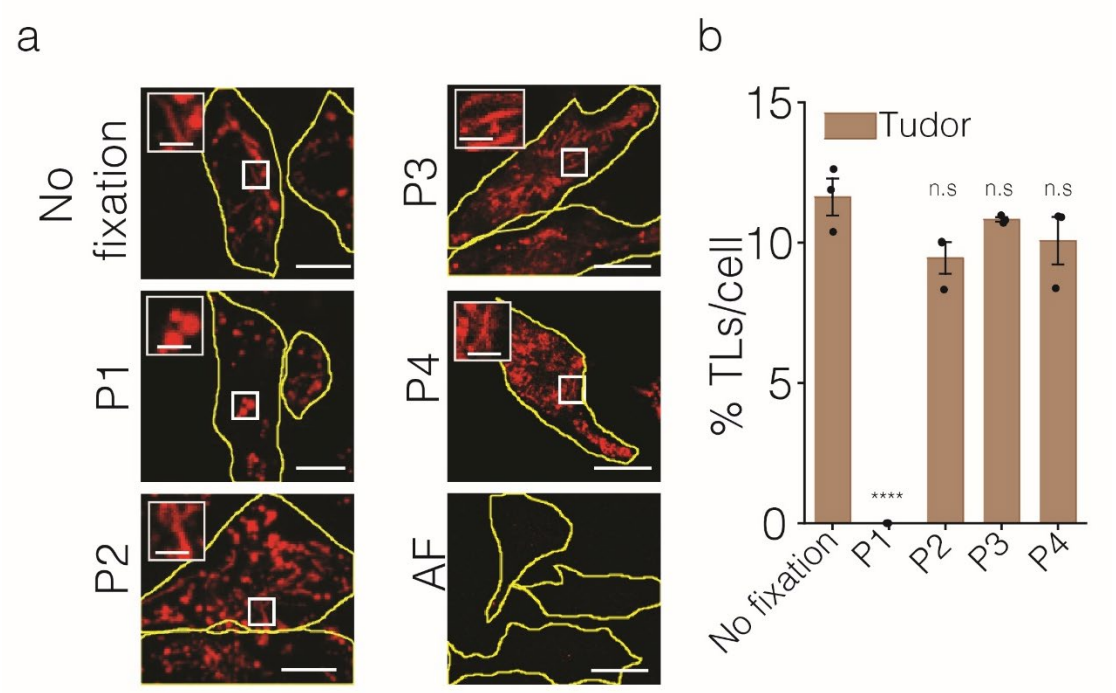

Fixation methods used
P1: 3% Glyoxal
P2: 1% Glyoxal
P3: 0.5% PFA+0.45% GA
P4: 2% PFA+0.2 GA

Figure. IV.3: Fixation protocol for tubular lysosomes. (a) Representative images of TMR dextran labeled lysosomes in RAW 264.7 cells either untreated (no fixation and AF) or fixed using various mentioned fixatives (P1-P4). Insets show magnified regions indicated. Describe bottom table, either use a new panel # or describe as upper and bottom. (b) Percentage TLs/cell upon treatment with various fixative compositions and in un-fixed cells (n = 20 cells). ****P< 0.0005 (one-way ANOVA with Tukey *post hoc* test), n.s: non-significant. Error bar represents s.e.m from three independent experiments. AF: Autofluorescence. Scale bar: 10 µM, with inset scale bar: 4 µm.

4.3b.1 Relative abundance of cathepsin B in vesicular and tubular lysosomes

Tudor and LPS treated cells were tested for their overall proteolytic activity levels by a DQ^{TM} BSA assay and proteolysis was found to be higher in vesicular lysosomes. This could be due to the differential distribution of Cathepsins between vesicular and tubular lysosomes. In order to test this hypothesis, vesicular and tubular lysosomes were probed for the endogenous levels of Cathepsin B enzymes (CTB). Immunofluorescence for CTB in dsDNA, *Tudor* and LPS treated

RAW 264.7 macrophages revealed that CTB was uniformly distributed across vesicular and tubular lysosomes irrespective of *Tudor* or LPS treatments (Figure IV.4 a, b).

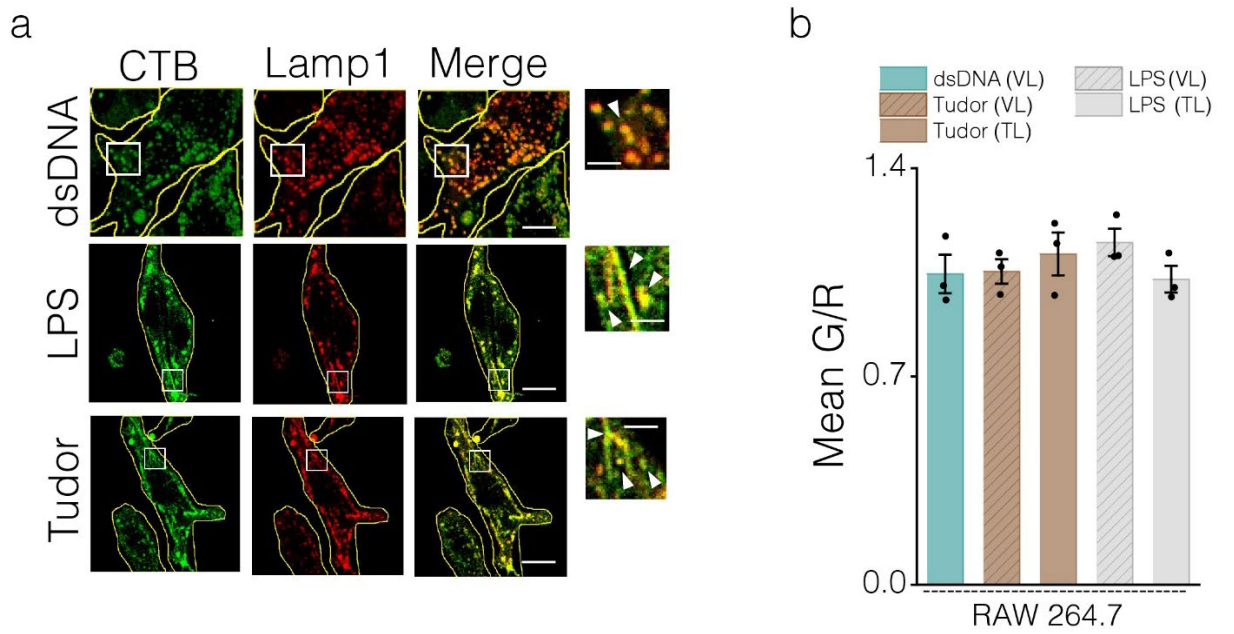

Figure IV.4: Cathepsin B levels in vesicular and tubular lysosomes. (**a**) Representative images of RAW 264.7 immunostained for CTB (green) and LAMP1 (red) upon treatment with dsDNA, *Tudor* and LPS. Magnified images are shown in white box (right). (**b**) Mean G/R plot showing fluorescence intensity from immunofluorescence of Cathepsin B (G) and LAMP1 (R) in presence of dsDNA, *Tudor* and LPS (n=15 cells) in RAW 264.7. Error bar represents s.e.m from three independent experiments. AF: Autofluorescence. Scale bar: 10 µM, with inset scale bar: 4 µm.

4.3c Targeting DNA nanodevices to lysosomes of BMDM

Since dsDNA consists of negatively charged phosphate backbone and is the ligand for ALBR (Class 2A Scavenger Receptors), it is targeted to lysosomes in several mammalian cell types and *in vivo* in model organisms[14,26,29–31]. DNA is trafficked to lysosomes by receptor mediated endocytosis[27,31,33]. Endocytic maturation is time dependent and hence the movement of endocytosed cargo can be precisely monitored as a function of time in concert with specific markers of the various endosomal stages of maturation[27,33]. In order to study the time taken by dsDNA to reach lysosomes of primary BMDMs, lysosomes in these cell types were marked with

TMR-dextran. Cells were pulsed for 30 minutes and chased in complete media over different time points. Murine primary macrophages, BMDM (M0, M1 and M2) were shown to uptake dsDNA at 30 mins of pulse and 30 mins of chased since it showed PCC of ≥ 0.8 at 30 mins of chase time (Figure IV.5 a-f).

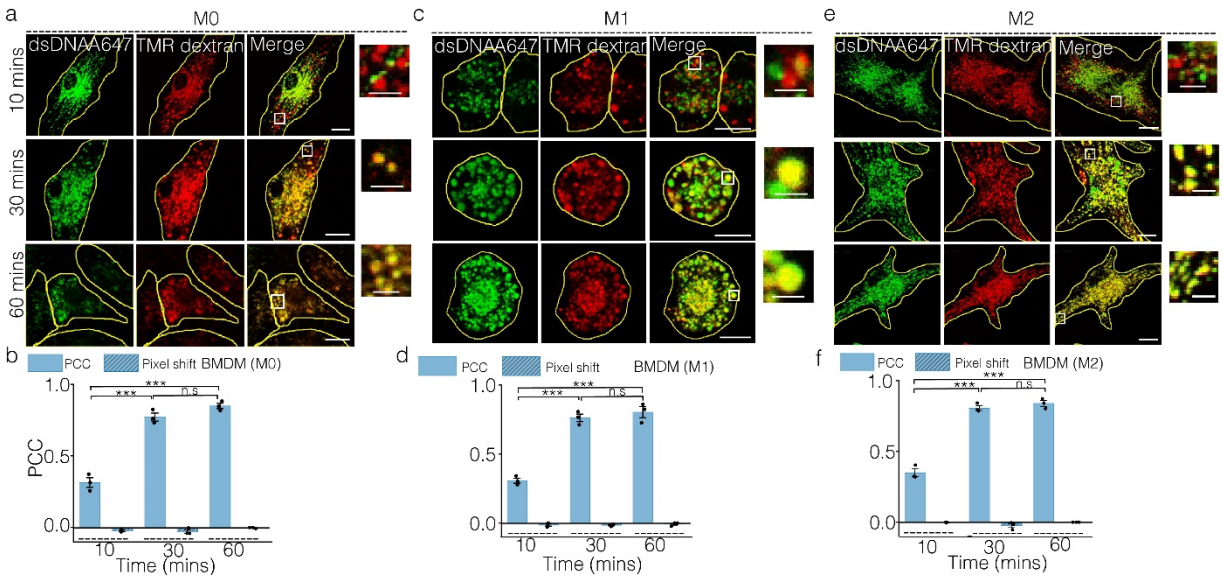

Figure IV.5: **Time dependent colocalization of dsDNA with lysosomes in BMDM**. Representative images of TMR dextran labeled lysosomes colocalized with dsDNA-A647 at different chase times of 10 mins; 30 mins and 60 mins in M0 (a); M1 (c) or M2 (e) BMDMs. Pearson's correlation coefficient (PCC) and pixel shift measured at each indicated chase time for M0 (b); M1 (d) and M2 (f). Images and data represented from three independent experiments and error bars represent s.e.m (n = 12 cells per experiment). ***P< 0.0005 (one-way ANOVA with Tukey *post hoc* test), n.s: non-significant. Scale bar: 10 µm. Inset scale bar: 4 µm.

4.3d: DNA based proteolytic activity measurements

4.3d.1 DNA based Cathepsin C reporter design and activity measurements in vesicular and tubular lysosomes

DQ^{TM} BSA degradation assay revealed the overall proteolytic activity within tubular lysosomes is lower compared to vesicular lysosomes (Figure. IV.2). Autophagy-stimulated tubules lack cathepsins B, D and acid phosphatase[4]. However in our hands, immunofluorescence of CTB showed uniform distribution in both vesicular and tubular lysosomes (Figure IV.4). We therefore

tested whether this differential proteolytic activity between vesicular and tubular lysosomes is due to differences in activity of cathepsin C (CTC), an of the abundant lysosomal cysteine protease. CTC is a well studied lysosomal cathepsin which strongly relies on the lysosomal lumenal ionic environment for its activity.

To study CTC activity, a previously reported DNA-based CTC reporter (Cat_C) was used[33]. Cat_C consists of two modules namely, (i) sensing module made of azido Rhodamine 110 is caged by a CTC cleavable motif namely a Gly-Phe dipeptide and a (ii) ratiometric module comprising of Alexa 647N (denoted as R) which is insensitive to enzymatic treatment or ion levels (Figure. IV.6a). Lysosomal CTC cleaves the N-terminus of Gly-Phe dipeptide, uncages Rhodamine 110 and enhances its fluorescence (denoted as G). DNA-based Cathepsin C ON probe (Cat_{ON}) consists of azido-Rhodamine 110 denoted as G, and Alexa 647N as R (Figure. IV.6a). Cat_{ON} reporter provides the measure of the maximum fluorescence signal for 100% cleaved reporter and provides the maximum attainable G/R ratio. Cat_C in presence of E64 (a pan cathepsin inhibitor) shows the lowest or basal cleavage of Cat_C reporter, therefore provides minimum G/R ratio. The perentage response of CTC activity within the vesicular and tubular lysosomes upon different treatments was quantified as described in Methods section at single lysosome resolution. CTC reporter in vesicular and tubular lysosomes of both cell lines (RAW 264.7) and murine primary macrophages (BMDM [M0, M1 and M2]) showed similar results as seen in the overall proteolytic activity levels given by the DQ™ BSA assay, Here too, vesicular lysosomes showed higher cathepsin C activity as compared to tubular lysosomes (Figure IV.7a-c and Figure IV.8a-f).

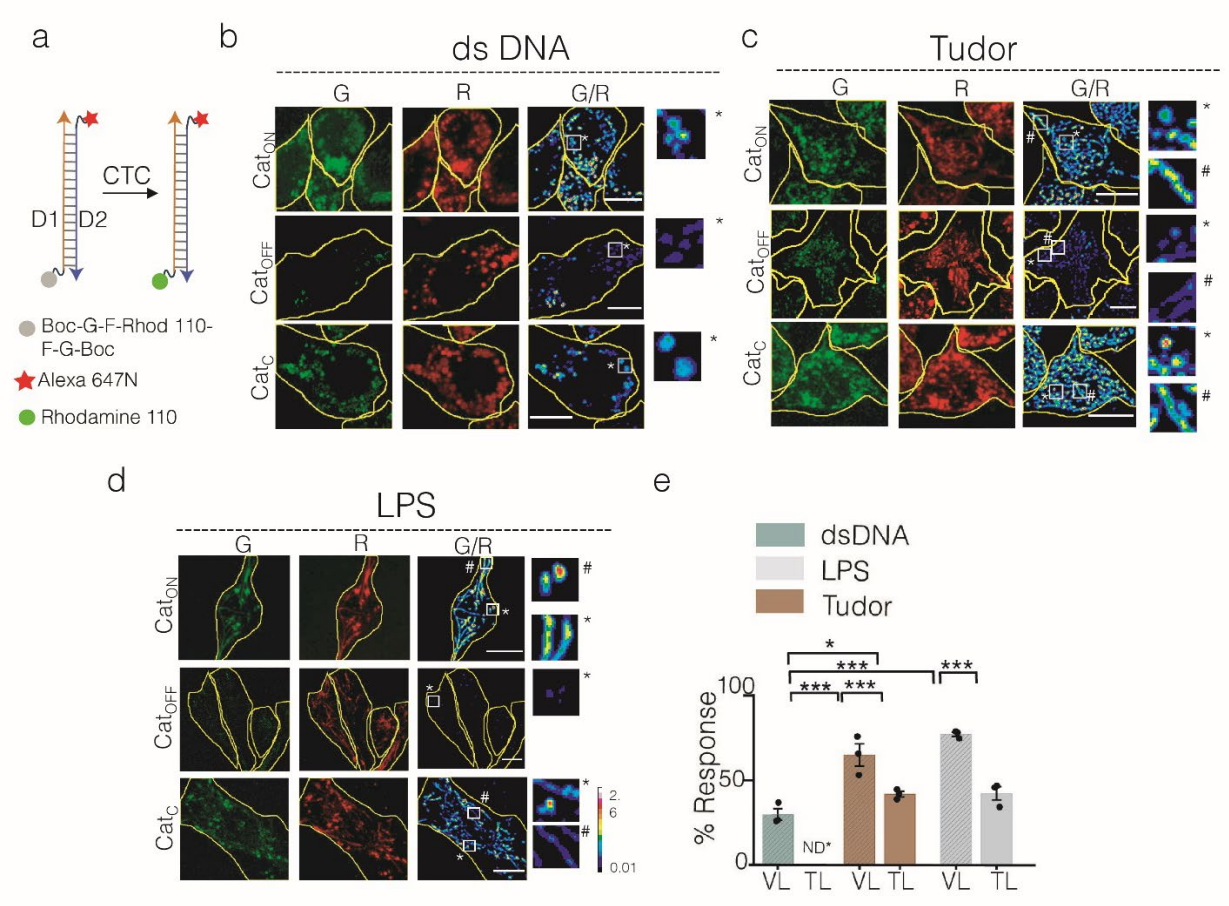

Figure IV.6: Cathepsin C activity in vesicular and tubular lysosomes in RAW 264.7. (**a**) Schematic of DNA based CTC activity reporter consisting of DNA duplex (orange and blue ladder) with sensing module (caged Rhodamine 110, grey) and normalizing module (Alexa 647N, red) and cleaved or always on module (Rhodamine 110, green). (b-d) Representative images of lysosomes in (b) dsDNA; (c) *Tudor* or (d) LPS treated RAW 264.7 cells labeled with CTC reporters (Cat_{ON} Cat_C and Cat_{OFF}) with or without E64 with pseudocolored G/R images of CTC activity reporter. Magnified images of the white boxed region (right). (**e**) Quantification of (b, c and d) as % response of CTC reporter in VLs and TLs in dsDNA, *Tudor* and LPS treated cells (n =50 cells, m=500 lysosomes). ***P< 0.0005 (one-way ANOVA with Tukey *post hoc* test), n.s: non-significant. Error bars represent standard error of mean (s.e.m). VLs (*) and TLs (#), Scale bar: 10 µm.

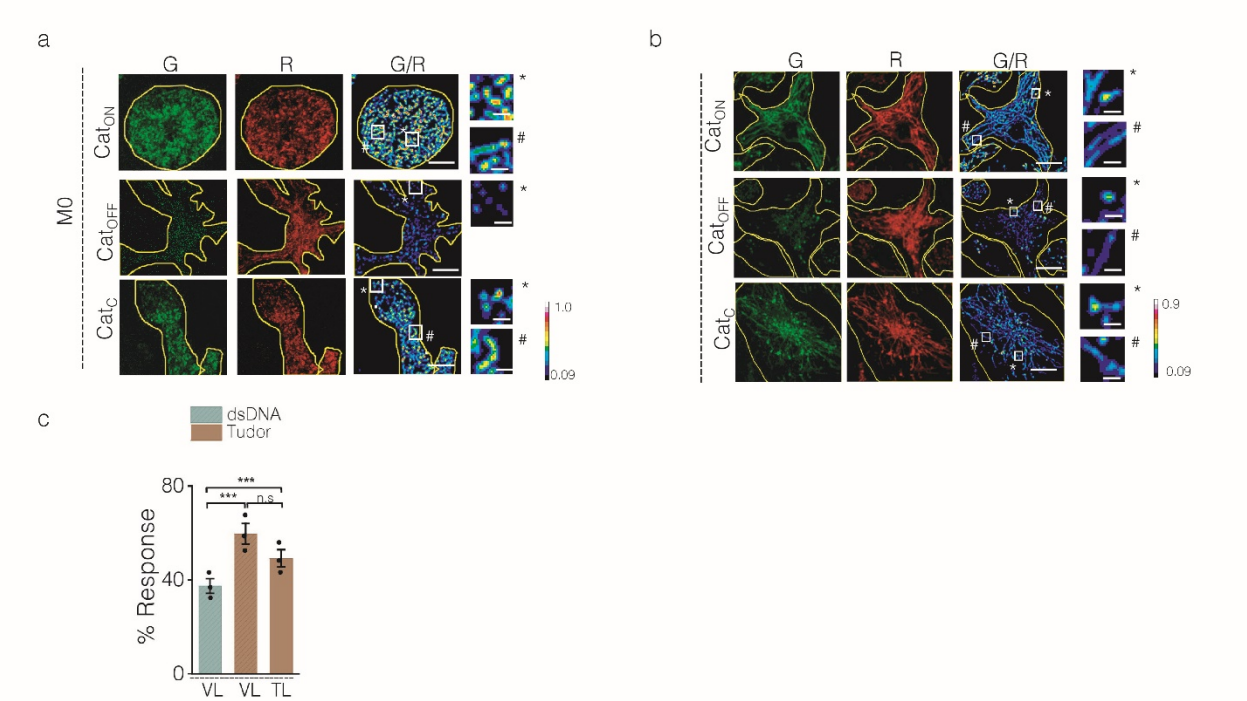

Figure IV.7: Cathepsin C activity in vesicular and tubular lysosomes in BMDM (M0). (**a**) Representative images of lysosomes in (a) dsDNA; (b) *Tudor* in BMDM (M0) cells labeled with CTC reporters (Cat_{ON} Cat_C and Cat_{OFF}) with or without E64 with pseudocolored G/R images of CTC activity reporter. Magnified images of the white boxed region (right). Quantification of (a and b) as % response in VLs and TLs of dsDNA and *Tudor* treated cells (n =50, m=500 lysosomes), *P< 0.05; ***P< 0.0005 (one-way ANOVA with Tukey *post hoc* test); n.s: non-significant. ND: not defined. White arrowheads show VLs (*) and TLs (#). Error bars represents standard error of mean (s.e.m) from three independent experiments. Scale bars: 10 µm; inset scale bars: 4 µm.

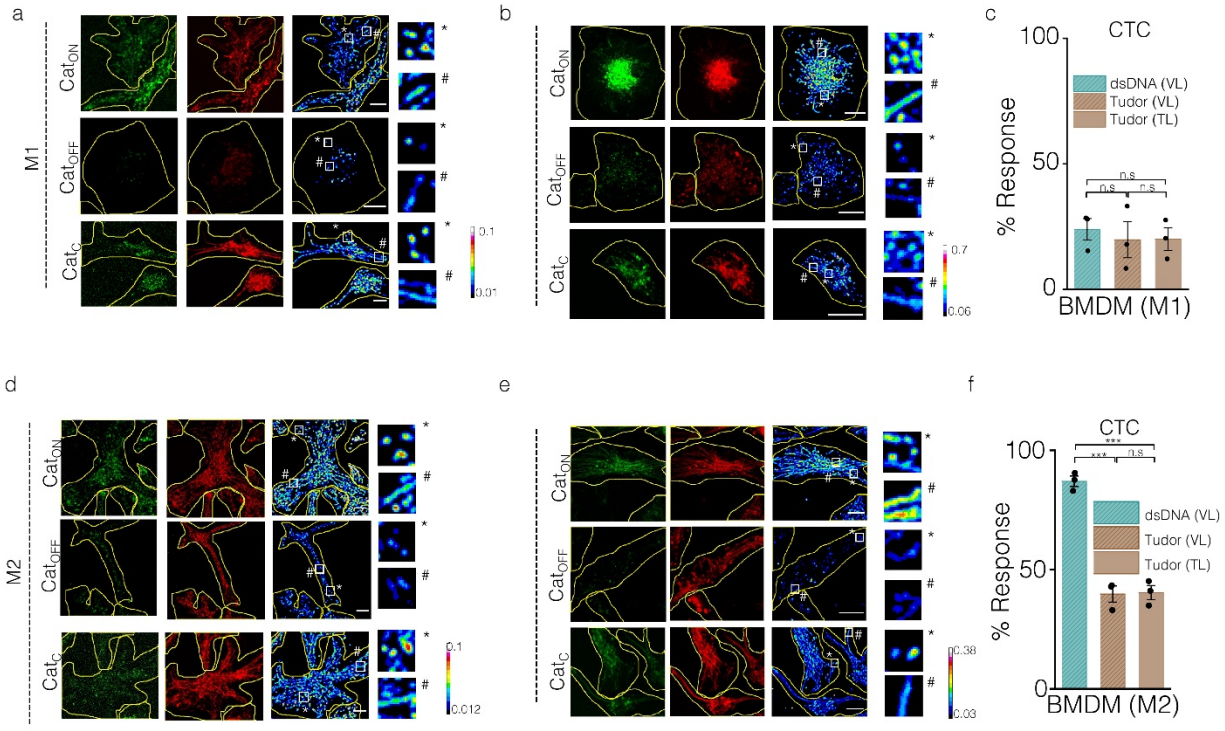

Figure IV.8: Cathepsin C activity in RAW 264.7 and BMDMs. (a) Representative images of lysosomes in (a) dsDNA and (b) *Tudor* treated BMDM (M1 and M2) cells labeled with CTC reporters (Cat_{ON} Cat_C and Cat_{OFF}) with or without E64. CTC activity measurement in dsDNA or *Tudor* treated BMDM (a and b) for M1 and (d and e) for M2. Inset shown in white box with * representing VLs and # represent TLs. (c, f) Quantification of % response of CTC in VLs and TLs upon treatment with dsDNA and *Tudor* in M1 and M2 BMDM respectively. All data obtained from three independent experiments with error representing s.e.m (n = 50 cells, m= 500 endosomes). ***P< 0.0005 (one-way ANOVA with Tukey *post hoc* test), n.s: non-significant. Scale bar: 10 µm. Inset scale bar: 4 µm.

4.3d.2 Cathepsin B activity levels in vesicular and tubular lysosomes

Cathepsin B (CTB) is an abundant lysosomal cysteine protease. Immunofluorescence of CTB revealed a uniform distribution of CTB across both vesicular and tubulay lysosomes. DNA based proteolytic activity reporters can be used to detect the activity of specific enzymes within the lumen of lysosomes. If the proteolytic activity is driven by the bio-availability of the enzyme present within the lysosomes then CTB activity should be similar within the lumens of vesicular and

tubular lysosomes. We found that the DNA-based CTB proteolytic activity based reporter revealed insignificant differences in the proteolytic activity of CTB in vesicular and tubular lysosomes of *Tudor* treated macrophages. The DNA-based CTB reporter (Cat_B) shares similar detection principles as the Cat_C reporter. Cat_B probe contains a different peptide substrate which is specific to Cathepsin B. Similar to Cat_C substrate contains a caged Rhodamine 110 that is susceptible to cleavage by Cathepsin B protease[33] (Refer to 4.3d, CTC proteolytic activity probe design). The substrate sequence used for Cat_B reporter is a Phe-Lys dipeptide which, upon cleavage by CTB within lysosomes uncages Rhodamine 110 fluorescence. Conjugation was confirmed by denaturing PAGE. D1 strand displaying caged Rhodamine 110 on Phe-Lys is annealed with D2 DNA displaying Alexa 647N (Figure IV.9). The reporter is targeted to lysosomes of macrophages by scavenger mediated endocytosis. The ratio of G/R provides the measure of CTB activity within lysosomes. DNA based Cat_B measurement revealed no significant changes between in vesicular and tubular lysosomes in RAW 264.7 and BMDM M0, M1 and M2 macrophages.

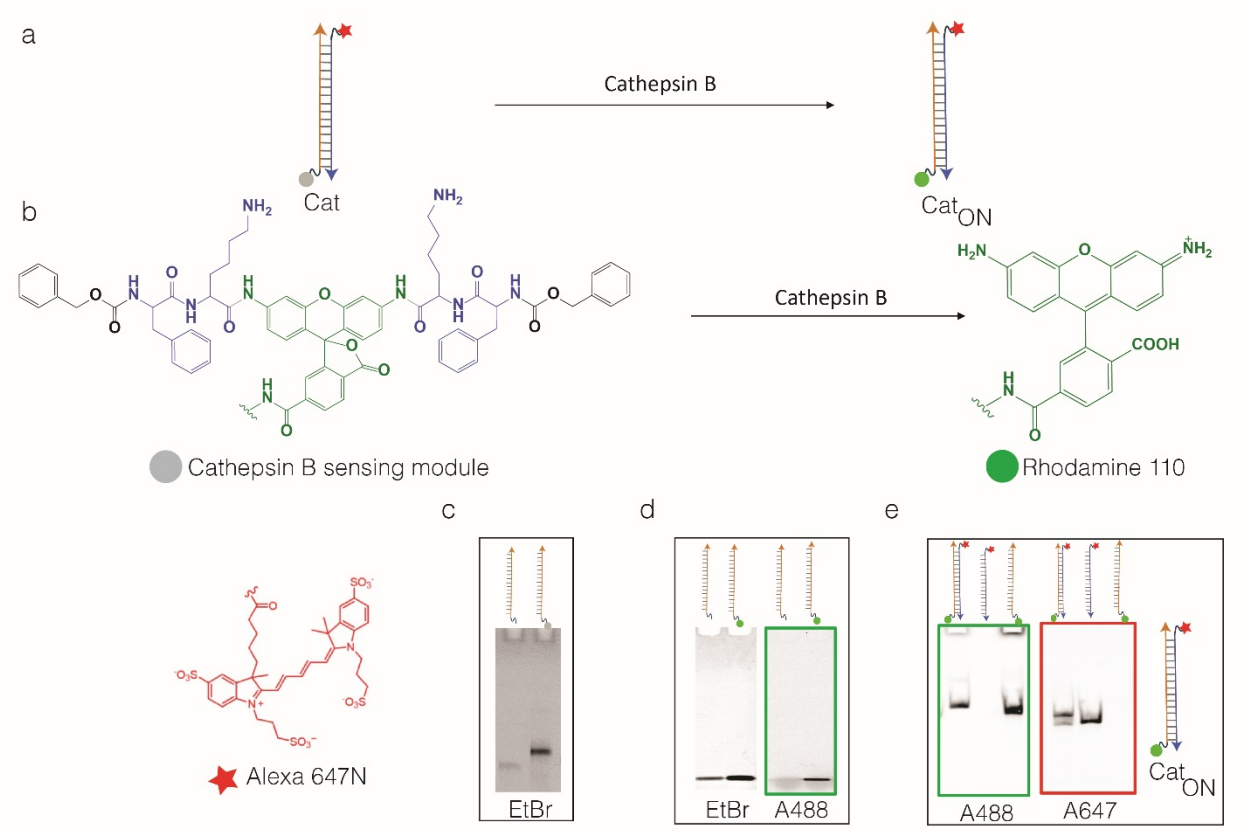

Figure IV.9: **Schematic and characterization of DNA based CTB reporter.** (**a**) Structure of CTB reporter containing ds DNA (orange and blue strands) consisting of sensing module (grey) and a normalizing module (red). (**b**) Sensing module for CTB activity reporter consists of Rhodamine 110 dye (green) protected by Phe-Lys motifs (blue) with amine protecting carboxybenzyl group (black). CTB cleaves the sensing motif uncaging rhodamine 110 and causing rhodamine 110 highly fluorescent (Cat_{ON}). (**c**) 18% Denaturing PAGE showing the conjugation of azido caged Rhodamine 110 to Dibenzocyclooctyl (DBCO) DNA (orange strand) with lane 1: DBCO-DNA; Lane 2: DBCO DNA conjugated to Azido caged rhodamine110 shown in EtBr channel. (**d**) 12% Denaturing PAGE showing the conjugation of azide containing rhodamine 110 and DBCO-DNA in EtBr and Alexa 488 channels with Lane 1: DBCO-DNA and Lane 2: Mixture of DBCO-DNA and azide-rhodamine 110. (**e**) Native PAGE (12%) showing the formation of Cat_{ON} reporter. Lane 1: DBCO-DNA and Azide-rhodamine conjugate; lane 2: Alexa 647N DNA and Lane 3: anneal product of equimolar concentration of both rhodamine 110 and Alexa 647N dye containing DNA shown in Alexa 488 and Alexa 647 channels and merge of both channels.

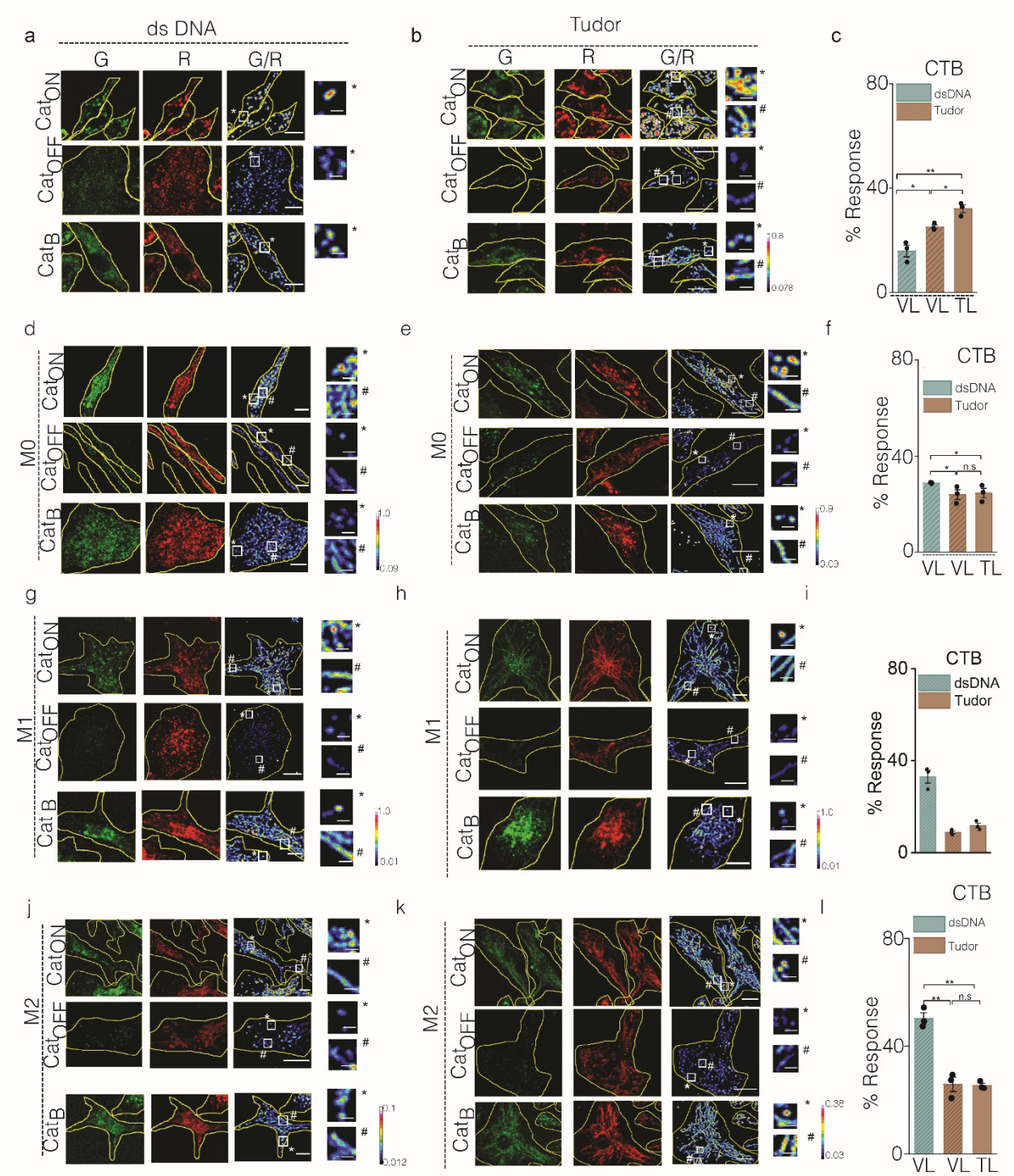

Figure IV.10: Cathepsin B activity in vesicular and tubular lysosomes in macrophages. (a and b) representative images of RAW 264.7 with lysosomes labeled with dsDNA and Tudor followed by treatment of Cat_{ON}, Cat_{OFF} and Cat_B (cathepsin B reporter) with pseudocolored G/R images of cells in Rhodamine 110 (G) and Alexa 647N (R) channels with insets shown on right. *

Figure IV.10, continued. represents VL and # represent TL. Scale bar : 10 µm and inset scale bar: 4 µm. (c, f, I and j) quantification showing % response of (a and b) in Raw 264.7; (d and e) in BMDM (M0); (g and h) M1 and (j and k) in M2 macrophages. All data obtained from three independent experiments with error representing s.e.m (n = 50 cells, m= 500 endosomes). ***P< 0.0005 (one-way ANOVA with Tukey *post hoc* test), n.s: non-significant.

4.4 Conclusion

Proteolytic degradation of cargo is one of the key functions of lysosomes driven by the hydrolytic enzymes present within its lumen[34]. Both *Tudor* and LPS induced tubular lysosomes showed overall lower proteolysis as compared to their vesicular counterparts. Immunofluorescence revealed that endogenous CTB was uniformly abundant across both vesicular and tubular lysosomes regardless of whether tubulation was induced by *Tudor* or LPS treatments. However, CTC activity in vesicular lysosomes was higher when compared to tubular lysosomes. In contrast, proteolytic differences based on CTB activity were insignificant, suggesting that the activity of specific enzymes are reduced within tubular lysosomes. These experiments also showed no biochemical differences between tubular lysosomes that were generated by LPS or *Tudor* treatment. Our experiments show that overall proteolytic activity within tubular lysosomes is lowere than in vesicular lysosomes, despite there being no discernable differences in lysosomal enzyme content. This can be further linked to lower enzymatic activity of specific enzymes and not a blanket overall reduction of the activity of all enzymes. This suggests that activity differences could arise due to differential ionic environment within vesicular and tubular lysosomes, which will be addressed in the next chapter.

4.5 References

1. Lawrence, R. E. & Zoncu, R. The lysosome as a cellular centre for signalling, metabolism and quality control. *Nat. Cell Biol.* **21,** 133–142 (2019).
2. Creasy, B. M. & McCoy, K. L. Cytokines regulate cysteine cathepsins during TLR responses. *Cell Immunol.* **267,** 56–66 (2011).
3. Cooper, P. H., Mayer, P. & Baggiolini, M. Stimulation of phagocytosis in bone marrow-derived mouse macrophages by bacterial lipopolysaccharide: correlation with biochemical and functional parameters. *J. Immunol.* **133,** 913–922 (1984).
4. Yu, L. *et al.* Termination of autophagy and reformation of lysosomes regulated by mTOR. *Nature* **465,** 942–946 (2010).
5. Murakawa, T., Kiger, A. A., Sakamaki, Y., Fukuda, M. & Fujita, N. An Autophagy-Dependent Tubular Lysosomal Network Synchronizes Degradative Activity Required for Muscle Remodeling. *BioRxiv* (2020). doi:10.1101/2020.04.15.043075
6. Miao, R., Li, M., Zhang, Q., Yang, C. & Wang, X. An ECM-to-Nucleus Signaling Pathway Activates Lysosomes for C. elegans Larval Development. *Dev. Cell* **52,** 21–37.e5 (2020).
7. Mrakovic, A., Kay, J. G., Furuya, W., Brumell, J. H. & Botelho, R. J. Rab7 and Arl8 GTPases are necessary for lysosome tubulation in macrophages. *Traffic* **13,** 1667–1679 (2012).
8. Hipolito, V. E. B. *et al.* Enhanced translation expands the endo-lysosome size and promotes antigen presentation during phagocyte activation. *PLoS Biol.* **17,** e3000535 (2019).
9. Saric, A. *et al.* mTOR controls lysosome tubulation and antigen presentation in macrophages and dendritic cells. *Mol. Biol. Cell* **27,** 321–333 (2016).
10. Gray, M. A. *et al.* Phagocytosis enhances lysosomal and bactericidal properties by activating the transcription factor TFEB. *Curr. Biol.* **26,** 1955–1964 (2016).
11. Yuan, H. *et al.* LPS-induced autophagy is mediated by oxidative signaling in cardiomyocytes and is associated with cytoprotection. *Am. J. Physiol. Heart Circ. Physiol.* **296,** H470–9 (2009).
12. Yadati, T., Houben, T., Bitorina, A. & Shiri-Sverdlov, R. The ins and outs of cathepsins: physiological function and role in disease management. *Cells* **9,** (2020).
13. Qiu, G.-F., Feng, H.-Y. & Yamano, K. Expression and purification of active recombinant cathepsin C (dipeptidyl aminopeptidase I) of kuruma prawn Marsupenaeus japonicus in insect cells. *J. Biomed. Biotechnol.* **2009,** 746289 (2009).
14. Chakraborty, K., Leung, K. & Krishnan, Y. High lumenal chloride in the lysosome is critical for lysosome function. *Elife* **6,** e28862 (2017).

15. Wang, Y. *et al.* Lysosome-Targeting Fluorogenic Probe for Cathepsin B Imaging in Living Cells. *Anal. Chem.* **88,** 12403–12410 (2016).

16. Li, J. *et al.* Substrate optimization for monitoring cathepsin C activity in live cells. *Bioorg. Med. Chem.* **17,** 1064–1070 (2009).

17. Gumpper, K., Sermersheim, M., Zhu, M. X. & Lin, P.-H. Skeletal muscle lysosomal function via cathepsin activity measurement. *Methods Mol. Biol.* **1854,** 35–43 (2019).

18. van Es, H. H., Veldwijk, M., Havenga, M. & Valerio, D. A flow cytometric assay for lysosomal glucocerebrosidase. *Anal. Biochem.* **247,** 268–271 (1997).

19. Yu, C., Sun, Q. & Zhou, H. Enzymatic screening and diagnosis of lysosomal storage diseases. *N Am J Med Sci (Boston)* **6,** 186–193 (2013).

20. Zani, I. A. *et al.* Scavenger receptor structure and function in health and disease. *Cells* **4,** 178–201 (2015).

21. Gowen, B. B., Borg, T. K., Ghaffar, A. & Mayer, E. P. The collagenous domain of class A scavenger receptors is involved in macrophage adhesion to collagens. *J. Leukoc. Biol.* **69,** 575–582 (2001).

22. PrabhuDas, M. R. *et al.* A consensus definitive classification of scavenger receptors and their roles in health and disease. *J. Immunol.* **198,** 3775–3789 (2017).

23. Canton, J., Neculai, D. & Grinstein, S. Scavenger receptors in homeostasis and immunity. *Nat. Rev. Immunol.* **13,** 621–634 (2013).

24. Kraal, G., van der Laan, L. J., Elomaa, O. & Tryggvason, K. The macrophage receptor MARCO. *Microbes Infect.* **2,** 313–316 (2000).

25. Miyatake, S. *et al.* Scavenger Receptor Class A1 Mediates Uptake of Morpholino Antisense Oligonucleotide into Dystrophic Skeletal Muscle. *Mol. Ther. Nucleic Acids* **14,** 520–535 (2019).

26. Narayanaswamy, N. *et al.* A pH-correctable, DNA-based fluorescent reporter for organellar calcium. *Nat. Methods* **16,** 95–102 (2019).

27. Saminathan, A. *et al.* A DNA-based voltmeter for organelles. *Nat. Nanotechnol.* (2020). doi:10.1038/s41565-020-00784-1

28. Leung, K., Chakraborty, K., Saminathan, A. & Krishnan, Y. A DNA nanomachine chemically resolves lysosomes in live cells. *Nat. Nanotechnol.* **14,** 176–183 (2019).

29. Surana, S., Bhat, J. M., Koushika, S. P. & Krishnan, Y. An autonomous DNA nanomachine maps spatiotemporal pH changes in a multicellular living organism. *Nat. Commun.* **2,** 340 (2011).

30. Saha, S., Prakash, V., Halder, S., Chakraborty, K. & Krishnan, Y. A pH-independent DNA nanodevice for quantifying chloride transport in organelles of living cells. *Nat. Nanotechnol.* **10,** 645–651 (2015).

31. Surana, S. & Krishnan, Y. A method to map spatiotemporal pH changes in a multicellular living organism using a DNA nanosensor. *Methods Mol. Biol.* **991,** 9–23 (2013).

32. Modi, S. & Krishnan, Y. A method to map spatiotemporal pH changes inside living cells using a pH-triggered DNA nanoswitch. *Methods Mol. Biol.* **749,** 61–77 (2011).

33. Dan, K., Veetil, A. T., Chakraborty, K. & Krishnan, Y. DNA nanodevices map enzymatic activity in organelles. *Nat. Nanotechnol.* **14,** 252–259 (2019).

34. Bonam, S. R., Wang, F. & Muller, S. Lysosomes as a therapeutic target. *Nat. Rev. Drug Discov.* **18,** 923–948 (2019).

Chapter 5. Lumenal pH and calcium levels in vesicular and tubular lysosomes

5.1 Introduction

Lysosomes are the most acidic organelles in a cell and have pH that can range between 4.5 and 5.0[1]. pH within the lysosomes is maintained predominantly by V-ATPases. V-ATPases are also important for several processes like amino acid metabolism, fusion events, PLASMA MEMBRANE repair, exocytosis, optimal functioning of lysosomal enzymes etc (Chapter 1, Figure I.1). pH maintenance is also important for lysosomal remodeling needed for cellular adaptation during conditions like autophagic lysosome reformation (ALR)[2]. The concentration of protons within the lysosomal lumen is also maintained by ClC transporters, Na^+/K^+ channels/transporters that provide counter ions[3]. Lysosomal proteolysis are heavily dependent on its lumenal acidic pH. The V-ATPase inhibitor, bafilomycin neutralizes the lysosomal pH by preventing proton translocation into lysosomes that in turn leads to the inhibition of mTORC1 and therefore inhibition of amino acid metabolism[4]. Lysosomal pH has also been linked to their different spatial positions within the cell[5–9].

The proton gradient across the lysosomal membrane regulates its lumenal calcium concentration[10]. Lysosomal alkalinization by ammonium chloride decreases lysosomal calcium levels.[11]. The dynamic nature of lysosomes and subsequent fission and fusion are determined by its lumenal calcium levels. Like pH, calcium also plays an important role in tubular lysosome formation. Lysosome tubulation can be stimulated by PI(3,5)P2-TRPML1-ALG-2-dynein signaling[12]. Acidic organelles such as phagolysosomes spatially cluster PIPs on its membrane to mediate ER contacts[13]. Further the formation of tubular lysosomes are also seen as a necessary step for phagosome resolution[13]. Although predicted ATP13A2 is so far the only lysosomal calcium importer, calcium release channels have been well characterized[14,15]. For instance, P2X4, calcium channels are hypothesized to be important for lysosomal fusion and require a hypo-acidic environment for their function, whereas TRPML1 regulates lysosomal fission events and require a more acidic lumen for its optimal function[16]. This has led to a hypothesis that there may be a pH gradient within the lumen of tubular lysosomes.

Spatial gradients of Ca^{2+} have been previously observed within tubular structures of dimensions similar to tubular lysosomes, known as primary cilia. The tip of the primary cilia is known to maintain high Ca^{2+} levels with respect to the cytoplasmic end due to activity of PKD1 channels at the tip. The low cytosolic Ca^{2+} act as a sink, thereby generating an active gradient across the tubular structure[17]. Formation and maintenance of this Ca^{2+} gradient is shown to be important for mechanosensation of external fluid flow by the cell. Similarly, pH and Ca^{2+} gradients are hypothesized to exist in TLs, due to selective activity of P2X4 and TRPML1. Further, V-ATPases that sets the pH gradient across lysosomal membrane, have been postulated to be spatially segregated along tubular lysosomes that are destined to fuse with phagosome. Thus, the active pH and Ca^{2+} spatial gradients posited to exist along the length of tubules could be related to the extension mechanism of tubular lysosomes. The extrusion of tubular lysosomes requires opposing pulling forces from Arl8b-SKIP-Kinesin and Rab7-RILP-dyenin complexes. In addition, these transport complexes regulate the spatial distribution of lysosomes facilitating different functions. For instance, peripheral lysosomes regulate PLASMA MEMBRANE repair and nutrient availability whereas perinuclear lysosomes fuse with autophagosomes to generate auto-lysosomes.

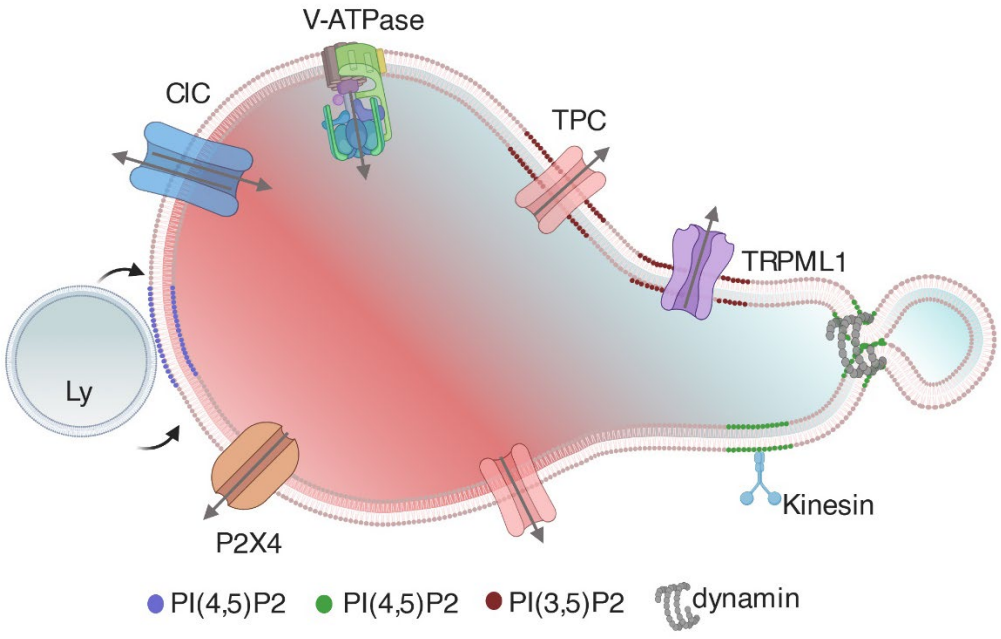

Figure V.1: Differential pH within the lysosomes regulates calcium channels. TRPML1 channels require acidic pH for effective function. TRPML is also activated by PI(3,5)P2 on lysosomal membrane. Activation of TRPML leads to fission in the presence of PI(4,5)P2. P2X4 calcium efflux channels need a hypo-acidic lumen for function and regulates lysosomal fusion.

5.2 Materials and methods

5.2a Chemicals and reagents: All oligonucleotides used in this study is shown in the table below.

Oligo Name	Sequence (5'-3')
C1	Amino-ATAACACATAACACATAACAAAATATATATCCTAGAACGACAGACAAACAGTGAGTC
C2	ATTO647-TATATTTTGTTATGTGTTATGTGTTAT
C3	DBCO-GACTCACTGTTTGTCTGTCGTTCTAGGATA

Table 5: Sequences of DNA used to make *CalipHluor 2.0*

5.2b *Tudor* formation, characterization, lysosomal tubulation assay and analysis, refer to Chapter 2, Material and methods 2.2b.

5.2c Measurement of extinction coefficient of 5(6)-Carboxy-2',7'-dichlorofluorescein (DCF): Primary stock of DCF was made by dissolving DCF in dry DMSO to create a primary stock of 50 mM. The primary stock was stored at -20 °C until used. Different dilutions of DCF in deionized water were prepared. Absorption spectra for each dilutions were measured using a UV spectrophotometer. Using Beer-Lambert's law, extinction coefficient for DCF in deionized water was estimated at different concentrations which was found to be 90000 $M^{-1}cm^{-1}$.

5.2d Conjugation of DCF to DNA and *ImLy2.0* preparation: Modification of DCF into its NHS ester form was performed according to previously described protocol[18]. 40 equivalence of DCF-NHS ester was added to 20 μM of the amine labeled 57 base strand (C1) oligoneucleotide in 20 mM sodium phosphate buffer pH 7.0. The mixture was stirred overnight at RT. Ethanol precipitation method was used to purify DCF conjugated DNA[19]. UV-absorption spectroscopy was used to quantify the conjugated DNA was measuring its absorbance at 260 nm for DNA and 504 nm for DCF. The reaction mixture was purified by amicon ultra 0.5 mL centrifugal unit with filter MWCO 3kDa. Purified DNA-DCF conjugate was further purified by ethanol precipitation to remove any residual free dye. Amicon and ethanol purified DNA-DCF conjugate was reconstituted in 20 mM Sodium phosphate buffer, pH 7.2. 20% Denaturing PAGE was using to confirm the efficiency of DNA to DCF conjugation. C1 (DCF containing DNA), C2 (Atto 647 dye containing DNA) and C3 (DBCO- modified DNA) were mixed in equimolar ratios to final concentration of 10 μM. This DNA mixture was annealed in 20 mM

Sodium phosphate buffer (pH 7.2). The formation of *ImLy 2.0* was confirmed by 15% native PAGE.

5.2e *In vitro* fluorescence measurements of *ImLy 2.0:* Fluoromax spectrophotometer (Horiba Scientific) was used to perform the *In vitro* calibration for *ImLy2.0* as reported earlier[20]. For all clamping experiments, following pH clamping buffer was used with following composition; Universal Buffer (UB): CaCl2 (50 µ M to 10 mM), HEPES (10 mM), MES (10 mM), sodium acetate (10 mM), EGTA (10 mM), KCl (140 mM), NaCl (5 mM), and MgCl2 (1 mM) and pH was set ranging between pH 3.5 and pH 7.2. 30 nM of *ImLy 2.0* was diluted in pH clamping buffer with pH ranging between 3.5 and 7.2 and allowed to equilibrate at RT for 30 mins. Each sample for DCF (G) was excited at 504 nM and emission spectra was collected between 512nm to 560 nm and similarly Alexa 647 (R) was excited at 647 nm and emission spectra was collected from 650 nm to 700 nm. The ratio of emission maxima of G and R which is 520nm:665 nm was measured. The normalized G/R values were plotted from three independent experiments as a function of pH to generate *in vitro* calibration curve.

5.2f *In cellulo* clamping of *ImLy 2.0*: 500 nM *ImLy 2.0* was pulsed in RAW 264.7 in Opti-MEM™ for 30 min. This was followed by a chase of 30 mins in complete media. Cells were washed with 1XPBS and fixed in 4% PFA in 1X PBS, 20mins. Cells were washed with 1X PBS. After washing, cells were incubated in clamping buffer (120 mM potassium chloride, 5 mM sodium chloride, 1 mM magnesium chloride, 1 mM calcium chloride, 20 mM HEPES, 20 mM MES, 20 mM sodium acetate) at various pH points each containing 50 µM Monensin and 50 µM Nigericin for 1 hour at RT. Cells were imaged in widefield microscope.

Image analysis: All images were background subtracted and thresholded. ROI was drawn around vesicular lysosomes. The ROIs were applied to background subtracted images of both G and R channels separately. The G and R values from green and red channels respectively were noted for each lysosome. G/R was plotted for each pH point in each experiment.

5.2g *In cellulo* pH measurements by *ImLy 2.0*: In order to measure pH of vesicular lysosomes in RAW 264.7, cells were used for pH measurements where cells were pulsed with 500 nM *ImLy 2.0* for 30 mins in Opti-MEM™. The cells were then chased in complete media for 30 mins. Cells were imaged in HBSS by widefield microscope. To measure the pH of tubular lysosomes,

lysosomes in RAW 264.7 cells were tubulated with 100 nM *Tudor* for 4 hours followed by incubation with 500 nM *ImLy 2.0* in Opti-MEM^{TM} for 30 mins (pulse) in presence of *Tudor*. Cells were chased of 30 mins in complete media containing *Tudor*. Cells were washed and imaged in HBSS. Image analysis: All image analysis was performed by Fiji. Background subtraction for all images were performed as follows, an ROI was drawn outside the cell on brightfield. The ROI is now applied to Green and Red channel images and mean intensity was noted. The mean intensity was subtracted from the both Green and Red channel images. Tubeness, a plugin in Fiji was used to highlight any tubular and vesicular structures in the R channel image. The image was then thresholded which was used to obtain ROIs for vesicular and tubular lysosomes. The ROIs were applied to background subtracted G and R images separately. The G and R values were noted for each lysosome. G/R was plotted for each pH point in each experiment.

5.2h *CalipHluor 2.0* preparation: 10 µM DBCO-C3 was conjugated to 1 mM of Rhod-5F-Azide in 100 µL of 20 mM sodium phosphate buffer pH 7.2. This mixture was stirred overnight at RT[14]. The DNA-Rhod-5F conjugation mixture was purified by ethanol precipitated to remove any free/unconjugated dye. DNA conjugated to Rhod-5F was reconstituted in 20 mM sodium phosphate buffer pH 7.2. 12% denaturing PAGE was used to confirmed the Conjugation. *CalipHluor 2.0* was prepared by annealing equi-molar concentrations of each oligonucleotides (5 µM) containing DCF, Rhod5F and a ratiometric dye (Atto 647N) in buffer containing 10 mM sodium phosphate buffer pH, 7.2. Gel mobility shift assay in 15% native PAGE was used to confirm the formation of *CalipHluor 2.0*.

5.2i *In vitro* bead calcium calibration: The *in vitro* calibration of CalipHluor 2.0 was performed as mentioned previoursly[14]. Briefly, 0.6 µm monodisperse silica beads was incubated with 500 nM of *CalipHluor 2.0* for 30 mins 20 mM sodium phosphate buffer, pH 5.1 containing 500 mM NaCl at RT. The beads were washed thrice by spinning at 10000 rpm for 10 mins each at room temperature. *CalipHluor 2.0* adsorbed silica beads were incubated for 30 mins in clamping buffer (HEPES (10 mM), MES (10 mM), sodium acetate (10 mM), EGTA (10 mM), KCl (140 mM), NaCl (500 mM), and $MgCl_2$ (1 mM)) at RT containing 0.1 µM or 10 mM free calcium buffers at pH (4.0, 4.6, 5.1, 6.0 and 7.2). The 2 µL of *CalipHluor 2.0* adsorbed beads were loaded on a glass slide and allowed to settle on the slide for 20-30 seconds. The glass slide was covered with a 1.5 mm coverslip and imaged in widefield microscope. Rhod-5F(O), Atto 647N (R) and DCF (G) was

excited at 545 nm, 647 nm and 504 nm respectively. O/R (calcium) and G/R (pH) from three independent experiments were plotted for each calcium concentrations as function of pH from individual images.

5.2j *In vitro* Calcium calibration: 100 nM of *CalipHluor 2.0* was incubated in calcium clamping buffer (with composition of the buffer mentioned in above protocol, 5.2i). 0.1 µM and 10 mM free calcium buffers were prepared at various pH buffers (4.0, 4.6, 5.1, 6.0 and 7.2). Rhod-5F(O), Atto 647 (R) and DCF (G) was excited at 545 nm, 647 nm and 504 nm respectively. Emission spectra for Rhod-5F, Atto 647N and DCF was collected from 570 nm to 620 nm, 650 to 700 nm and 512 to 560 nm respectively. Mean emission maxima of G/R and O/R were plotted from three independent experiments for each calcium concentrations as function of pH and calcium. The *in vitro* pH and calcium calibration performed on fluoromax was compared with the *in vitro* bead calibration performed on widefield microscope. Free calcium concentrations for a given pH for both *in vitro* calibrations by fluoromax and bead calibrations were found using https://somapp.ucdmc.ucdavis.edu/pharmacology/bers/maxchelator/CaEGTA-NIST.htm

5.2k *In cellulo* pH and Calcium clamping: *In cellulo* clamping for calcium was performed as described in previously published literature[14]. Cells were pulsed with 500 nM of *CalipHluor 2.0* for 30 mins. Cells were washed well in 1X PBS and chased of 30 mins in complete media such that *CalipHluor 2.0* is targeted to all vesicular lysosomes. Before clamping, cells were fixed in 4% PFA for 20 mins, RT. Cells were thoroughly washed and incubated in clamping buffer, pH 6.5 containing ethylene glycol-bis(β-aminoethyl ether)-N,N,N′,N′-tetraacetic acid) (EGTA) (10 mM), 10 mM free calcium along with ionophores, nigericin (50 µM); monensine (50 µM) and ionomycin (20 µM) for 1 hour, RT. Cells were imaged in clamping buffer using confocal microscope. The mean intensity of G/R and O/R values for approximately over 500 endosomes were considered from three independent experiments where G corresponds to mean fluorescence intensity of DCF; O corresponds to Rhod-5F and R to Atto 647N. A pH calibration curve for *CalipHluor 2.0* was obtained using mean G/R from clamped lysosomes at pH 6.5 and comparing the values with previous calibration curve from *ImLy 2.0*. This calibration curve was used to measure the pH in real time using *CalipHluor 2.0.* O/R values were recorded and considered to be O/R_{max} at pH 6.5.

5.2l pH and calcium measurements: Lysosomes in RAW 264.7 cells were tubulated as per protocol mentioned in Chapter 2, 2.2f with 100 nM *Tudor* (tubular and vesicular lysosomes). Similarly, cells were also treated with 100 nM dsDNA for 4 hours (vesicular lysosomes). 500 nM *CalipHluor 2.0* was pulsed and chased of 30 mins in both *Tudor* and dsDNA treated cells. Cells were imaged in confocal microscope. Quantification and calculation of free calcium in lysosomes were performed according to previously published method[14].

5.2m Abolishment of pH and calcium gradients with Tubular lysosomes: The pH and calcium gradients were abolished by neutralizing the pH within the tubular lysosomes. This was done by treatment of cells with 10 mM ammonium chloride. lysosomes (VLs and TLs) in cells were pulsed with 500 nM *CalipHluor 2.0* followed by a wash in 1X PBS and chase for 20 mins in DMEM and 20 mins of chase in Medium1(M1: 150 mM NaCl, 5 mM KCl, 1 mM $CaCl_2$, 1mM $MgCl_2$, 20 mM HEPES, pH 7.2) buffer containing 10 mM ammonium chloride at 37 °C. Cells were imaged in confocal microscope in Opti-MEM™ or HBSS.

5.2n Analysis of pH/Ca^{2+} gradient within TLs: All images were background subtracted. Tubeness plugin in Fiji was used to highlight any tubular and vesicular structures in the R (Atto 647N) channel. Images were then thresholded and used to obtain ROIs for VL and TLs. All TLs in a cell were considered for analysis except for those which are parallel to the nucleus. The ROIs were applied to background subtracted images of G, O and R separately. G/R and O/R images were constructed by dividing G channel image and O channel image with the R channel image respectively. ROI was drawn around the nucleus. A box which corresponds to the approximate size of a vesicular lysosome, 5 X 5 pixels (length and breadth) was drawn. This box was used to quantify the G/R and O/R value along the TL starting from the side closest to the nucleus and progressing towards the Plasma Membrane. The length of 5 X 5 pixel ROI was kept constant throughout the analysis process while the width varied depending on the width of TLs. The mean intensity of each ROI was noted as a function of length of the tubule in G, R and O channels. The G/R and O/R values were noted for each TLs. G/R values were converted into pH using the equation obtained from the pH calibration curve and O/R values were converted into free lumenal calcium concentration using equations shown in previously published literature[14]. Both pH and calcium values were normalized to its respective first value. Normalized pH and calcium values of each TLs were fitted to a straight line to obtain a slope. TLs were segregated based on positive;

negative or no change (increase/decrease or no change) given by the slopes of pH and calcium values for each TL. Therefore, TLs were segregated into population A, B or no gradient (n.g).

5.2o Time lapse imaging: The temporal maps of pH and calcium levels in vesicular and tubular lysosomes for RAW 264.7 were performed using *CalipHluore 2.0* by imaging in Leica TCS SP5 II STED laser scanning confocal microscope with 63X, 1.4 NA objective in G, O and R channels as per protocol mentioned above. The images were acquired for upto a maximum time point of 10 mins with 15 secs time intervals between each acquisition. Images were background subtracted and bleach corrected. There images were further processed to construct pH and calcium (log) Images according to previously published literature[14].

5.2p Stability of *Tudor* in TLs: DBCO-PEG-NHS conjugation to A2-NH2 was performed as per previously reported literature[21]. Cupper free click chemistry was used to conjugate A2-PEG-DBCO with azido-Alexa 488[22]. Unconjugated azide containing Alexa 488 was removed by amicon ultra 0.5 mL centrifugal filters MWCO 3 kDa (Millipore Sigma) which also led to concentration of ssDNA. UV quantification was used to quantify the amount of conjugation. 10 µM of Alexa 488 A2 DNA was annealed with Atto-647N labeled A1 in 10 mM potassium phosphate buffer, 100 mM KCl, pH 7.4. Annealing of dual labeled *Tudor* with Atto 647N and PEG-Alexa 488 was performed similar to protocol mentioned in Chapter 2, Material and methods, 2.2b. Lysosomes in RAW 264.7 were labeled with 0.5 mg/mL of TMR dextran. Cells were then pretreated with 100 nM unlabeled *Tudor* for 4 hours for formation of TLs. After 4 hours, cells were pulsed with 500 nM of dual labeled *Tudor* containing Atto 647N (R) and PEG-Alexa 488(G) for 30 mins and chased over time. Cells were imaged in wide field microscope with time.

Image Analysis: Tubeness from Fiji was used to highlight the tubular lysosomes. Cells were background subtracted. ROI generated by analyze particles were used to obtain the G and R mean intensity values respectively. The individual G and R values were plotted as a function of chase time.

5.2q Stability of dsDNA in lysosomes of RAW 264.7 macrophages: Cupper free click chemistry-based conjugation of azido Alexa488 to DBCO-PEG-ssDNA (D1) was performed as mentioned above (5.2 q). 10 µM of Alexa 488 ss-DNA (D1) was annealed with 10 µM of Atto 647N (D2) labeled DNA in 10 mM Potassium phosphate buffer, 100 mM KCl, pH 7.4. Annealing

was performed as mentioned previously. Cells were pulsed with 100 nM of dsDNA for 30 mins in RAW 264.7 with lysosomes labeled with (0.5 mg/mL) TMR dextran and chased over time. Cells were imaged in wide field microscope over different time points. Alexa 488 was considered as (G) and Atto 647N (R). Image Analysis: Image analysis was performed by Fiji. Images were background subtracted. ROI was drawn around the whole cell and whole cell intensities were plotted at both G and R channels as a function of chase time.

5.3 Results and discussion

5.3a Stability of DNA in vesicular and tubular lysosomes in macrophages

Endo-lysosomal compartments contain nucleases that degrade nucleic acids resident in the lumen [20,23,24]. Lysosomes of macrophages clear nucleic acid-related debris from apoptotic cells[25]. Quantitative maps of DNA degradation within lysosomes of macrophages have been obtained using single molecular counting[26]. Since the reporters used to study the lumenal environment within the vesicular and tubular lysosomes are DNA based nanodevices, the stability of DNA nanodevices was studied in both vesicular and tubular lysosomes in RAW 264.7 to identify the appropriate duration within which the DNA based reporters can reliably measure the analyte prior to degradation. The stability of DNA was studied using dual labeled DNA dsDNA (D1 and D2 DNA) containing Atto647N (R) and Alexa488 (G) dyes which was previously reported[24]. Atto647N dye is membrane permeable and upon degradation leaks through the membrane and therefore exits the lysosome. Hence the intensity of Atto647N decreases as the DNA nanodevice degrades. The presence of a PEG linker connecting Alexa 488 to the nanodevice leads to a high molecular weight of Alexa488 upon degradation of the DNA nanodevice. The high molecular weight blocks the release of Alexa 488 into cytoplasm upon degradation of the DNA nanodevice. Further, Alexa 488 being negatively charged, has very low membrane permeability and therefore remains within the lumen of the lysosome. Hence the fluorescence of Alexa 488 remains reasonably constant within the lysosomes over the timescales of the stability experiments. For the analysis, total cell intensity in both Alexa 488 and Atto 647N channels was plotted where the intensities of (G) and (R) were normalized to the initial intensity at time t=0. Our experiments revealed that dsDNA is stable up to 90 mins after reaching lysosomes of RAW 264.7 (Figure IV. 2a, b). In order to study the stability of *Tudor* within the tubular lysosomes, *Tudor* was constructed with internally labeled Atto 647N on A3 strand and Alexa 488 conjugated to A2 strand. G and R mean intensity values were plotted for each tubular lysosomes over different chase times. This

experiment revealed that *Tudor* can reliably stable for up to 2 hours within the tubular lysosomes (Figure IV. 2c, d).

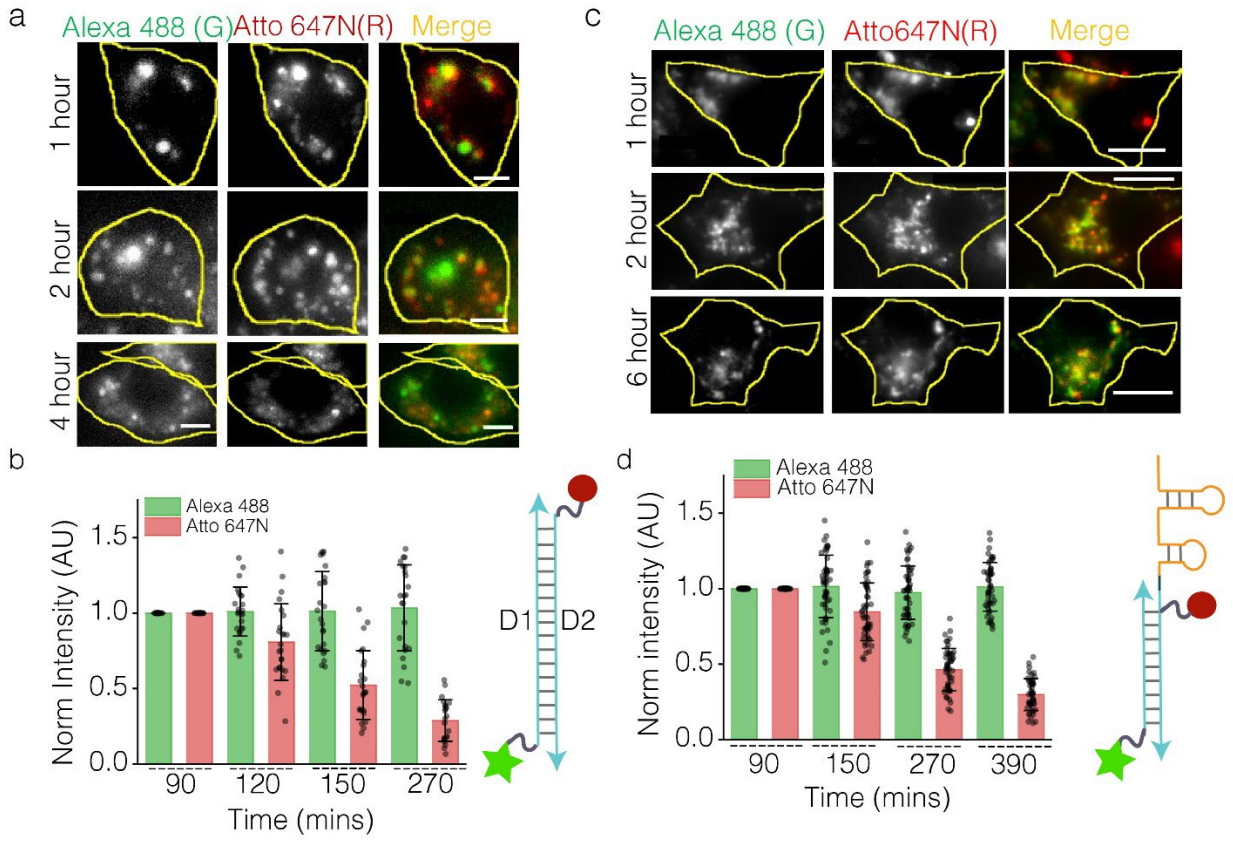

Figure. V.2: Stability of DNA nanodevices in VLs and TLs (a) Representative images of RAW 264.7 cells showing dsDNA (Schematic shown below) uptake containing PEG-Alexa 488 (G) and Atto 647N (R) at different indicated chase times. Scale bar: 5 µm. (b) Whole cell intensities of G and R as a function of chase times (n= 20 cells). (c) Representative single plane wide field images of *Tudor* treated RAW 264.7 labeled with *Tudor* containing Atto 647N (R) and PEG-Alexa 488 (G) Schematicon the right shows the structure in TLs at various chase times. (d) Normalized intensity of TLs in R and G channels at different chase times. (n = 15 cells, m = 50 TLs per experiment). Error bars indicate standard deviation (SD). Scale bar: 10 µm. Data from three independent experiments.

5.3b *ImLy 2.0*, a new pH reporter for tubular and vesicular lysosomes

To measure unknown pH levels within lysosomes upon tubulation, we designed our pH reporter to be capable of measuring a pH range from 4.0 to 6.0 reliably. Fluorescein (λex: 490 nm and λem: 515 nm) is a well-known pH reporter used to measure pH from 5.2 to 7.2. Hence, it is not suitable for this study. Further fluorescein has poor photo stability making it undesirable reporter for real-time imaging. Introducing halogens on the fluorescein core not only increases its photostability, but the negative inductive effect shifts its regime of pH sensitivity. Orgone Green (OG) 488 (λex: 450 nm and λem: 510 nm) is a difluoro fluorescein which is pH sensitive at acidic pH with pKa of 4.6 which we used to measure pH of lysosomes in *ImLy*[20]. OG488 in *ImLy* works best between pH 4.0 and 5.4 reliably, but we wanted an extended pH regime upto pH 6.0. Hence 5(6)-Carboxy-2',7'-dichlorofluorescein (DCF) was chosen. The dichloro moiety pushes the pKa of DCF to 5.1 and was ideal for acidic pH between 4.0 and 6.0. Hence DCF was used to generate a new DNA-based pH reporter, *ImLy 2.0*.

ImLy2.0 comprises 3 DNA strands, C1, 58 nt DNA strand consist of amino modification on 5' end which is used to conjugate DCF (the pH reporting dye with excitation maxima, λ_{ex} = 504 nm and emission maxima λ_{em} = 520 nm). Conjugation of DCF to amino labeled DNA was confirmed by denaturing polyacrylamide gel electrophoresis. C2, 28 nt strand complementary to one half of C1 is labeled with Atto 647N (pH and calcium insensitive dye with, λ_{ex} = 647 nm and emission maxima λ_{em} = 670 nm) which acts as reference dye and C3, 30 nt strand which is also complementary to the other half of C1. The formation of *ImLy2.0* was confirmed by mobility shift assay by native PAGE. *ImLy2.0* was characterized by measuring the excitation and emission spectra in DCF (G) and Atto 647 (R) channels in universal buffer by varying pH ranging from pH 3.5 to pH 6.5. The ratio of G/R was plotted which was fitted to sigmoidal curve with Boltzmann fit. *In cellullo* calibration for *ImLy 2.0* was performed in RAW 264.7 using protocols mentions in the methods section (5.2g-5.2h). The R/G ratios were computed from single lysosomes in cells treated clamped at various pH. The ratios were plotted similar to *in vitro* calibration curve. The *in cellulo* calibration curve recapitulated *in vitro* calibration curve revealing that *ImLy2.0* indeed could measure pH from 4.0 to 6.0. We then proceeded to measure the pH of both vesicular and

tubular lysosomes in RAW 264.7 using the pH calibration curve generated using pH clamping of cells at varying pH points.

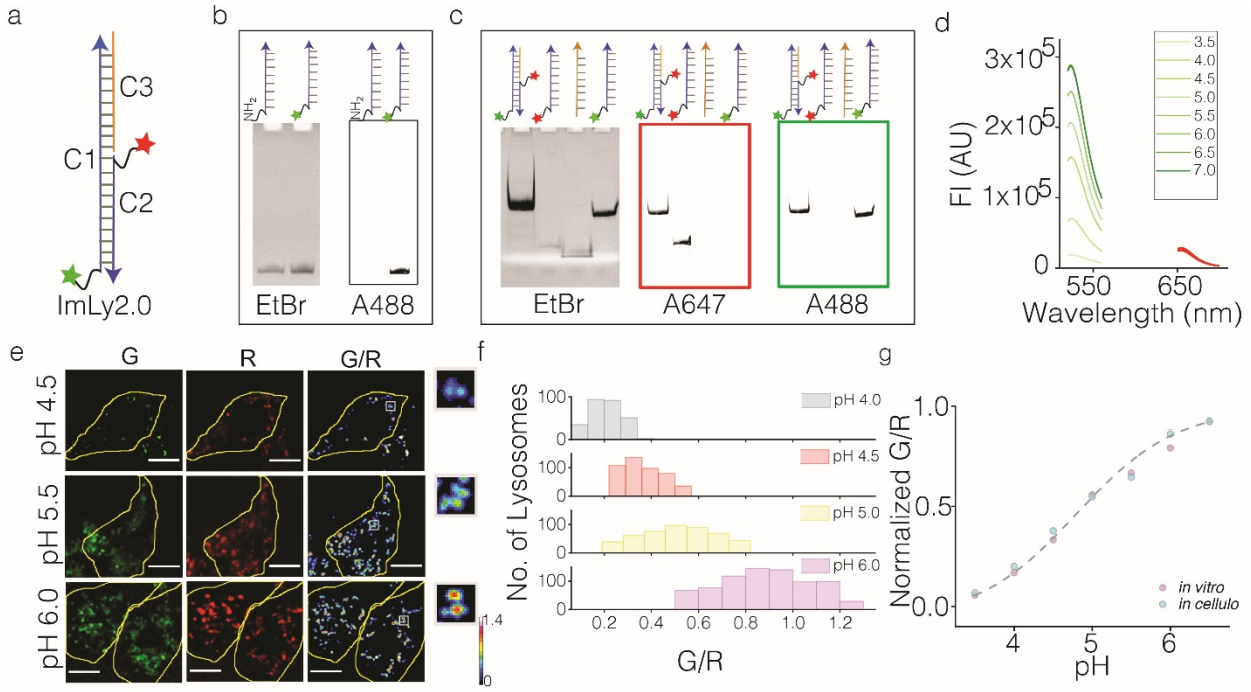

Figure. V.3: Characterization of *ImLy2.0*. (a) Schematic of *ImLy 2.0* showing 5(6)-Carboxy-2',7'-dichlorofluorescein (DCF) on 58 nt (C1) oligo (green), Atto 647N (red) on the complimentary 28 nt oligo (C2) and unlabeled 30 nt oligo (C3). (b) Denaturating PAGE (15%) showing the conjugation of DCF to amine containing C1 in EtBr and Alexa 488 channels. (c) Gel mobility shift assay showing the formation of *ImLy 2.0* by 15% native PAGE imaged in EtBr, Alexa 647 and Alexa 488 channels. (d) Emission spectra of *ImLy 2.0* at pH ranging from 3.5 and 7.0. (e) Representative images of RAW 264.7 showing the uptake of *ImLy 2.0* and pixel wise pseudocolored images of G/R clamped at indicated pH. Inset showing the zoomed in area shown in the white box. Scale bar: 10 µm. (f) Histogram of G/R ratios of lysosomes clamped at indicated pH (n= ≥ 90 cells, m = ≥ 500 lysosomes). (g) pH calibration (*in vitro*) for *ImLy 2.0* showing normalized G/R ratios versus indicated pH values. Error bars represents s.e.m from three independent experiments.

5.3c pH correctable calcium reporter, *CalipHluor 2.0*

The design of *CalipHluor 2.0* was inspired by the previously designed *CalipHluor*^{mLY14}. *CalipHluor 2.0* consists of three modules; pH sensing module, DCF; ratiometric module: Atto 647N dye as it is pH and calcium insensitive, and a calcium sensing dye, Rhod5F. Rhod5F consists

of 1,2-bis(o-aminophenoxy) ethane-N,N,N′,N′-tetra acetic acid (BAPTA) core, rhodamine fluorophore with a linker with azide for click mediated conjugation. pH sensing module by DCF is explained in (section *ImLy 2.0*). In the absence of calcium, the rhodamine dye (excitation maxima λ_{ex} = 560 nm and emission maxima λ_{em} = 580 nm) is quenched by photoinduced electron transfer (PeT) from the nitrogen of BAPTA and hence is non fluorescent. In presence of calcium, the nitrogen of BAPTA is now engaged with the calcium ion in a pH dependent manner and hence relieves rhodamine to fluoresce. pH mediated protonation of nitrogen in BAPTA can also relieve the PeT quenching of rhodamine. Hence the fluorescence output by rhodamine will be determined not just by the affinity of BAPTA to calcium but also the *Kd* of BAPTA in the surrounding pH. Therefore, it is crucial to have pH module in Rhod5F based calcium reporter.

CalipHluor 2.0 consists of 3 strands of DNA where C1 strand is conjugated to DCF (pH reporter) C2 with Atto 647N (ratiometric reporter) and DBCO modified C3 strand is conjugated Rhod5F (calcium reporter) containing azide by copper free click chemistry (Figure IV.4a). The confirmation of conjugation was shown by denaturation polyacrylamide gel electrophoresis (Figure IV. 4b) and formation of *CalipHluor 2.0* was shown by gel mobility shift assay by native polyacrylamide gel electrophoresis (Figure IV. 4c).

Since BAPTA binding to calcium is pH dependent manner, DCF was used to provide a pH measure. Hence *Kd* of BAPTA can be calculated based on the pH of the surrounding given by DCF. While, maximum [Ca2+] (O/R_{max}) (with O representing mean fluorescence intensity of rhodamine and R representing fluorescence intensity of Atto 647N) can be obtained from *in cellulo* calcium clamping at 10 mM free calcium at a given pH (Methods 5.2l). The fold change of *Caliphluor 2.0* was at various pH was experimentally determined (Figure IV.4d). O/R_{min} (O/R in low [calcium] at same pH) can be calculated using the fold change in O/R as function of pH. The free calcium within the lumen of lysosomes (VLs and TLs) were obtained as function of Kd, O/R_{min} and O/R_{max}.

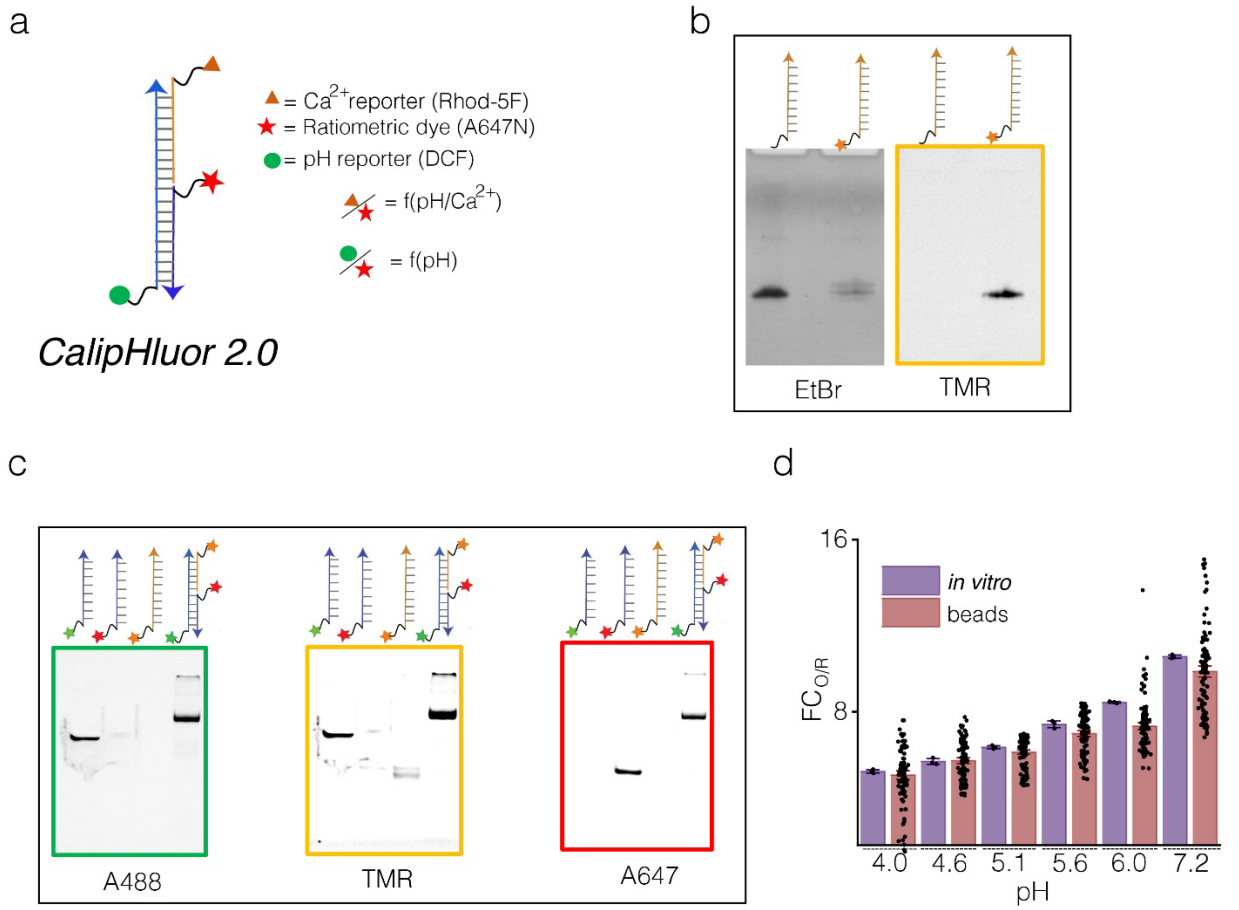

Figure V.4: Characterization of *CalipHluor 2.0.* (a) Schematic of ratiometric fluorescent pH correctable Ca^{2+} reporter, *CalipHluor 2.0*. It consists of Ca^{2+} sensitive dye, Rhod-5F (orange triangle); pH sensing dye, DCF (green circle) and ratiometric dye, Atto 647N (red star). (b) Denaturing PAGE (15%) showing the conjugation of Rhod-5F to DBCO containing D3 oligo in EtBr and TMR channels. (c) Native PAGE (15%) showing gel mobility shift of *Caliphluor 2.0* in Alexa 488, TMR and Alexa 647 channels. (d) Comparison of *in vitro* (purple) and on beads (pink) fold change of O/R ($FC_{O/R}$) ratios of *CalipHluor 2.0* from pH 4.0 - 7.2 (n = 100 beads).

5.3c.1 pH and calcium measurements in vesicular and tubular lysosomes

Tubular and vesicular lysosomes showed differential proteolytic activity although expression levels of cathepsins were comparable between the two morphologically distinct forms of lysosomes. Proteolytic activity also is dictated by lumenal pH of the lysosomes. Tubular lysosomes have been previously found to be hypo-acidic compared vesicular lysosomes in autophagic conditions in cultured cells. In contrast, within the hypodermis of *C. elegans* during development,

they have proved to be comparable[2,27]. Lysosomes are highly fusogenic and contain P2X4 and TPC2 channels that promote lysosome fusing while TRPML1 is imperative for lysosome fission[28–30]. TRPML1 channels tubulate lysosomes by activating ALG2 due to the local increase of calcium efflux from the lysosome lumen[12]. TRPML1 requires more acidity for its functionality while P2X4 requires less acidity for its functionality. This has led to the hypothesis that ion gradients might exist within tubular lysosomes.

Using *CalipHluor 2.0*, we have measured lumenal pH and calcium simultaneously within tubular and vesicular lysosomes in RAW 264.7 macrophages. For this, lysosomes in RAW 264.7 macrophages tubulated with *Tudor* and LPS followed by an 30 min pulse of *CalipHluor 2.0* and 30 mins chase in complete media such that *CalipHluor 2.0* localizes in both vesicular and tubular lysosomes (Figure IV 5a). *CalipHluor 2.0* labeled cells were imaged in DCF (G); Rhod5F (O) and Atto 647N (R) channels and analyzed as described in methods, (5.2l - 5.2n). The overall pH and calcium in vesicular and tubular lysosomes were found to be comparable (Figure IV 5c-d). The imaging methods to obtain pH and calcium images were as performed as previously described[14]. (i) The pseudocolored G/R images were obtained from G and R channel images and converted into the corresponding pH image (ii). (iii) pH images are then converted into K_d maps using the corresponding pH image where K_d for a given pixel is determined by the pH value at that pixel. (iv) The K_d image is then multiplied by pseudocoloured O/R image to obtain calcium map (v) (Figure IV 5e).

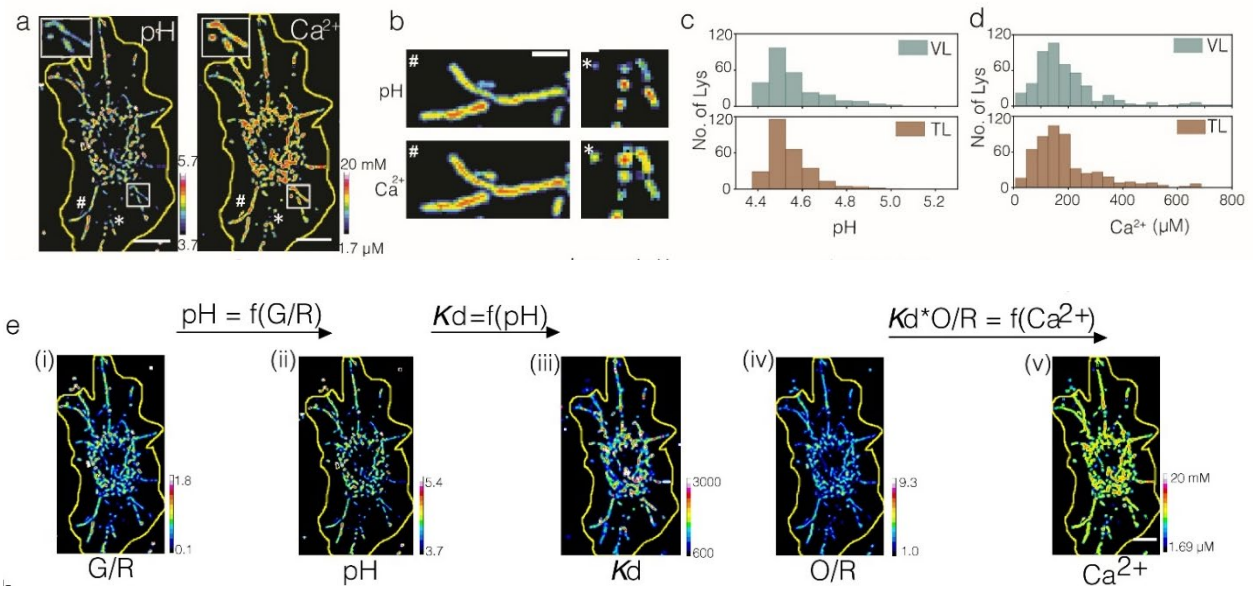

Figure V.5: pH and calcium measurements in macrophages.

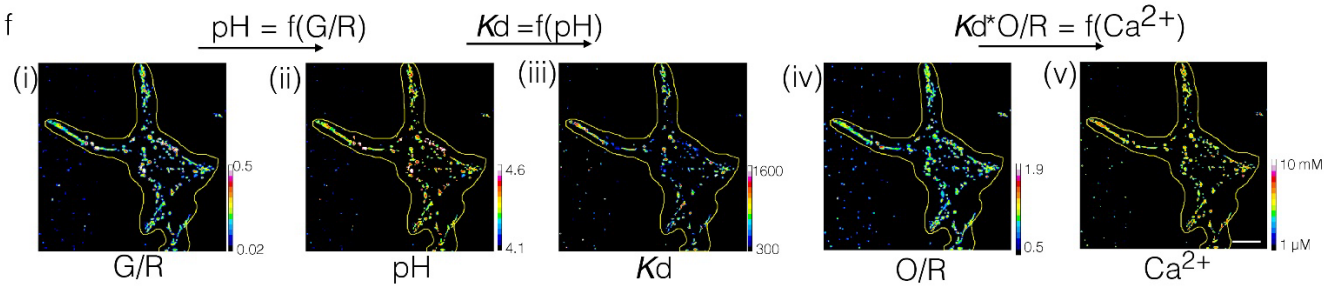

Figure V.5, continued. pH and calcium measurements in macrophages. (**a**) Representative pH and Ca2+ images of *CalipHluor 2.0* labeled RAW 264.7 cells pretreated with *Tudor*. (**b**) Representative pH and Ca2+ maps in TLs and VLs. (**c** and **d**) Histograms of lysosomal pH (c) and Ca2+ (d) distribution in VLs of dsDNA treated RAW 264.7 and TLs of Tudor treated cells, (n= 20 cells, m = 300 VLs (n=20 cells; m=100 TLs). (**e-f**) Representative images from *Tudor* (e) and LPS (f) treated RAW 264.7 cells pulsed with *CalipHluor 2.0* followed by chase in complete media. f(x): function of. Scale bar: 10 µm, inset scale bars: 4 µm.

5.3c.2 pH and calcium gradients within tubular lysosomes

Although the overall vesicular and tubular lysosomes showed comparable pH and calcium levels, the lumen of tubular lysosomes revealed the existence of pH and calcium gradients (Figure VI. 5). More than 90% of all Tubular lysosomes radiated outwards from the nucleus towards PLASMA MEMBRANE. The lumenal pH and calcium levels in tubular lysosomes changed as they propagated from the center of the cell to the periphery (Figure IV. 5a-c). In order to better analyze these qualitative observations, we classified the tubular lysosomes into two categories. Those that showed their high acidity termini at the nucleus were considered as one population (population B), and those that had their high acidity termini at the PLASMA MEMBRANE were considered another population (population A) (Figure IV.5 d-e). We found that more than ~53% of tubular lysosomes had their high acidity termini positioned closer to the nucleus (population B) while around ~29% of corresponded to population A and ~13% showing no ion gradient, denoted n.g. (Figure IV.5 f, g). Similar pH and calcium gradients and population distributions were observed for LPS-mediated tubular lysosomes (Figure IV.5h, g).

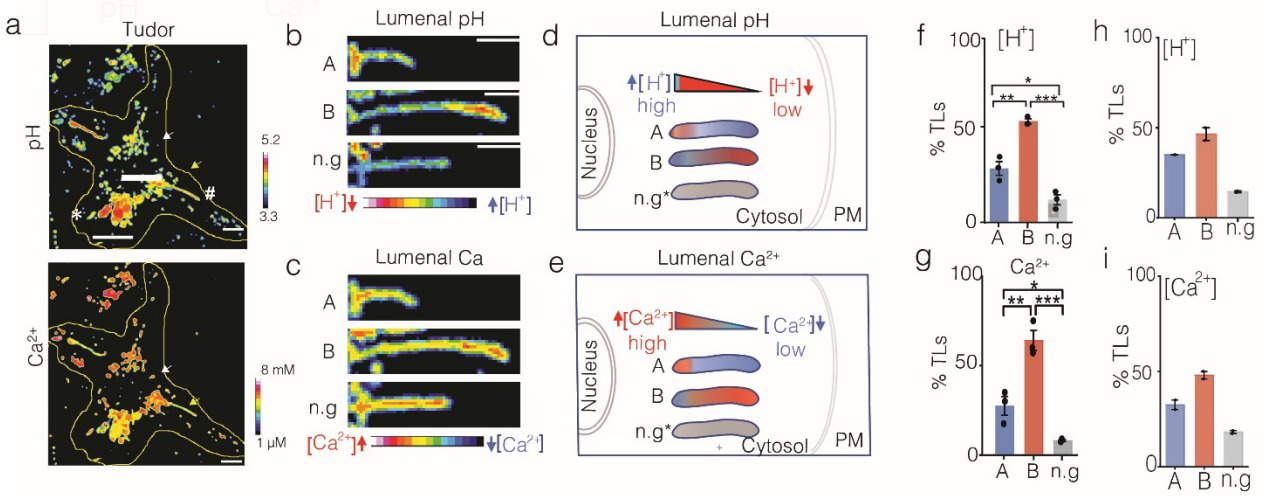

Figure V.6: pH and calcium ion gradients in tubular lysosomes. (a) Representative pH and Ca^{2+} images respectively of *Tudor* treated RAW 264.7 showing both VLs and TLs. Scale bar: 10 µm. (**b** - **c**) Representative images of pH and Ca^{2+} maps of TLs. (**d** and **e**) Schematics of the different TL according to their lumenal pH and Ca^{2+} gradients and orientation in the cell. n.g represents no gradient, scale bars: 4 µm. (**f-i**) Quantification of TL populations (A), (B) and (n.g) respectively. ***P< 0.0005; **P< 0.005; *P< 0.05 (one-way ANOVA with Tukey *post hoc* test) in *Tudor* (f and g) (n=20 cells, m=100 TLs), and LPS treated (h and i) cells ((n=15 cells, m=50 TLs). Error bars represents standard error of mean (s.e.m) from three independent experiments.

5.3c.3 Ammonium chloride neutralizes ion gradients within tubular lysosomes.

Previous reports have shown that neutralizing the pH in the lysosomes (both vesicular and tubular lysosomes) by inactivating V-ATPases breaks down tubular lysosomes into vesicular ones suggesting that acidity is important for maintaining the tubulated state[31]. Inhibition or over-expression of TRPML1 also breaks down tubular lysosomes into vesicular ones[12]. Ammonium chloride neutralizes pH within lysosomes[32] and causes lysosomal calcium efflux thereby reducing lumenal calcium and potentially destroying calcium homeostasis within tubular lysosomes[10]. To test whether the gradients we observed might have been due to imaging or analysis artifacts, we repeated our experiments in the presence of 10 mM Ammonium chloride. Although ammonium chloride drastically reduced the number of tubular lysosomes in cells, those tubular lysosomes that still existed showed no pH or calcium gradients (Figure IV. 6).

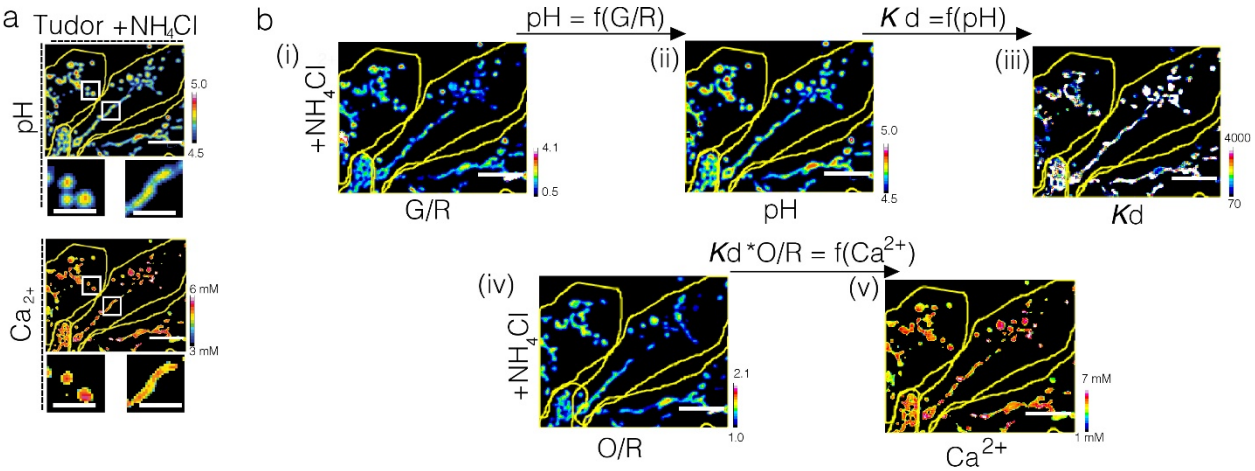

Figure V.7: pH and calcium measurements in presence Ammonium chloride. (a and **b)** Representative images of *Tudor* treated RAW 264.7 cells pulsed with *CalipHluor 2.0* followed by chase in complete media containing 10 mM Ammonium chloride. Scale bar: 10 µm, inset scale bars: 4 µm.

5.4 Conclusion

Quantitative pH and calcium maps of tubular lysosomes revealed the existence of pH and calcium gradients along the long axis of tubular lysosomes, even though the overall levels of pH and calcium were similar to those in vesicular lysosomes. Approximately ~ 53% of the radially oriented tubular lysosomes were oriented such that their more acidic termini were nearer the nucleus (population B). A minor population (29%) were oriented in the reverse direction and ~13% showed no ion gradients. A similar calcium spatial gradient is also seen in the primary cilium, an organelle with similar dimensions as tubular lysosomes where the tip of the cilium has high calcium due to PKD1 channel activity and the base has lower calcium as it is continuous with the cytosol which acts as a calcium sink. Importantly pH gradients, calcium gradients and population distributions observed for tubular lysosomes induced by either *Tudor* and LPS proved to be nearly identical suggesting that the nature of the tubular lysosomes is conserved. However, the differently oriented populations suggest that tubular lysosomes may have associated functionalities.

5.5 References

1. Mindell, J. A. Lysosomal acidification mechanisms. *Annu. Rev. Physiol.* **74,** 69–86 (2012).
2. Yu, L. *et al.* Termination of autophagy and reformation of lysosomes regulated by mTOR. *Nature* **465,** 942–946 (2010).
3. Xu, H. & Ren, D. Lysosomal physiology. *Annu. Rev. Physiol.* **77,** 57–80 (2015).
4. Fedele, A. O. & Proud, C. G. Chloroquine and bafilomycin A mimic lysosomal storage disorders and impair mTORC1 signalling. *Biosci. Rep.* **40,** (2020).
5. Leung, K., Chakraborty, K., Saminathan, A. & Krishnan, Y. A DNA nanomachine chemically resolves lysosomes in live cells. *Nat. Nanotechnol.* **14,** 176–183 (2019).
6. Pu, J., Guardia, C. M., Keren-Kaplan, T. & Bonifacino, J. S. Mechanisms and functions of lysosome positioning. *J. Cell Sci.* **129,** 4329–4339 (2016).
7. Cabukusta, B. & Neefjes, J. Mechanisms of lysosomal positioning and movement. *Traffic* **19,** 761–769 (2018).
8. Johnson, D. E., Ostrowski, P., Jaumouillé, V. & Grinstein, S. The position of lysosomes within the cell determines their luminal pH. *J. Cell Biol.* **212,** 677–692 (2016).
9. Ballabio, A. & Bonifacino, J. S. Lysosomes as dynamic regulators of cell and organismal homeostasis. *Nat. Rev. Mol. Cell Biol.* **21,** 101–118 (2020).
10. Christensen, K. A., Myers, J. T. & Swanson, J. A. pH-dependent regulation of lysosomal calcium in macrophages. *J. Cell Sci.* **115,** 599–607 (2002).
11. Reeves, W. H. Antibodies to the p70/p80 (Ku) antigens in systemic lupus erythematosus. *Rheum Dis Clin North Am* **18,** 391–414 (1992).
12. Li, X. *et al.* A molecular mechanism to regulate lysosome motility for lysosome positioning and tubulation. *Nat. Cell Biol.* **18,** 404–417 (2016).
13. Levin-Konigsberg, R. *et al.* Phagolysosome resolution requires contacts with the endoplasmic reticulum and phosphatidylinositol-4-phosphate signalling. *Nat. Cell Biol.* **21,** 1234–1247 (2019).
14. Narayanaswamy, N. *et al.* A pH-correctable, DNA-based fluorescent reporter for organellar calcium. *Nat. Methods* **16,** 95–102 (2019).
15. Yang, J., Zhao, Z., Gu, M., Feng, X. & Xu, H. Release and uptake mechanisms of vesicular Ca2+ stores. *Protein Cell* **10,** 8–19 (2019).
16. Saffi, G. T. & Botelho, R. J. Lysosome fission: planning for an exit. *Trends Cell Biol.* **29,** 635–646 (2019).
17. Su, S. *et al.* Genetically encoded calcium indicator illuminates calcium dynamics in primary cilia. *Nat. Methods* **10,** 1105–1107 (2013).

18. Adamczyk, M., Fishpaugh, J. R. & Heuser, K. J. Preparation of succinimidyl and pentafluorophenyl active esters of 5- and 6-carboxyfluorescein. *Bioconjug. Chem.* **8,** 253–255 (1997).

19. Moore, D. Purification and concentration of DNA from aqueous solutions. *Curr. Protoc. Immunol.* **Chapter 10,** Unit 10.1 (2001).

20. Chakraborty, K., Leung, K. & Krishnan, Y. High lumenal chloride in the lysosome is critical for lysosome function. *Elife* **6,** e28862 (2017).

21. Veetil, A. T., Jani, M. S. & Krishnan, Y. Chemical control over membrane-initiated steroid signaling with a DNA nanocapsule. *Proc. Natl. Acad. Sci. USA* **115,** 9432–9437 (2018).

22. *Click chemistry for biotechnology and materials science*. (John Wiley & Sons, Ltd, 2009). doi:10.1002/9780470748862

23. Surana, S., Bhat, J. M., Koushika, S. P. & Krishnan, Y. An autonomous DNA nanomachine maps spatiotemporal pH changes in a multicellular living organism. *Nat. Commun.* **2,** 340 (2011).

24. Saminathan, A. *et al.* A DNA-based voltmeter for organelles. *Nat. Nanotechnol.* (2020). doi:10.1038/s41565-020-00784-1

25. Odaka, C. & Mizuochi, T. Role of macrophage lysosomal enzymes in the degradation of nucleosomes of apoptotic cells. *J. Immunol.* **163,** 5346–5352 (1999).

26. Prakash, V. *et al.* Quantitative mapping of endosomal DNA processing by single molecule counting. *Angew. Chem. Int. Ed. Engl.* **58,** 3073–3076 (2019).

27. Murakawa, T., Kiger, A. A., Sakamaki, Y., Fukuda, M. & Fujita, N. An Autophagy-Dependent Tubular Lysosomal Network Synchronizes Degradative Activity Required for Muscle Remodeling. *BioRxiv* (2020). doi:10.1101/2020.04.15.043075

28. Cao, Q. *et al.* Calcium release through P2X4 activates calmodulin to promote endolysosomal membrane fusion. *J. Cell Biol.* **209,** 879–894 (2015).

29. Wang, X. *et al.* TPC proteins are phosphoinositide- activated sodium-selective ion channels in endosomes and lysosomes. *Cell* **151,** 372–383 (2012).

30. Cao, Q., Yang, Y., Zhong, X. Z. & Dong, X.-P. The lysosomal Ca2+ release channel TRPML1 regulates lysosome size by activating calmodulin. *J. Biol. Chem.* **292,** 8424–8435 (2017).

31. Johnson, A. E., Shu, H., Hauswirth, A. G., Tong, A. & Davis, G. W. VCP-dependent muscle degeneration is linked to defects in a dynamic tubular lysosomal network in vivo. *Elife* **4,** (2015).

32. Poole, B. & Ohkuma, S. Effect of weak bases on the intralysosomal pH in mouse peritoneal macrophages. *J. Cell Biol.* **90,** 665–669 (1981).

Chapter 6. Tubular lysosomes promote the early stages of phagocytosis

6. 1 Introduction

Innate immune cells like neutrophils, macrophages and dendritic cells are specialized phagocytes that internalize foreign or infectious particles, cellular debris, tumor and apoptotic cells[1]. Lipopolysaccharide (LPS) activates macrophages and enhances phagocytosis[2,3]. LPS stimulation activates the TLR4 signaling to enhance phagocytosis by activating the PI3k-AKT-mTOR cascade which activates S6Kinase and 4E-BP[4,5]. This pathway leads to the upregulation of several lysosomal and phagosomal proteins needed for phagosomal maturation and increased phagocytosis[5].

Cargo containing phagosomes enters the cells through a series of well-studied mechanisms beginning with identifying of particle to be ingested[6]. Macrophages and dendritic cells possess massive membrane ruffles on their Plasma Membrane which aids in constant surveillance of its surrounding as it migrates[6]. Exposure to growth factors or immune stimulants like LPS, further increases membrane ruffling[7,8]. Membrane ruffles occur by cell surface GPCR and calcium sensitive receptor (CaSR) activation that mediates downstream signaling of the formation of PI(3,4,5)P3, Phosphatidic acid (PA)[6,9]. This activates the WASP family verprolin homolog (WAVE) complex and the guanine nucleotide exchange factor (GEF) needed to activate Cdc42 and Rac to bring about Arp2/3 complex dependent actin remodeling underneath the Plasma Membrane[6,10].

The recognition of phagocytic cargo could also happen passively as cells like macrophages constantly surveil the system for foreign or dead cell debris to be cleared[11]. Bacterial movement can also attract macrophages to its vicinity[6]. Recognition could also occur by either complement opsonized particles or by chemoattractant[12]. For example, macrophages and neutrophils move with increased speed towards the gradient of chemoattractant N-formyl-methionyl-leucyl-phenylalanine (fMLP) to ingest bacteria[12]. “Find-me signals” like sphingosine 1-phosphate or fractalkine released by dying cells are recognized by the phagocytes and ingested[13–16]. Once the phagocyte identifies the particle to be ingested, the process begins with recognition of particle through receptors such as FcγR, SR-B2[9]. Inadvertent activation of receptors is eliminated by large phosphates on cytosolic sides of receptors brought about Src Kinase family protein, C-terminal Src Kinase (CsK)[6]. Upon interaction with particle for ingestion, inhibiting phosphates are removed

and dimerization of receptors occurs leading to PI3K mediated Rho GTPases activation[6]. PI3K activation leads to increased PI(3,4,5)P3 on PLASMA MEMBRANE[17]. Rho GTPases activate nucleation promoting factors (NPF) like WAVE complex bringing about actin remodeling by activating Arp2/3 needed for Plasma Membrane protrusions around the particle to be engulfed[6]. BAR domain proteins further assist in Plasma Membrane remodeling[6]. Meanwhile phospholipase Cγ (PLCγ) converts diacyl glycerol (DAG) into inositol (1,4,5) triphosphate (IP_3)[6]. PLCγ mediated cytosolic calcium elevation activates myosin together with PI(3,4,5)P3 on Plasma Membrane leading to phagosomal cup formation[6]. Myosin activation, and actin polymerization mediated by BAR domain containing proteins and recruitment of dynamin on either side of enclosing membranes eventually seals the phagosome[6,18].

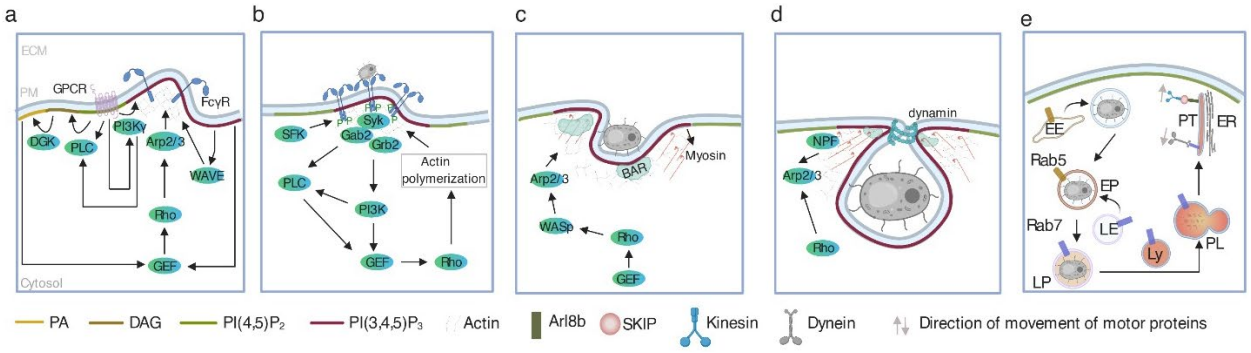

Figure VI.1: Mechanism of formation, maturation and resolution of phagosomes. (a) Cytoskeletal remodeling under Plasma Membrane forming membrane ruffles as macrophage surveil looking for dead cell or debris or foreign particles. (b) Receptor dimerization upon recognition of the particle to be ingested. (c) Internalization of particles (formation of a phagosome). (d) completion of phagosome formation. (e) Phagosomal maturation and its resolution. Early endosome (EE); early phagosome (EP); late endosome (LE); late phagosome (LP); Ly (lysosome); phagolysosome (PL); endoplasmic reticulum (ER) and phagosomal tubule (PT); extracellular matrix (ECM); phosphatidic acid (PA); diacyl glycerol(DAG); G protein coupled receptor (GPCR); diacyl glycerol kinase (DGK); phosphor lipase Cγ(PLC); phosphatidylinositol 3- kinase γ(PI3Kγ); actin related protein 2/3 complex (Arp2/3); Rho family GTPase(Rho); WASP family verprolin homolog (WAVE); Src family kinases (SFK); spleen tyrosine kinase (SyK); growth factor receptor bound protein 2 (Grb2); guanine nucleotide exchange factor(GEF); nucleation promoting factor(NPF)

The internalized phagosome interacts with endosomes via a mechanism called “kiss and run”[19]. During this process, phagosomes interact with early endosomes (EE) forming the early phagosome which contains EE marker, Rab5[18]. The early phagosome matures into late phagosome mainly by fusing with late endosomes (LE). Hence late phagosomes contain LE markers like Rab7 and

LAMP[18]. At this stage, the pH of late phagosome matches with that of LE[18]. The late phagosome fuses with lysosomes and finally matures into phagolysosome[20,21]. Phagolysosomes contain lysosomal hydrolases, cathepsins and other degradative enzymes which bring about the degradation of the cargo[22,23]. Phagolysosomes contain PI4P on its membrane[24]. Phagolysosomes lacking PI_4P tubulate into phagosomal tubules. Phagosomal tubules contain Arl8b on outer membrane bound to SKIP. SKIP loads the phagosomal tubules onto kinesin dragging the phagosomal tubules towards the Plasma Membrane[25]. As it progresses towards Plasma Membrane, it makes contact with endoplasmic reticulum for its resolution[25]. Fusion of phagosome to lysosomal maturation step is one of key steps in phagosomal maturation.

Phagosomes do not just fuse with lysosomes, both phagosomes and lysosomes are involved in bi-directional signaling. Phagocytes like macrophages upon initial cycles of phagocytosis leads to TFEB translocation into the cell nucleus bringing about the transcription of lysosomal genes[26]. Activation of Fcγ receptor leads to the activation of lysosomal genes[27]. Further, inhibition of Mucolipin1 (MCOLN1) leads to reduction in phagocytosis[27]. Also, the phagocytic trigger in macrophages enhances the degradation capacity of lysosomes[27]. All these point to the possibility of signaling between lysosomes and phagosomes.

The morphologically distinct tubular lysosomes are crucial for phagocytosis and antigen presentation in macrophages and dendritic cells respectively[5,28–31]. Tubular lysosomes deliver V-ATPases to phagosomes to acidify the lumen of phagosomes[32]. LPS and *Tudor* stimulated tubular lysosome initially activate different players but converges on a common pathway namely, the PI3K-Akt mTOR cascade[33]. LPS treated macrophages show higher fluid retention, increased phagocytosis and these correlate with an increase in tubular lysosomes abundance [5]. Studying the role of tubular lysosomes in phagocytosis in resting immune cells is challenging mainly because by forming tubular lysosomes with LPS, it is not possible to decouple increased phagocytic behavior and the immune response. However, *Tudor*, can tubulates lysosomes without activating macrophages. Thus, we can test whether tubular lysosomes affect phagocytosis without immune signaling occurring in macrophages.

6.2 Material and methods

6.2a Immunofluorescence:

Plasma Membrane labeling of Phosphatidylinositol (3,4,5) triphosphate: Sequential immunofluorescence method was employed which is as follows; Cells were incubated with PI3K inhibitor, ZSTK474 (1 μM) for 30 mins; mTOR inhibitor, Torin 1 (100 nM) for 1 hour. This was followed by treatment of cells with 100 nM *Tudor* in presence or absence of the inhibitor for 4 hours in DMEM with 10% FBS. Fixation protocol is as follows; 5% PFA+0.45% GA in 1X PBS for 10 mins at RT followed by thorough wash in 1X PBS. Quenching protocol is as follows; 100 mM Glycine, 1% BSA in 1X PBS for 5 mins followed by thorough washing. Permeabilization protocol was performed by incubation of cells in 0.2% saponin for 3 mins. Cells were washed and blocked in 5% FBS, 1% BSA in 1X PBS for 1 hour at room temperature. Cells were then incubated with primary antibody (PIP3 antibody, (1:100)) for1 hour at room temperature in moist chamber. Cells were incubated in secondary antibody for 30 mins in blocking buffer at room temperature. Cells were blocked again the second time with 4% FBS, 3% BSA for 30 mins, RT. Cells were then incubated with Pan cadherin antibody overnight at 4° C. Cells were then incubated with secondary antibody for 1 hour, RT, washed and imaged.

6.2b Zymosan pHrodo™ Red conjugation: 5 mg/mL zymosan was freshly dissolved in 10 mM sodium phosphate buffer, pH 7.2 containing 0.2% Tween 20. The particle solution was sonicated for total time of 1 min (pulse of 10 seconds and interval of 10 seconds). 100 nM of pHrodo™ Red succinimidyl ester was mixed with 0.5 mg/mL of zymosan in 10 mM sodium phosphate buffer, pH 7.2 for 4 hours with continuous shaking at room temperature. The conjugated zymosan was centrifuged at 5000 rpm for 5 mins at RT and stored at 4 °C until used.

6.2c Imaging parameters for pHrodo™ Red conjugated zymosan: pHrodo™ Red conjugated zymosan particles were incubated for 5 mins at room temperature in universal buffer with following composition; (UB) ($CaCl_2$ (1 mM), HEPES (20 mM), MES (20 mM), sodium acetate (20 mM), KCl (120 mM), NaCl (5 mM), and $MgCl_2$ (1 mM)) at pH 5.0. 0.5 μL of the above solution was loaded on glass slide, covered with 1.5mm coverslip. The pHrodo™ Red conjugated zymosan particles on coverslip was imaged before any phagocytosis assay to set up the appropriate imaging conditions. Multiple stage positions were set to image various fields of cells. Zymosan was added (t=0 mins).

6.2d pHrodo^{TM} Red conjugated zymosan uptake analysis in cells: 0.5 uL of pHrodo^{TM} Red conjugated zymosan particles were added to 100 uL of media containing monolayered cells and imaged by Leica TCS SP5 II STED laser scanning confocal microscope using the above imaging conditions with time intervals of 3 mins all the way upto 60 mins. The images obtained were z-projected with maximum intensity projection. The images were background subtracted in each stack. Each z-stacked image from time t=0 mins upto 60 mins were further stacked together to form a time lapse showing internalizing of zymosan into phagosomes. Number of pHrodo^{TM} Red zymosan particles uptaken into cells were counted with time and plotted.

6.2e Zymosan uptake assay: ~$8x10^4$-10^5 number of RAW 264.7, BMDMs, P mac cells were plated in 1mm coverslip containing 3mm culture dishes. Cells were either treated with 100 ng/mL LPS, 100 nM dsDNA or *Tudor*, or only culture media (untreated, UT) for 4 hours. After 4 hours of incubation of nanodevice or LPS, cells were treated with pHrodo^{TM} Red conjugated zymosan (t=0 min) (excitation maxima λ_{max} = 560 nm). Cells were imaged at 37° C from 0 mins to 1 hour using a widefield or confocal microscope.

6.2f Zymosan uptake in presence of inhibitor: ~$8x10^4$-10^5 number of RAW 264.7 were treated with following inhibitors, PI3K inhibitor (1 μM, Zstk474, 30 mins); mTOR1/2 inhibitor (100 nM Torin1, 1 hour); MMP9 inhibitor (100 μM, MMP9-I, 1 hour) or siRNA against *Arl8b1 and 2* for 72 hours. This was followed by treatment of 100 nM *Tudor* for 4 hours in absence or presence of inhibitors, siRNA. The phagocytic cargo, pHrodo^{TM} Red conjugated zymosan were then pulsed on cells for 30 mins at 37 °C. Cells were imaged in confocal microscopy and scored for internalized zymosans into the cells. Zymosan uptake was analyzed for ~100 cells in each condition and compared to Tudor treated cells in the absence of inhibitor or si*Scrambled* siRNA.

6.2g Phagosome lysosome fusion assay: Lysosomes in RAW 264.7, P macs (M0, M1 and M2) and BMDM (M0, M1 and M2) cells were labeled with 10 kDa Alexa 488 dextran. Lysosomal labeling of dextran in cells (Refer to Chapter 2, Materials and methods, 2.2g). Cells were either incubated with *Tudor*, dsDNA or only culture media (untreated, UT) followed by the addition of 0.5 μL pHrodo^{TM} Red conjugated zymosan for 30 mins at 37 °C. These cells were imaged by confocal microscope. Imaging conditions before each experiment were set as described in above protocol, 6.2c.

Image Analysis: The fusion of phagosome to lysosome was analyzed in single plane confocal microscope images. Alexa 488 dextran was denoted as green (G) and pHrodo^{TM} Red as red channel (R). All images were background subtracted. ROI was drawn on the plasma membrane of the cell in the R channel using Fiji. The same ROI was applied to Alexa 488 channels and intensity profiles were obtained for both G and R channels. The R/G ratios were plotted which represents the fusion of phagosome with lysosome, respectively. To quantify the phagosome lysosome contacts, the number of Alexa 488 dextran containing TLs (G) making contact with a single phagosome (R) were counted per cell and plotted.

6.3 Results and discussion

6.3a Tudor or LPS-treatment enhances phagocytosis in macrophages

We first studied the rate of phagocytosis in cells treated either with dsDNA (negative control), LPS and *Tudor*. We used the phagosome marker, pHrodo^{TM} Red conjugated zymosan as a probe to assay phagocytic uptake in RAW 264.7 macrophages. pHrodo^{TM} Red zymosan is an ideal probe to study phagocytosis as pHrodo^{TM} Red is a pH sensitive turn-on sensor which, upon conjugation to zymosan, marks acidic phagosomes within live cells (Figure VI.2 a, b). A plot of the number of phagosomes in 60 LPS and *Tudor* treated RAW 264.7 cells as a function of time revealed a higher rate of phagocytosis than untreated or dsDNA treated cells (Figure VI.2c). This suggests that those cells with more tubular lysosomes showed enhanced phagocytic uptake.

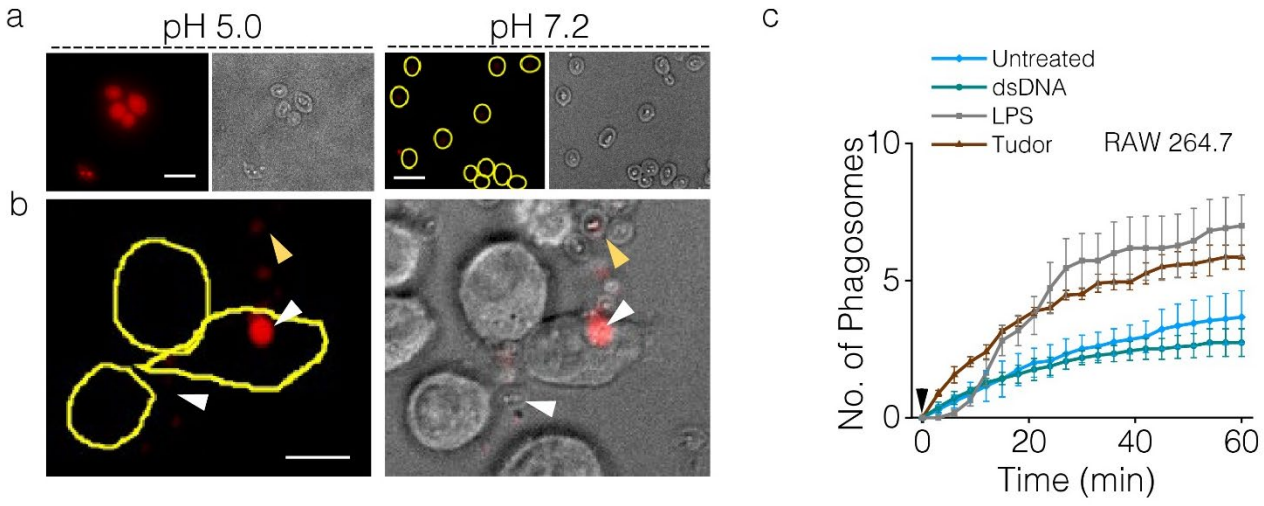

Figure VI.2: *Tudor* enhances phagocytosis.

Figure VI.2, continued. (**a** and **b**) Representative widefield images of pHrodo™ Red labeled zymosan imaged at (a) pH 5.0 and (b) pH 7.2. (**c**) Quantification of the mean number of pHrodo™ Red conjugated zymosan particles uptaken into RAW 264.7 macrophages over time upon treatment with untreated (culture media), dsDNA; *Tudor* and LPS. Arrow at t=0 min shows the time at which zymosan was added (n = ~60 cells). Error bars represents standard error of mean (s.e.m) from three independent experiments.

6.3a.1Tudor treatment enhances phagocytosis in primary macrophages

Both BMDMs and P macs have tubular lysosomes[5,29,32]. M0 (naïve) macrophages from both BMDM and Pmac show more tubulated lysosomes upon *Tudor* treatment unlike adipose tissue macrophages (ATM) that showed no significant change in tubulation (Figure II.6). Between BMDMs and P macs, M0 macrophages from P macs showed more lysosomal tubulation upon treatment with LPS or *Tudor* (Figure II.6). To test whether tubular lysosomes upregulated phagocytosis in primary macrophages, we studied the rate of phagocytosis in primary macrophages (M0, M1 and M2 macrophages of BMDMs and P macs origin) as previously described.

BMDM showed no significant change in phagocytic behavior in M0, M1 and M2 macrophages (Figure VI.5 a-f). However, M0 P macs showed significant enhanced phagocytosis upon treatment with *Tudor* but not dsDNA while M1 and M2 P macs showed no significant change in phagocytosis (Figure VI.5 g-l).

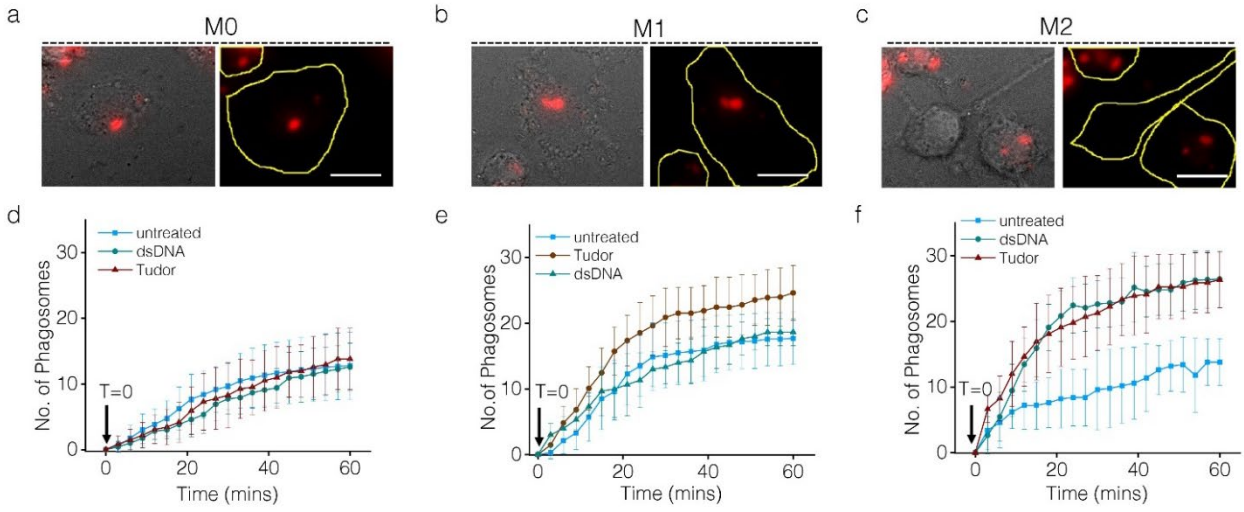

Figure VI.3: The rate of phagocytosis in BMDMs and P macs.

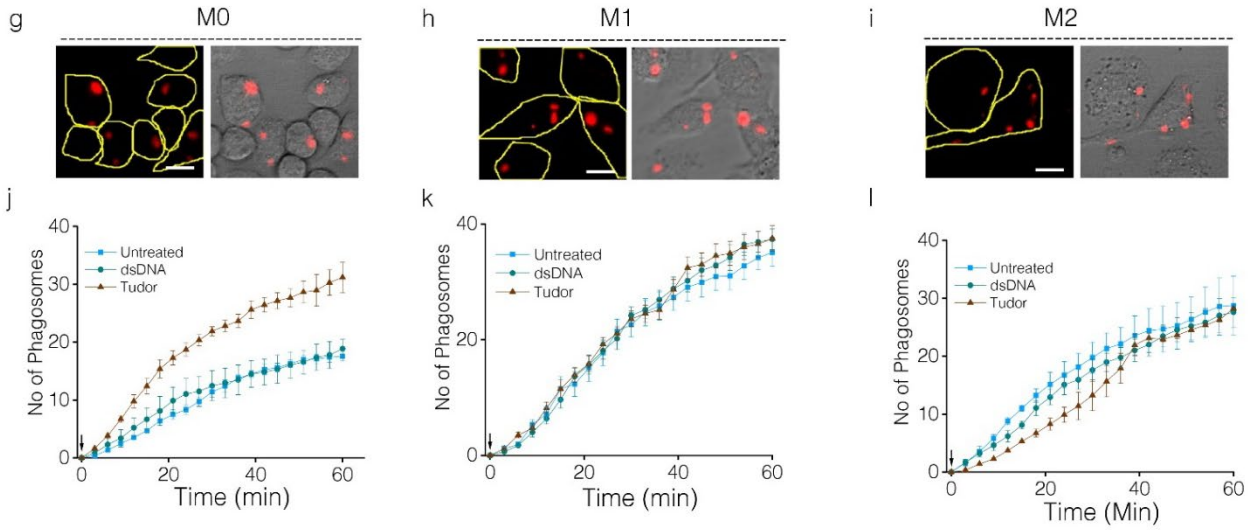

Figure VI.3, continued. The rate of phagocytosis in BMDMs and Pmacs. (**a-c** and **g-i**) Representative widefield images of BMDM (a-c) and Pmacs (g-i) showing pHrodo^{TM} Red-zymosan uptake (fluorescence image, left and brightfield image, right). (**d-f** and **j-l**)) Number of phagocytosed particles uptaken upon treatment with dsDNA and *Tudor* in BMDM (d-f) and Pmac (j-l). Arrowhead at t=0 min shows pHrodo^{TM} Red-zymosan addition to cells (n = ~30 cells). Error bars represent s.e.m from three independent experiment. Scale bar: 10 µm.

6.3b Tubular lysosomes enhanced phagosome lysosome fusion

Phagosome lysosome fusion is one of the key steps in phagosomal maturation leading to pathogen degradation. Tubular lysosomes contact late phagosomes to deliver V-ATPases needed for further acidification of phagosomal lumen before its fusion with lysosomes[32]. Disturbing phagosomal acidification affects the phagosome maturation and impedes its fusion with lysosomes. We therefore developed an assay to study the role of tubular lysosomes in phagosome-lysosome fusion

if any. Here, lysosomes in *Tudor* treated macrophages were labeled with pH insensitive Alexa 488 dextran and then subjected to uptake of pHrodo ^{TM} Red conjugated zymosan particles, which gave

rise to phagosomes. Fusion between lysosomes and phagosomes can be probed by the relative intensity of Alexa 488 and pHrodo^{TM} Red in the cell as shown in the schematic (Figure VI.3).

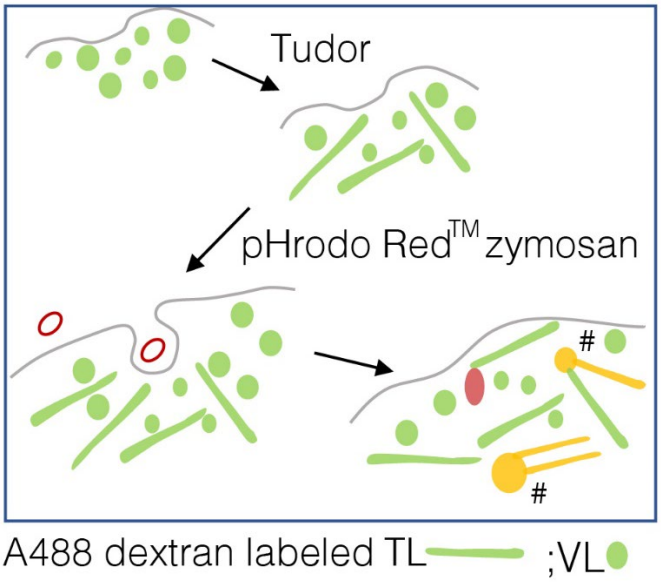

Figure VI.4: Schematic of the phagosome lysosome fusion assay.

When tubular lysosome formation was triggered by *Tudor* it led to more phagosome lysosome fusion (Figure VI.4a, c). Note that the basal uptake efficiency of cells was unaltered upon various treatment with dsDNA or *Tudor* (Figure VI.4b). Tubular lysosomes were also found to make more number of contacts with phagosomes (Figure VI.4d, e). Increased contacts also translated to increased phagosome-lysosome fusion which correlated with increased number of tubular lysosomes in cells (Figure VI.4e).

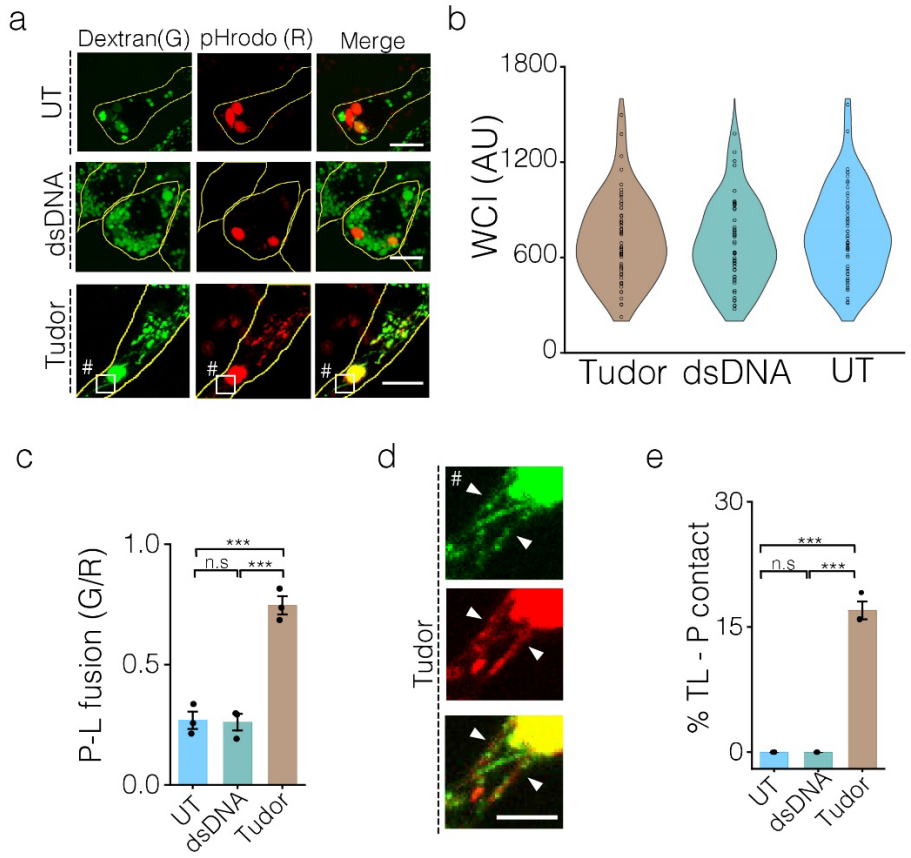

Figure VI.5: Tubular lysosomes enhance phagosome lysosome fusion. (a) Representative confocal images of lysosomes marked with Alexa 488 dextran (G) and pHrodo™ Red conjugated zymosan particles (R) in presence or absence of dsDNA; *Tudor* in RAW 264.7, Scale bars: 4 µm. (**b**) Distribution of whole cell intensity (WCI), (n= 50 cells). (**c**) Quantification of phagosome lysosome fusion (P-L fusion) represented by mean G/R (n = 20 cells, m = ~100 phagosomes). (**d**) Percentage of TLs making contact with phagosome (TL-P contact) in RAW 264.7 macrophages (n = 30 cells). (**e**) Inset for white box with # representing tubular lysosomes in *Tudor* treated RAW 264.7 in (a), inset scale bars: 4 µm. ***P< 0.0005; **P< 0.005; *P< 0.05 (one-way ANOVA with Tukey *post hoc* test). Error bars represent standard error of mean (s.e.m) from three independent experiments with similar results. AU: arbitrary units; n.s: non-significant.

6.3b.1 Tubular lysosomes enhance phagosome-lysosome fusion in primary macrophages

M0 naïve macrophages of peritoneal origin (M0 Pmacs) showed increased phagocytic behavior compared to other macrophages. We then tested whether these macrophages showed any change in the extent of phagosome lysosome fusion using the previously described method. *Tudor* treated M0 macrophages showed enhanced phagosome-lysosome fusion and with ~30% of total tubular lysosomes within the cell making contact with phagosomes in the cell (Figure VI. 6 a-d).

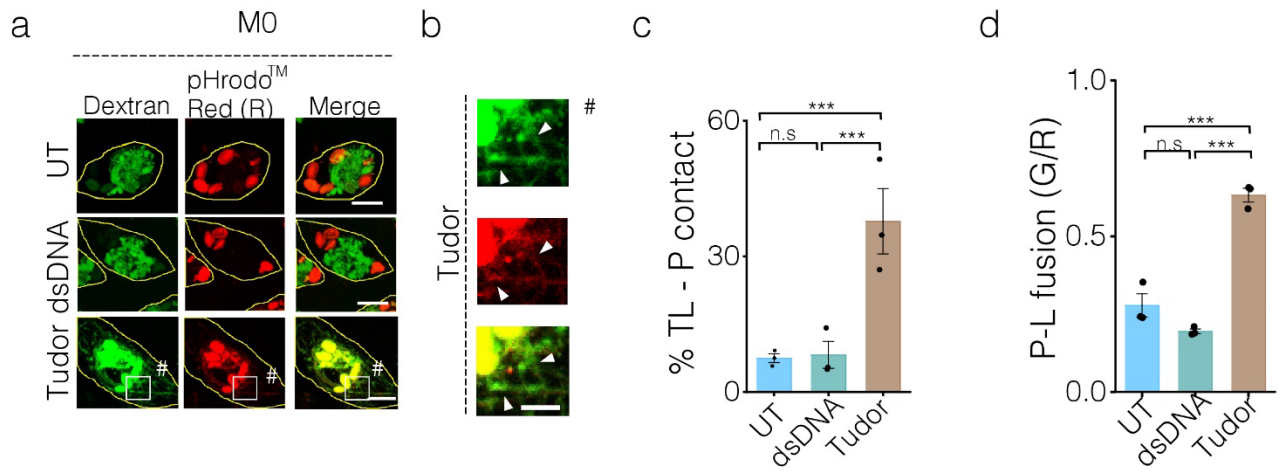

Figure VI.6 *Tudor* regulates phagosome lysosome fusion in M0 of Pmac. (a) Representative confocal images of lysosomes marked with Alexa 488 conjugated dextran (G) and pHrodo™ Red conjugated zymosan (R) in Pmacs upon treatment with culture media (untreated); dsDNA, *Tudor,* Scale bars: 10 µm. (b) Zoomed image of white box containing # in (a) with white arrow heads showing TL contacting phagosome, Scale bars: 4 µm. (c and d) Quantification of mean G/R represented as % tubular lysosomes making contact with phagosomes (TL-P contact) (c) and phagosome lysosome fusion (P-L fusion) (d), (n = 50 cells, ~300 phagosomes). ***P< 0.0005 (one-way ANOVA with Tukey *post hoc* test). n.s: non-significant. Error bars represent standard error of mean (s.e.m) from three independent experiment.

Phagosome lysosome fusion was then studied in M1 and M2 Pmacs. Both M1 and M2 macrophages did not show significant increase in lysosome tubulation, however they did show more phagosome-lysosome fusion. Since these macrophages are already activated into either M1 or M2 like phenotypes, the increase in lysosomal tubulation is not much as these cells are already at their full capacity in terms of lysosomal tubulation. This data from phago-lysosomal fusion assay suggests that *Tudor* binding to Ku70/80 heterodimer present on the plasma membrane stimulates phagosome-lysosome fusion unlike that seen in dsDNA or untreated (UT) M1 and M2 Pmacs (Figure VI.7 a-d). Note that though M0, M1 and M2 macrophages showed increased phagosome-lysosome fusion, the overall endocytic behavior in these polarized macrophages were unchanged as shown in (Figure VI.8 a-c).

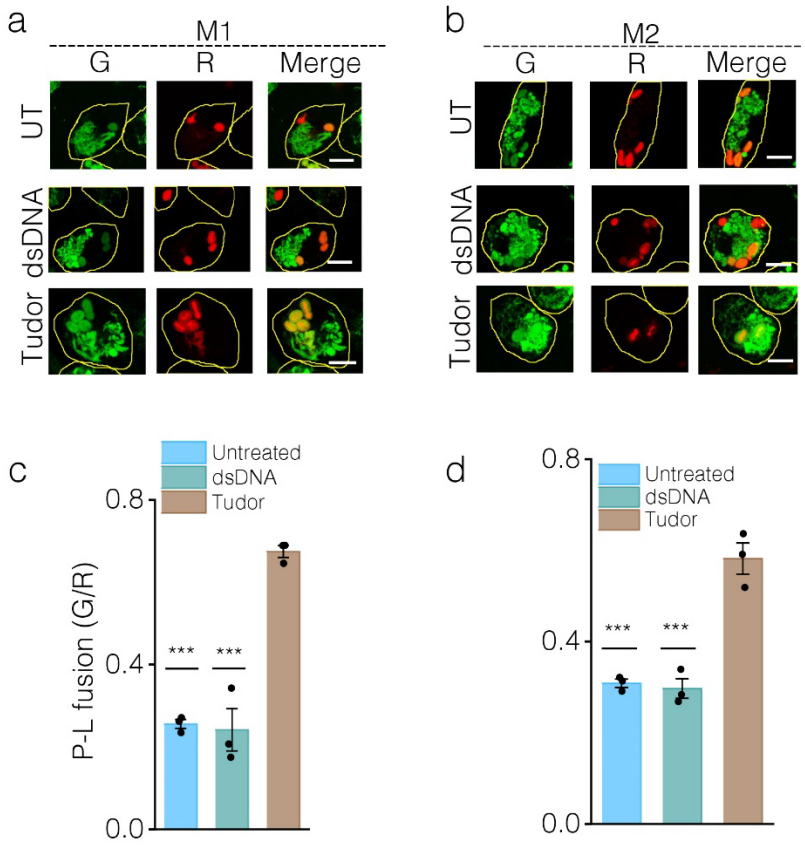

Figure VI.7: *Tudor* Mediated increase in Phago-lysosomal fusion in M1 and M2 macrophages of Pmac. (a, b) Representative confocal images of lysosomes marked with Alexa 488 conjugated dextran (G) and pHrodo^{TM} Red conjugated zymosan (R) in Pmacs upon treatment with culture media (untreated); dsDNA, *Tudor*. (**c** and **d**) Quantification of mean G/R showing the phagosome lysosome fusion (P-L fusion) in P macs (n = 50 cells, ~300 phagosomes). ***P< 0.0005 (one-way ANOVA with Tukey *post hoc* test). All errors showed here represent s.e.m from three independent experiments. Scale bars: 10 µm.

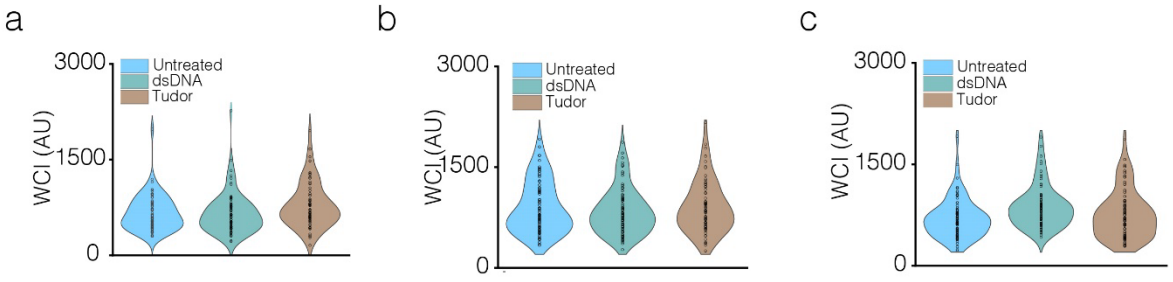

Figure VI.8: P macs (M0, M1 and M2) showed unchanged endocytic during phagolysosomal fusion. (**a-c**) Total cell intensity of Alexa 488 dextran containing lysosomes in M0 (a), M1 (b) and M2 (c) of P macs upon untreated and treatment with dsDNA and *Tudor* (n=50 cells).

6.3c MMP9 is necessary for tubulation of lysosomes

Macrophages are constitutive producers of MMP9[36]. The presence of MMP9 is important for remodeling extracellular matrix for migration of macrophages[37]. When macrophages are triggered by immune stimulants like bacterial infection or LPS it further increases MMP9 expression and enhances phagocytosis[38]. Chemical inhibition of MMP9 abolishes lysosome tubulation in diverse macrophages (Chapter 3, Figure III.3, III.5). Thus, MMP9 plays a key role in tubular lysosome formation. We therefore tested whether MMP9 knockout cells, that lacked the ability to tubulate their lysosomes also showed altered phenotypes of phagocytic behavior in primary macrophages using the previously developed assayed. We found that BMDMs (M0, M1 and M2) lacking MMP9 indeed showed reduced phagocytosis revealing that tubular lysosomes indeed enhance phagocytic uptake in macrophages (Figure VI. 9a-f)

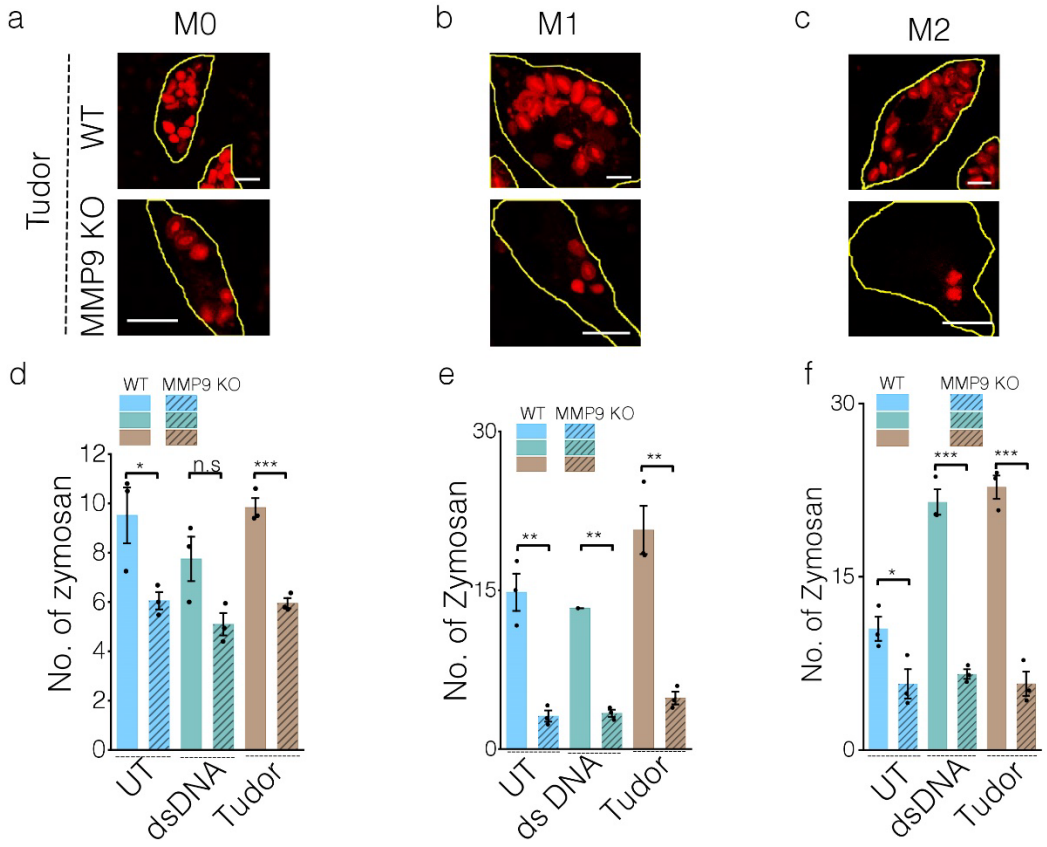

Figure V.9: MMP9 is important for lysosome tubulation in BMDM. (a-c) Representative images of *Tudor* treated M0 (a), M1 (b) and M2 (c) macrophages from wildtype and MMP9 knockout (KO) mouse showing the uptake of pHrodo™ Red™ conjugated zymosan shown in red. (b-f) Quantification showing the number of zymosan uptaken in M0 (d), M1 (e) and M2 (f), (n-50

cells). ***P< 0.0005 (one-way ANOVA with Tukey *post hoc* test). All errors showed here represent s.e.m from three independent experiments. Scale bars: 10 µm.

We then tested whether knocking out MMP9 affected phagosome- lysosome fusion using the previously assays (Figure VI.2) in M0, M1 and M2 BMDMs isolated from MMP9 KO mice. Indeed, we found that *Tudor* treated M0 macrophages from MMP9 KO BMDM showed lower phagosome lysosome fusion (Figure VI.10a-c) even though there was no change in their relative endocytic uptake whether or not they were treated with dsDNA or *Tudor* (Figure VI.10 d and e).

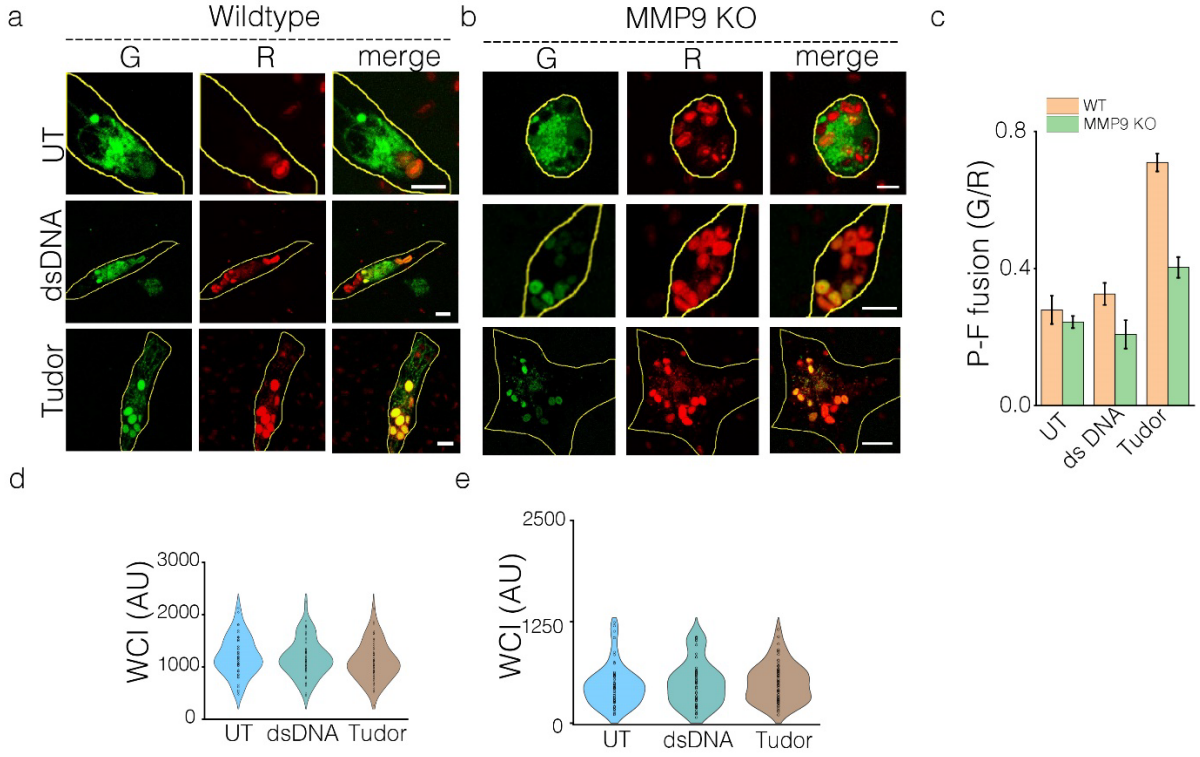

Figure V.10: MMP9 is important for the phagosome lysosome fusion in M0 BMDMs. (a and **b**) Representative confocal images of lysosomes marked with Alexa 488 conjugated dextran (G) and pHrodo™ Red conjugated zymosan (R) in M0 of BMDMs untreated (UT); dsDNA, *Tudor*. (**b**) Quantification of Phagosome-Lysosome (P-L) fusion showing the ratio of G over R, read out for phagosome lysosome fusion (P-L fusion) in M0 of BMDMs (n = 50 cells, ~300 phagosomes). (**d** and **e**) Total cell intensity of Alexa 488 dextran containing lysosomes in M0 of BMDM with UT, dsDNA and *Tudor* (n=50 cells). All errors showed here represent s.e.m from three independent experiments. Scale bars: 10 µm.

M1 polarized BMDMs lacking MMP-9 indeed showed reduced phagosome lysosome fusion as compared to wildtype M1 macrophages upon *Tudor* treatment (Figure VI.11 a-c) . Note that here

too, there was no change in the overall endocytic uptake in M1 BMDMs whether or not they were treated with dsDNA or *Tudor* (Figure VI.11 d and e).

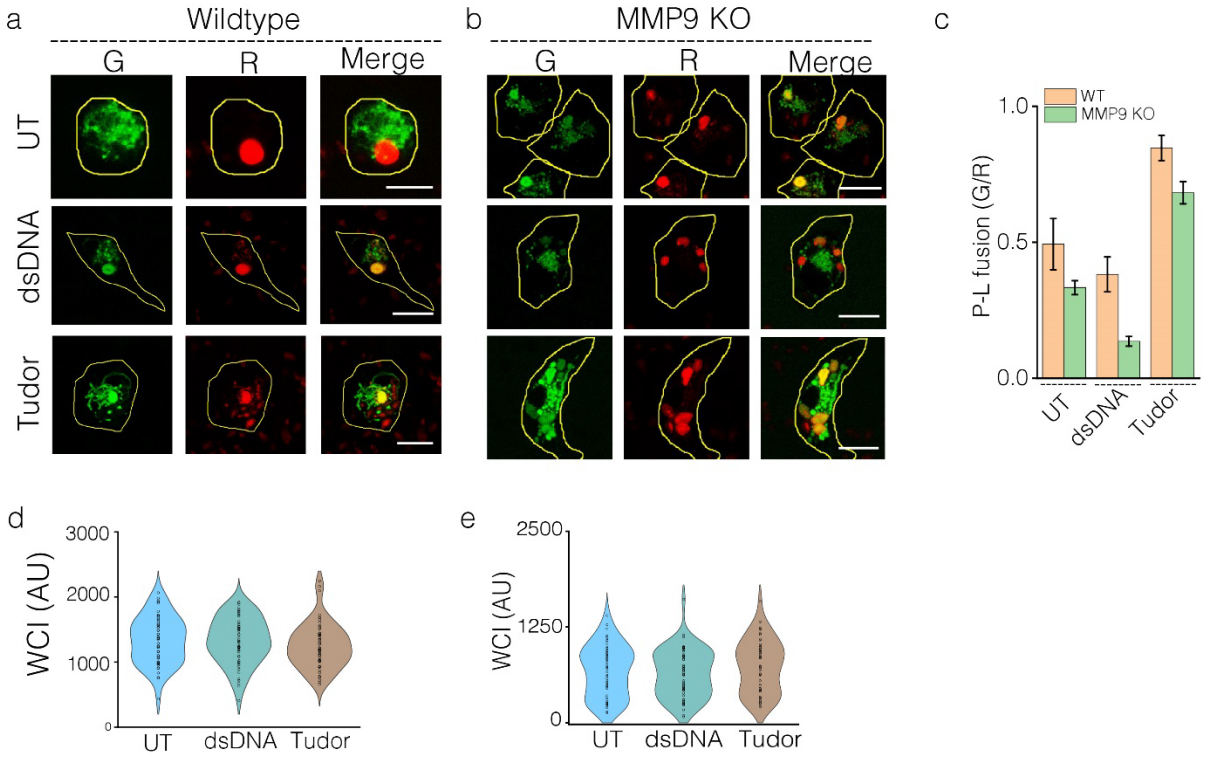

Figure VI.11: MMP9 is important for the phagosome lysosome fusion in M1 BMDMs. (a and **b**) Representative confocal images of lysosomes marked with Alexa 488 conjugated dextran (G) and pHrodo™ Red conjugated zymosan (R) in M1 of BMDMs untreated (UT); dsDNA, *Tudor*. (**b**) Quantification of Phagosome-Lysosome (P-L) fusion showing the ratio of G over R, read out for phagosome lysosome fusion (P-L fusion) in M1 of BMDMs (n = 50 cells, ~300 phagosomes). (**d** and **e**) Total cell intensity of Alexa 488 dextran containing lysosomes in M1 of BMDM with UT, dsDNA and *Tudor* (n=50 cells). All errors showed here represent Standard error of mean (s.e.m) from three independent experiments. Scale bars: 10 µm.

Similarly, M2 BMDMs lacking MMP9 showed drastically reduced phagosome lysosome fusion compared to their counterparts from wildtype mice upon *Tudor* treatment (Figure VI.12 a-c). Note that here too, there was no change in the overall endocytic uptake in M2 BMDMs whether or not they were treated with dsDNA or *Tudor* (Figure VI.12 d, e).

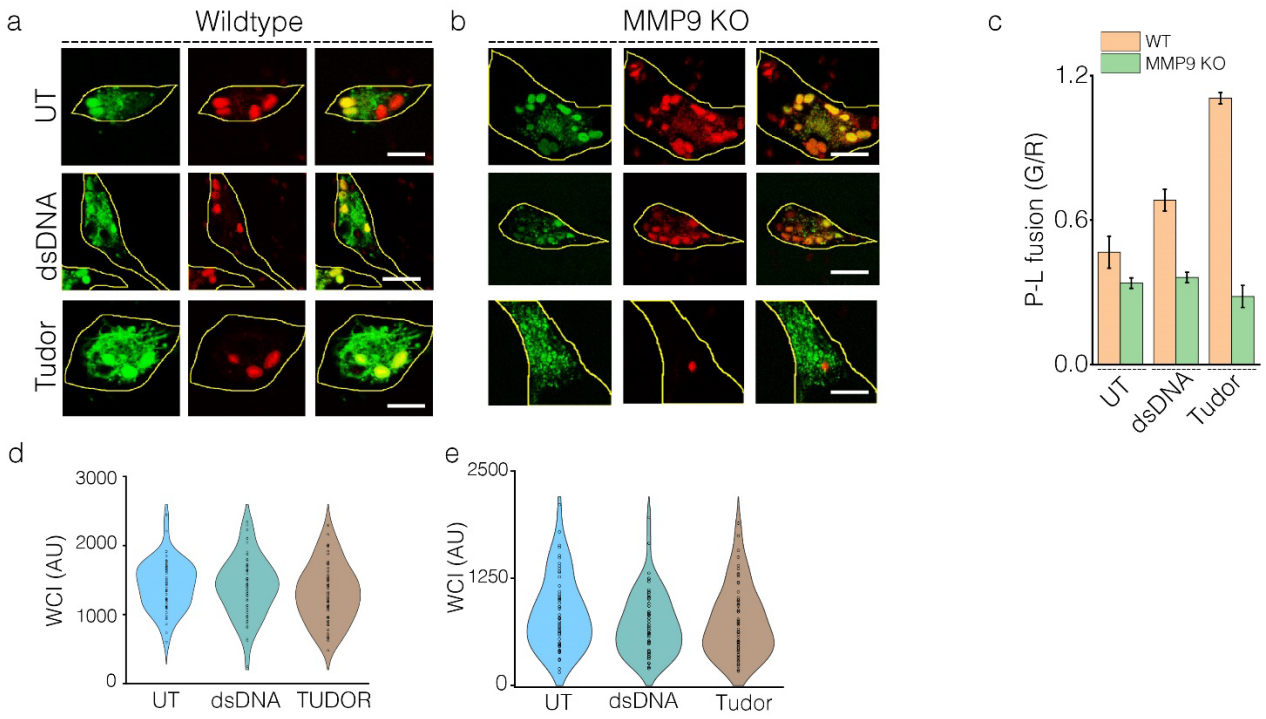

Figure V.12: MMP9 is important for the phagosome lysosome fusion in M2 BMDMs. (a and **b**) Representative confocal images of lysosomes marked with Alexa 488 conjugated dextran (G) and pHrodo™ Red conjugated zymosan (R) in M2 of BMDMs untreated (UT); dsDNA, *Tudor*. (**b**) Quantification of Phagosome-Lysosome (P-L) fusion showing the ratio of G over R, read out for phagosome lysosome fusion (P-L fusion) in M2 of BMDMs (n = 50 cells, ~300 phagosomes). (**d** and **e**) Total cell intensity of Alexa 488 dextran containing lysosomes in M2 of BMDM with UT, dsDNA and *Tudor* (n=50 cells). All errors showed here represent standard error of mean (s.e.m) from three independent experiments. Scale bars: 10 µm.

6.3d *Tudor* promotes phagocytosis

To explicitly study the effect of tubulation *per se* on phagocytosis, we studied phagocytic uptake in cells where players such as MMP9, PI3K and mTOR were pharmacologically inhibited. Arl8b is not implicated upstream of mTOR activation but is involved in actually tubulating the lysosome once mTOR has been activated. We compared the effects of inhibition players upstream of tubulation as well as downstream of mTOR. *Tudor* treatment on cells where PI3K, mTOR and MMP-9 led to loss of tubulation but also reduced phagocytosis. However, knocking down Arl8b by siRNA and treatment with *Tudor* indeed affected the phagocytic uptake in RAW 264.7

macrophages, even though the mTOR activation was still ongoing (Figure VI.13 a-b). This explicitly reveals a role for tubular lysosomes in promoting phagocytosis.

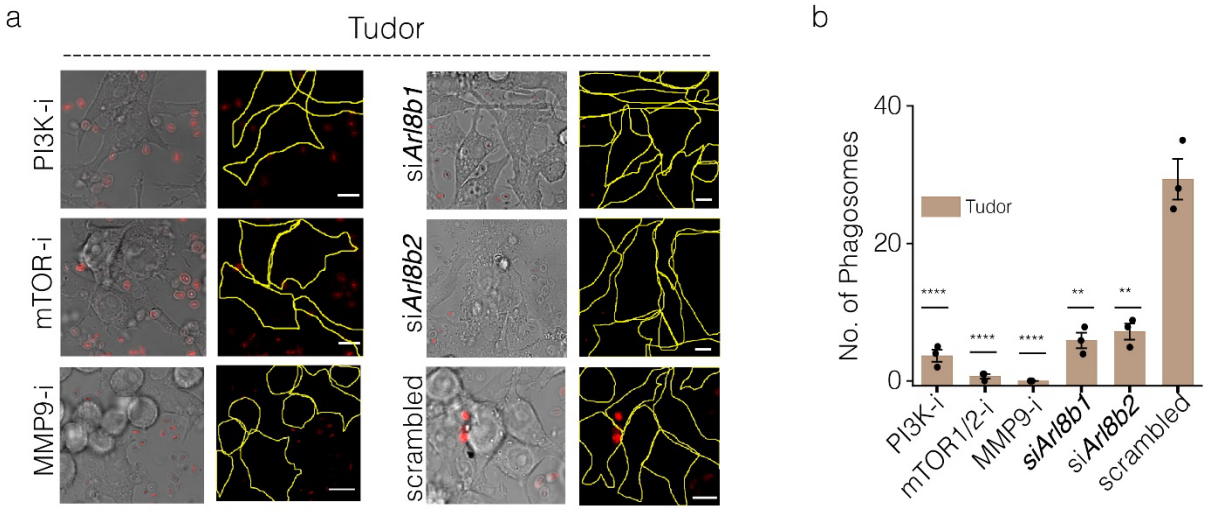

Figure V.13: *Tudor* mediated tubular lysosomes pathway is for important for phagocytosis. **(a)** Representative images of *Tudor* treated RAW 264.7 cells in presence of inhibitors of mentioned proteins (protein-i) showing its brightfield image (left) and pHrodo™ Red conjugated zymosan shown as red (right). (**b**) Quantification for (a) showing the number of phagosomes, (n=100 cells). Error bars represent standard error of mean (s.e.m) from three independent experiment. (***P< 0.0005; **P< 0.005; *P< 0.05 (one-way ANOVA with Tukey *post hoc* test). Scale bar: 10 µm.

PI_3K activity modulates the levels of phosphatidylinositol phosphates (PIPs) on the inner leaflet of the plasma membrane. PI_3K phosphorylates $PI(4,5)P_2$ that is abundant in the plasma membrane to $PI(3,4,5)P_3$ and the latter facilitates phagosome cup formation[6,18] (Figure VI.1). Accordingly, *Tudor* treated macrophages showed elevated levels of $PI(3,4,5)P_3$ at the plasma membrane which was reduced in presence of PI3K inhibitor. Inhibition of mTOR did not affect PI(3,4,5)P3 labeling on plasma membrane significantly, suggesting that even though the $PI(3,4,5)P_3$ needed for phagocytic cup formation were present, reduced phagocytosis could be pinpointed to the lack of tubular lysosomes . This demonstrates that the tubular lysosomes pathway promote the early stages in phagosome formation (Figure VI.14 a, b).

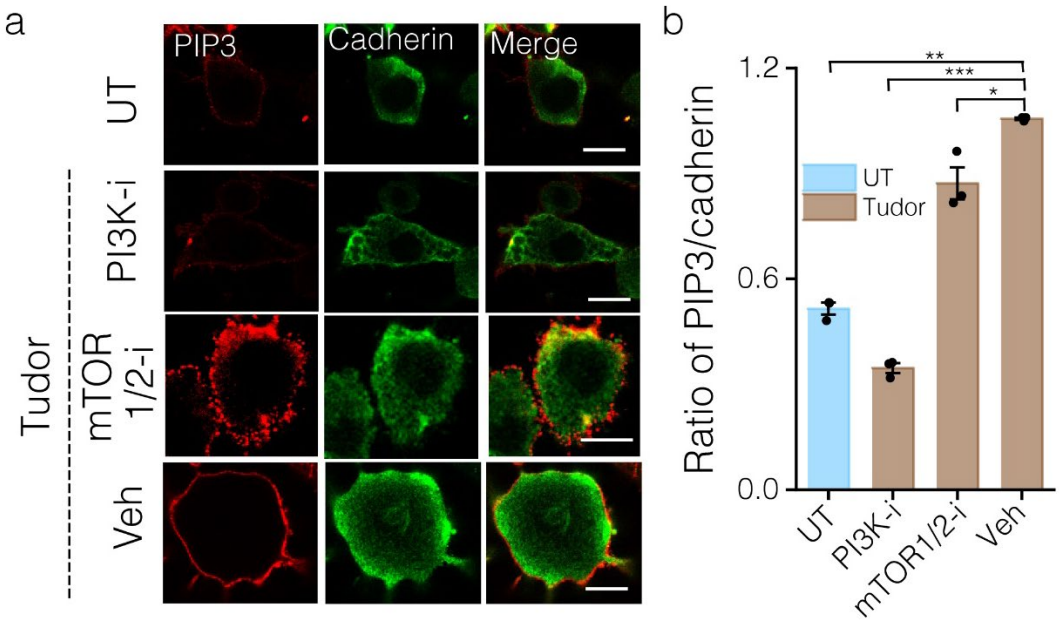

Figure V.14: Tubular lysosomes promote phagosome formation. (**a**) Representative confocal images of *Tudor* treated RAW 264.7 with immunofluorescence against PI(3,4,5)P3 (PIP3) and Pan cadherin in untreated (UT);PI3K inhibitor; mTOR1/2 inhibitor . (**b**) Quantification of (a) showing the ratio of PIP3 to Pan cadherin, (n=50 cells). Error bars represented standard error of mean from three independent experiment. ***P< 0.0005; **P< 0.005; *P< 0.05 (one-way ANOVA with Tukey *post hoc* test). Scale bar: 10 µm.

6.3e Model showing the impact of tubular lysosomes on phagocytosis

Based on our experiments, we propose a model for how tubular lysosomes might drive phagosome formation. Ku80 of Ku70/Ku80 heterodimer proteins interacts with pro-MMP9 and activates MMP9 on the plasma membrane. Activated MMP9 could bind to an as yet unidentified receptor tyrosine kinase (RTK) that could in turn activate PI3K through its SH2 domain[39]. Activation of PI_3K converts PI(4,5)P2 into PI(3,4,5)P3 on the inner leaflet of the plasma membrane which is needed for the phagosomal cup formation during the early stages of phagocytosis[6]. PI(3,4,5)P3 activates the serine/threonine kinase, Akt[39,40]. PI3K-Akt activation is known to promote the secretion of pro-MMP9 onto the plasma membrane such that more MMP9 is available for activation by *Tudor*[41]. This results in a positive feedback loop where more PI3K is activated setting up a mechanism for sustained tubulation of lysosomes.

Akt activation leads to mTOR activation. mTOR docks on the cytosolic side of the lysosomal membrane and brings about lysosomal tubulation via Arl8b[28]. Inhibition of Arl8b, despite allowing the upstream signaling to proceed, inhibits phagocytosis as tubular lysosome formation cannot be even if the positive feedback loop is operational. This explicitly reveals the requirement for lysosome tubulation for phagocytosis.

Two other protein players which were found to be essential *Tudor* mediated tubulation of lysosomes, namely, LKB1 and AMPK. LKB1 is a direct activator of AMPK and AMPK negatively regulates mTOR by phosphorylating it at positions, S722 and S792. This likely prevents runaway activation of mTOR[42,43]. Calcium levels within the lumen of lysosomes must be maintained just right for lysosomal tubulation which in turn must depend on the appropriate activity of mTOR (Figure VI.15). The calcium rich domain in tubular lysosomes might be the source of calcium needed for activation of dynamin for phagosome formation. Calcium rich tips of tubular lysosomes facing plasma membrane might be helping in its fusion with the latter. This could be a mechanism by which cells obtain extra membrane needed for phagocytosis and plasma membrane remodeling.

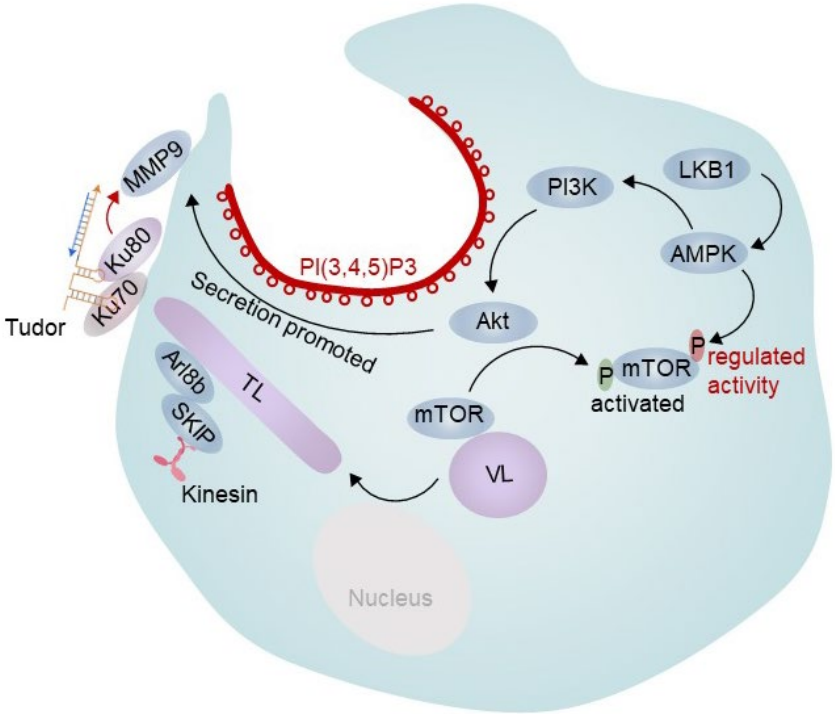

Figure V.15: Proposed model showing how lysosomal tubulation promotes phagocytosis.

6.4 Conclusion

Our experiments reveal tubular lysosomes poise macrophages for phagocytosis and promote phagosome-lysosome fusion. In activated macrophages, despite the background of cytokine signaling, the tubulation of lysosomes makes the cells more phagocytic. Phagocytosis is enhanced due to the existence of a positive feedback mechanism between PI3K activation that stimulates MMP9 secretion on the cell surface that is in turn activated by *Tudor*. Thus, inhibiting tubular lysosome formation, or inhibiting MMP-9 significantly impeded phagocytosis as sustained tubulation does not occur. The involvement of both PI3K-Akt activation which positively regulates mTOR and LKB1-AMPK activation which negatively regulates mTOR serve to prevent mTOR hyper activation and maintain judicious level of mTOR activity which in turn sculpts the lumenal Ca^{2+} levels needed for tubulation. Tubular lysosomes also promote phagosome-lysosome fusion, indicating that they are important in both early and late stages of phagocytosis. A reagent such as *Tudor* which can promote tubulation without immunostimulation or cell starvation, can be used to identify newer and as yet unknown roles for tubular lysosomes in resting cells.

6.5 References

1. Lim, J. J., Grinstein, S. & Roth, Z. Diversity and versatility of phagocytosis: roles in innate immunity, tissue remodeling, and homeostasis. *Front. Cell Infect. Microbiol.* **7,** 191 (2017).
2. Mazgaeen, L. & Gurung, P. Recent advances in lipopolysaccharide recognition systems. *Int. J. Mol. Sci.* **21,** (2020).
3. Islam, M. A. *et al.* Alveolar macrophage phagocytic activity is enhanced with LPS priming, and combined stimulation of LPS and lipoteichoic acid synergistically induce pro-inflammatory cytokines in pigs. *Innate Immun* **19,** 631–643 (2013).
4. Schaeffer, V. *et al.* Role of the mTOR pathway in LPS-activated monocytes: influence of hypertonic saline. *J. Surg. Res.* **171,** 769–776 (2011).
5. Hipolito, V. E. B. *et al.* Enhanced translation expands the endo-lysosome size and promotes antigen presentation during phagocyte activation. *PLoS Biol.* **17,** e3000535 (2019).
6. Levin, R., Grinstein, S. & Canton, J. The life cycle of phagosomes: formation, maturation, and resolution. *Immunol. Rev.* **273,** 156–179 (2016).
7. Yoshida, S., Pacitto, R., Yao, Y., Inoki, K. & Swanson, J. A. Growth factor signaling to mTORC1 by amino acid-laden macropinosomes. *J. Cell Biol.* **211,** 159–172 (2015).
8. Koivusalo, M. *et al.* Amiloride inhibits macropinocytosis by lowering submembranous pH and preventing Rac1 and Cdc42 signaling. *J. Cell Biol.* **188,** 547–563 (2010).

9. Rosales, C. & Uribe-Querol, E. Phagocytosis: A fundamental process in immunity. *Biomed Res. Int.* **2017,** 9042851 (2017).

10. Canton, J. *et al.* Calcium-sensing receptors signal constitutive macropinocytosis and facilitate the uptake of NOD2 ligands in macrophages. *Nat. Commun.* **7,** 11284 (2016).

11. Kohyama, M. *et al.* Role for Spi-C in the development of red pulp macrophages and splenic iron homeostasis. *Nature* **457,** 318–321 (2009).

12. Westman, J., Grinstein, S. & Marques, P. E. Phagocytosis of necrotic debris at sites of injury and inflammation. *Front. Immunol.* **10,** 3030 (2019).

13. Devosse, T. *et al.* Formyl peptide receptor-like 2 is expressed and functional in plasmacytoid dendritic cells, tissue-specific macrophage subpopulations, and eosinophils. *J. Immunol.* **182,** 4974–4984 (2009).

14. Lee, C.-Y., Herant, M. & Heinrich, V. Target-specific mechanics of phagocytosis: protrusive neutrophil response to zymosan differs from the uptake of antibody-tagged pathogens. *J. Cell Sci.* **124,** 1106–1114 (2011).

15. Ravichandran, K. S. Find-me and eat-me signals in apoptotic cell clearance: progress and conundrums. *J. Exp. Med.* **207,** 1807–1817 (2010).

16. Truman, L. A. *et al.* CX3CL1/fractalkine is released from apoptotic lymphocytes to stimulate macrophage chemotaxis. *Blood* **112,** 5026–5036 (2008).

17. Kamen, L. A., Levinsohn, J. & Swanson, J. A. Differential association of phosphatidylinositol 3-kinase, SHIP-1, and PTEN with forming phagosomes. *Mol. Biol. Cell* **18,** 2463–2472 (2007).

18. Flannagan, R. S., Jaumouillé, V. & Grinstein, S. The cell biology of phagocytosis. *Annu. Rev. Pathol.* **7,** 61–98 (2012).

19. Duclos, S. *et al.* Rab5 regulates the kiss and run fusion between phagosomes and endosomes and the acquisition of phagosome leishmanicidal properties in RAW 264.7 macrophages. *J. Cell Sci.* **113 Pt 19,** 3531–3541 (2000).

20. Kinchen, J. M. & Ravichandran, K. S. Phagosome maturation: going through the acid test. *Nat. Rev. Mol. Cell Biol.* **9,** 781–795 (2008).

21. Lee, H.-J., Woo, Y., Hahn, T.-W., Jung, Y. M. & Jung, Y.-J. Formation and Maturation of the Phagosome: A Key Mechanism in Innate Immunity against Intracellular Bacterial Infection. *Microorganisms* **8,** (2020).

22. Uribe-Querol, E. & Rosales, C. Control of phagocytosis by microbial pathogens. *Front. Immunol.* **8,** 1368 (2017).

23. Hackam, D. J., Rotstein, O. D. & Grinstein, S. in *Phagocytosis: The Host* **5,** 299–319 (Elsevier, 1999).

24. Jeschke, A. & Haas, A. Deciphering the roles of phosphoinositide lipids in phagolysosome biogenesis. *Commun Integr Biol* **9,** e1174798 (2016).

25. Levin-Konigsberg, R. *et al.* Phagolysosome resolution requires contacts with the endoplasmic reticulum and phosphatidylinositol-4-phosphate signalling. *Nat. Cell Biol.* **21,** 1234–1247 (2019).

26. Inpanathan, S. & Botelho, R. J. The lysosome signaling platform: adapting with the times. *Front. Cell Dev. Biol.* **7,** 113 (2019).

27. Gray, M. A. *et al.* Phagocytosis enhances lysosomal and bactericidal properties by activating the transcription factor TFEB. *Curr. Biol.* **26,** 1955–1964 (2016).

28. Saric, A. *et al.* mTOR controls lysosome tubulation and antigen presentation in macrophages and dendritic cells. *Mol. Biol. Cell* **27,** 321–333 (2016).

29. Hipolito, V. E. B., Ospina-Escobar, E. & Botelho, R. J. Lysosome remodelling and adaptation during phagocyte activation. *Cell Microbiol.* **20,** (2018).

30. Swanson, J., Burke, E. & Silverstein, S. C. Tubular lysosomes accompany stimulated pinocytosis in macrophages. *J. Cell Biol.* **104,** 1217–1222 (1987).

31. Mrakovic, A., Kay, J. G., Furuya, W., Brumell, J. H. & Botelho, R. J. Rab7 and Arl8 GTPases are necessary for lysosome tubulation in macrophages. *Traffic* **13,** 1667–1679 (2012).

32. Sun-Wada, G.-H., Tabata, H., Kawamura, N., Aoyama, M. & Wada, Y. Direct recruitment of H+-ATPase from lysosomes for phagosomal acidification. *J. Cell Sci.* **122,** 2504–2513 (2009).

33. Suresh, B. *et al.* Tubular lysosomes harbor active ion gradients and poise macrophages for phagocytosis. *BioRxiv* (2020). doi:10.1101/2020.12.05.413229

34. Kratz, M. *et al.* Metabolic dysfunction drives a mechanistically distinct proinflammatory phenotype in adipose tissue macrophages. *Cell Metab.* **20,** 614–625 (2014).

35. Reardon, C. A. *et al.* Obesity and Insulin Resistance Promote Atherosclerosis through an IFNγ-Regulated Macrophage Protein Network. *Cell Rep.* **23,** 3021–3030 (2018).

36. Fanjul-Fernández, M., Folgueras, A. R., Cabrera, S. & López-Otín, C. Matrix metalloproteinases: evolution, gene regulation and functional analysis in mouse models. *Biochim. Biophys. Acta* **1803,** 3–19 (2010).

37. Gong, Y., Hart, E., Shchurin, A. & Hoover-Plow, J. Inflammatory macrophage migration requires MMP-9 activation by plasminogen in mice. *J. Clin. Invest.* **118,** 3012–3024 (2008).

38. Bergin, P. J., Sicheng, W., Qiang, P.-H. & Marianne, Q.-J. Secretion of matrix metalloproteinase-9 by macrophages, in vitro, in response to Helicobacter pylori. *FEMS Immunol. Med. Microbiol.* **45,** 159–169 (2005).

39. Castellano, E. & Downward, J. RAS Interaction with PI3K: More Than Just Another Effector Pathway. *Genes Cancer* **2,** 261–274 (2011).

40. Hemmings, B. A. & Restuccia, D. F. PI3K-PKB/Akt pathway. *Cold Spring Harb. Perspect. Biol.* **4,** a011189 (2012).

41. Thant, A. A. *et al*. Fibronectin activates matrix metalloproteinase-9 secretion via the MEK1-MAPK and the PI3K-Akt pathways in ovarian cancer cells. *Clin Exp Metastasi*s **18**, 423–428 (2000).

42. Gwinn, D. M. *et al.* AMPK phosphorylation of raptor mediates a metabolic checkpoint. *Mol. Cell* **30,** 214–226 (2008).

43. Inoki, K., Kim, J. & Guan, K.-L. AMPK and mTOR in cellular energy homeostasis and drug targets. *Annu. Rev. Pharmacol. Toxicol.* **52,** 381–400 (2012).